SPECTRAL CHARACTERISTICS OF BOUNDARY LAYER OVER IRREGULAR TERRAIN

RAE ANN EVERSOLE

Atmospheric Scienc
PAPER NO.
314

US ISSN 0067-0340

DEPARTMENT OF ATMOSPHERIC SCIENCE
COLORADO STATE UNIVERSITY
FORT COLLINS, COLORADO

SPECTRAL CHARACTERISTICS OF BOUNDARY LAYER TURBULENCE OVER IRREGULAR TERRAIN

Rae Ann Eversole

The research reported here has been jointly supported by Zonta International through the Amelia Earhart Fellowship Award, and by the Wave Propagation Laboratory of the National Oceanic and Atmospheric Administration through a contract to Colorado State University.

Department of Atmospheric Science
Colorado State University
Fort Collins, Colorado 80523

June, 1979

Atmospheric Science Paper No. 314

ABSTRACT

The spectral behavior of turbulence in a convectively unstable boundary layer over undulating terrain is discussed. The wind and temperature fluctuations were measured with fast response sensors mounted on the 300 m tower at the Boulder Atmospheric Observatory (BAO). The boundary layer is divided into three layers (surface, matching, and mixed). The spectra of each layer are normalized using the appropriate scaling rules. The generalized spectra follow similarity theory. This paper compares the BAO results with the data obtained during AFCRL's field experiments in Kansas (1968) and Minnesota (1973) over flat, uniform terrain.

The spectra in the inertial subrange decrease in the surface layer and become constant in the mixed layer. The ratio of the spectral intensities between the transverse and longitudinal velocity components is 4/3, the -5/3 power law exists, and the cospectra vanish in the inertial subrange; consequently, local isotropy is observed.

The wavelength corresponding to the logarithmic spectral peak is greater over rolling terrain than flat terrain for all the spectra in the surface, matching, and mixed layers. Both the horizontal and vertical velocity components exhibited larger length scales in the mixed layer than $1.5z_i$ as observed at Minnesota. At BAO, the fluctuating temperature and vertical velocity component energy containing eddies were of comparable size. Since this was not observed over flat terrain, the irregular terrain may be a contributing factor to the observed differences.

The dissipation rates of turbulent kinetic energy are examined in the surface and mixed layers. In the surface layer BAO dissipation rates agree well with those calculated in Minnesota, but increased more rapidly than the Kansas dissipation rates. In the mixed layer, however, the dissipation rate of turbulent kinetic energy is high at BAO and Minnesota for unknown reasons. In addition, the normalized standard deviation of vertical velocity and temperature are compared with the Kansas results and found to agree well.

ACKNOWLEDGEMENTS

The author wishes to express the deepest gratitude to Dr. J. C. Kaimal for providing guidance, suggestions, and expertise throughout this research. The constructive comments and general support of Dr. W. H. Schubert have also been appreciated. Through such efforts, including the critical review of this manuscript, this research has been an invaluable educational experience. In addition, the author is thankful for the careful preparation and typing of the manuscript by Ms. M. Birchfield.

The research reported here has been jointly supported by Zonta International through the Amelia Earhart Fellowship Award, and by the Wave Propagation Laboratory of the National Oceanic and Atmospheric Administration through a contract to Colorado State University.

DEDICATION

I would like to dedicate this thesis to someone who has provided the continuous emotional support and understanding required to surmount the challenges of graduate study -- Richard E. Dougherty.

TABLE OF CONTENTS

TABLE OF CONTENTS continued

LIST OF TABLES

LIST OF ILLUSTRATIONS

LIST OF ILLUSTRATIONS continued

LIST OF ILLUSTRATIONS continued

LIST OF ILLUSTRATIONS continued

LIST OF ILLUSTRATIONS continued

Chapter I

INTRODUCTION

Studies of turbulence spectra conducted over the last two decades have yielded significant information on the structure and dynamics of the atmosphere's boundary layer. To a large extent, these advances were possible because of developments in sensor design and data acquisition methods enabling the collection and processing of large quantities of high quality atmospheric data. The study of turbulence in the boundary layer is complicated not only by the presence of a wide range of eddy sizes, but also by the influence of several factors such as height, wind speed, thermal stability, and surface roughness. A full explanation of spectral behavior requires the proper identification of all factors involved. Our present understanding has been achieved by comparing the results from several carefully designed experiments with the Monin-Obukhov and mixed-layer similarity hypotheses.

Taylor (1938) laid the foundations for spectral interpretation of atmospheric data, but a systematic approach to the study of spectra did not emerge until the mid-1950's, when Panofsky and his co-workers analyzed data from the Brookhaven National Laboratory. In 1960 Panofsky and McCormick presented, for the first time, a generalized form for the vertical velocity spectrum near the ground. When plotted against a dimensionless frequency, spectra of vertical velocity fluctuations measured under conditions of varying stability and wind speed and at many different locations displayed similar shapes with the maxima corresponding to a wavelength roughly equal to four times the height above the ground. The parameter plotted was the logarithmic spectral density (frequency times the spectral density or the variance

produced per unit logarithmic frequency increment). Although the horizontal velocity spectra failed to show the same systematic behavior, this labeling system became the foundation of spectral investigations that have followed.

As more precise data from different sites became available in the 1960's, Busch and Panofsky (1968) attempted to derive averaged curves for each site from composite plots of wind velocity spectra separated into broad stability categories. By normalizing the logarithmic spectral densities with the friction velocity squared, they reduced the spread of the data points along the ordinate. The composite vertical velocity spectra obeyed the Monin-Obukhov similarity theory within the lowest 50 meters of the atmosphere. However, the composite longitudinal velocity spectra did not follow this theory; there were some differences in spectral behavior between sites. All the spectra followed the predicted -5/3 power law within the Kolmogorov universal equilibrium range, also referred to as the inertial subrange. In this range, the ratio of the spectral densities between the transverse and longitudinal velocity components agreed well with the 4/3 ratio required for isotropy.

Not until the late-1960's were temperature spectra investigated. At Round Hill in Massachusetts a complete set of the temperature fluctuations was recorded under a variety of stability conditions. Although the individual spectra failed to demonstrate any systematic variation with height, the composite plots of temperature spectra followed Monin-Obukhov similarity theory. Panofsky (1969) observed the peak value of the normalized logarithmic spectral density curve shift toward higher frequencies as the stability increased. The slope of the temperature

spectra at high frequencies followed the predictions of the inertial subrange.

A clear understanding of spectral behavior in the "surface layer" (approximately the first 30 meters of the boundary layer) did emerge eventually from an experiment conducted by scientists of the Air Force Cambridge Research Laboratories (AFCRL)(Haugen et al., 1971) over unusually flat terrain in southwestern Kansas. Three-axis sonic anemometers and fine platinum wire thermometers mounted at three levels on a 32 m tower were used to measure the velocity and temperature fluctuations respectively. For the first time, a computer controlled the acquisition of data. By using similarity arguments to nondimensionalize the logarithmic spectral densities, Kaimal et al. (1972) were able to reduce each of the velocity and temperature spectra to a family of curves which merged into a single curve in the inertial subrange. In the energy-containing region of the lower frequencies, within a stable boundary layer the spectral curves separated systematically as a function of the stability parameter, z/L (where z is the height above ground and L is the Obukhov length), following similarity theory. However, the unstable velocity and temperature spectra were not arranged according to the stability parameter, but tended to randomly cluster with a band. The notable exceptions were still the horizontal velocity spectra which did not appear to conform to the scaling laws in the surface layer. It became apparent that the low frequency portion of those spectra was responding to a scaling parameter external to the surface layer.

The 1973 Minnesota experiment, designed to investigate the turbulence structure within a convectively unstable boundary layer, provided answers to some important questions raised by the Kansas

experiment. This experiment, conducted jointly by the Air Force Cambridge Research Laboratories (AFCRL) and the Meteorological Research Unit (MRU) at Cardington (England), was located on a flat and uniform site with little or no vegetation in northwestern Minnesota. The instrumentation included five turbulence probes suspended from the tethering cable of a large, captive balloon in addition to the fixed sensors mounted at several levels of a 32 m tower. The data showed, among other things, that Monin-Obukhov scaling is valid only to a height of $z_i/10$, where z_i is the height of the lowest inversion base. In the "mixed layer", which encompasses the upper 9/10 of the atmospheric boundary layer, z_i emerged as the controlling length scale (Kaimal et al., 1976). A new set of universal curves were developed to describe the wind velocity spectral behavior in the context of the mixed layer scaling. Not surprisingly, z_i turned out to be the parameter controlling low frequency behavior in the surface layer horizontal velocity spectra (Kaimal, 1978). Unlike velocity spectra, no systematic trend in the low frequency spread of the composite plot of the normalized logarithmic temperature spectra emerged due to the run-to-run variations of the low frequency variance.

Panofsky (1978) pointed out that the so-called "free-convection layer", sandwiched between the surface and mixed layers provided the necessary transition between the scaling laws in the two layers. In this intermediate region, which he renamed the "convective matching layer", both scaling laws apply and the spectral formulations there become the limiting forms for the universal curves derived independently for the surface and mixed layers.

While the Kansas and Minnesota experiments provided the basic framework for describing boundary layer structure over an ideal, flat plane (under homogeneous and steady-state conditions), they provided no clues on how the various functional relationships would be modified by changes in surface roughness. The opportunity to examine this effect presented itself in the spring of 1978 when the new 300 m tower at the Boulder Atmospheric Observatory (BAO) began its operation. The data used for this investigation were obtained during an intensive two-week observation period when the tower data were augmented by measurements from an instrumented aircraft and a surface network of wind and temperature sensors. The experiment was a cooperative venture undertaken by the National Oceanic and Atmospheric Administration (NOAA), the National Center for Atmospheric Research (NCAR), and the University of Washington. This study will focus on one of the many aspects of the experiment--the effect of the undulating terrain at the BAO site on wind velocity and temperature spectra in the first 300 m of the atmosphere.

This report has been divided into several chapters. The experimental details including the site characteristics, the facilities and the instrumentation used at BAO are given in Chapter II. The fluctuating components of velocity and temperature are measured by a sonic anemometer and resistance thermometer, respectively. The outputs of these in situ sensors, available in the form of time series, are reduced to spectral energy diagrams by utilizing the procedures described in Chapter III.

Chapter IV reviews the similarity theories and scaling rules corresponding to the various strata within the boundary layer. These

scaling rules, previously used in developing the universal spectral curves for the Kansas and Minnesota experiments, were also applied to the BAO data set.

A discussion of the individual velocity and temperature spectra within the unstable boundary layer overlying a nonhomogeneous terrain is the theme of Chapter V. The predominant length scales and dissipation rates of turbulent kinetic energy at BAO are also presented in this chapter. The behavior of the normalized logarithmic spectral densities as compared with the previously developed set of universal spectral curves over smooth terrain for both surface and mixed layer becomes the subject of Chapter VI. Finally, Chapter VII discusses the conclusions of this investigation and offers suggestions for further research.

Chapter II

EXPERIMENTAL DETAILS

2.1 Site

The BAO site is situated between Boulder, Colorado, 25 km to the west, and the South Platte River basin, 16 km to the east. The tower lies on gently rolling agricultural land, as illustrated in Figure 1, dedicated to growing dryland wheat. The terrain to the west, north, and east of the tower gently slopes downward; a small hill is located to the south. This terrain and the drainage flow along the Platte River basin influences the surface winds at the BAO site. At night the drainage flow is predominantly south-southwesterly; reversing to the north-northeasterly direction during the day. Also affecting the tower, constructed in the shadow of the Rocky Mountains, are occasionally strong zonal winds which are invariably from the west.

2.2 Instrumentation

To assure proper exposure, the sensors were mounted upwind on the northwestern boom of the tower during the April experiment. A variety of fast response and slow response sensors are installed at each of the eight standard levels (10 m, 22 m, 50 m, 100 m, 150 m, 200 m, 250 m, 300 m), Figure 2. The fast response sensors, sampling five times per second, on each level include a sonic anemometer and a fine platinum wire resistance thermometer. The aspirated quartz thermometer and the cooled-mirror dewpoint hygrometer were the only slow response sensors, sampling once each second, mounted at each level.

The three-axis fixed array sonic anemometer (Ball Brothers Research Corporation model 125-197) utilizes acoustic techniques to measure the mean and fluctuating components of the velocity field. The

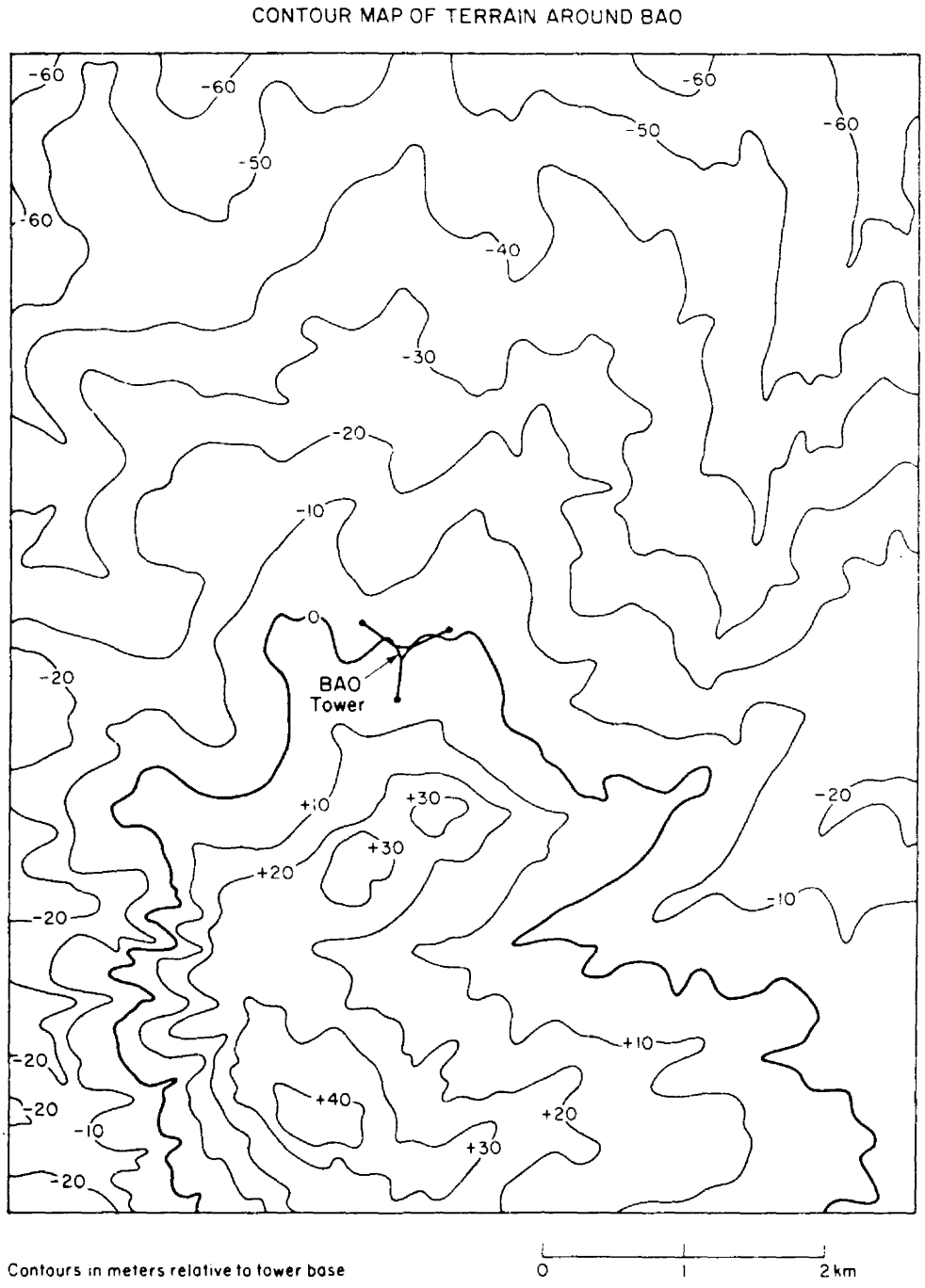

Figure 1. Topography at the Boulder Atmospheric Observatory. The tower is 1576 m above sea level. This figure was prepared by Dr. J. Wieringa of the Royal Netherlands Meteorological Institute.

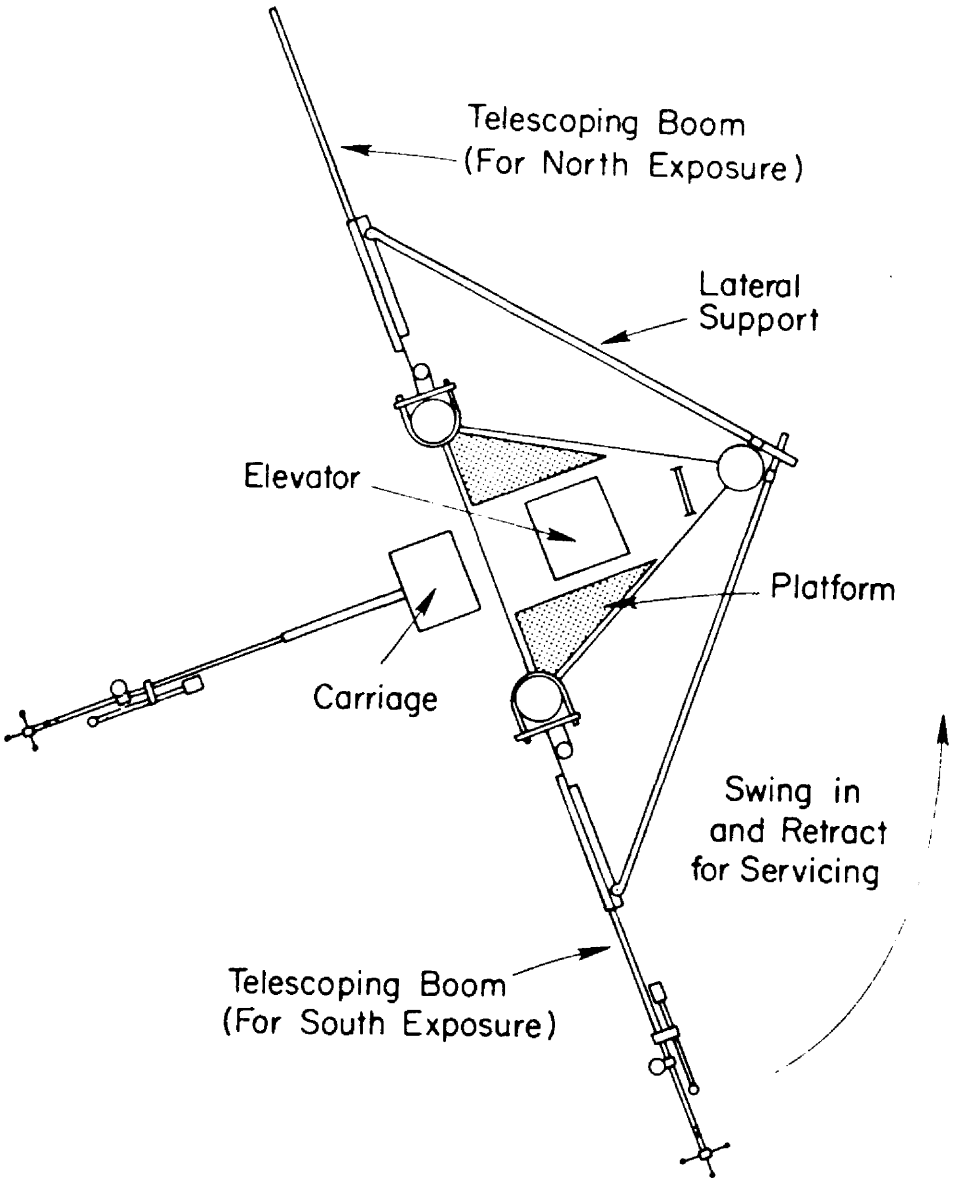

Figure 2. A standard level of BAO's instrumented tower as viewed from above. During April 1978 experiment the instruments were mounted on the northwest boom.

time difference between two acoustic pulses which propagate in opposite directions across the fixed path provides a direct measure of the velocity component along the path (Kaimal et al., 1974). Since this device responds rapidly to velocity fluctuations, it is well suited for turbulence studies. The three orthogonal axes of the array are aligned in directions along, across, and vertical to the supporting boom. An underestimation of the horizontal velocity components results if the wind blows directly along a horizontal axis causing the upwind transducer to block a portion of the acoustic path. This limitation can be corrected during data processing by utilizing a first approximation of the wind direction. The vertical velocity component is relatively free of this error. The Atmospheric Instrumentation Research Corporation's platinum wire resistance type thermometer (model DTIA) is nestled within the sonic anemometer. This design minimized the errors in the heat flux calculations due to the spatial separation between w and θ. The frequency response of the temperature sensor is roughly comparable to the path averaged response of the vertical sonic wind measurements.

To determine the mean wind of the atmospheric flow, information collected by the sonic anemometer was used. The sonic anemometer fixed at the end of the instrument boom measures the wind velocity along the three orthogonal directions. The mean wind is then obtained by calculating the average along each transducer leg of the sonic anemometer array before taking the vector mean. Finally the components of the velocity fluctuations are defined with respect to this vector mean wind.

Twenty minute summaries of each run, see Table 1 for an example, provide the mean values of the temperature and velocity components for each level resulting in profiles which extend 300 m into the boundary layer. Other information which can be found in the BAO data summaries includes the Obukhov length, the second and third order moments of turbulence. The Obukhov length, L, is an important length scale in surface layer similarity and is used to define the stability parameter, z/L. The variances of the fluctuating temperature or velocity components, second order moments, are equivalent to the integral of the spectral intensities over all frequencies. The covariances, also second order moments, are useful in obtaining characteristic boundary layer quantities such as the Reynolds stresses, $\overline{uw}$, etc., and temperature flux, $\overline{w\theta}$.

On several days during this experiment, NCAR's Queen Air aircraft made constant level flights (at approximately 150 m and 300 m) in the vicinity of the tower recording data on wind, temperature, and humidity from turbulence probes mounted on its nose. The primary objective of these flights was to compare the spatial scales measured by the aircraft with the temporal scales measured by the sensors on the tower. On most of these days the aircraft made periodic vertical soundings to determine the height of the lowest inversion base, z_i. This height is an important scaling parameter for the mixed layer.

2.3 Data Description

During April nineteen runs resulted in a total of 62 hours of data collected. Nine periods, each one hour in length, were chosen for detailed data analysis. All nine runs, classified as convectively unstable cases ($z/L < 0$), occurred during clear or partly cloudy sky

BOULDER ATMOSPHERIC OBSERVATORY DATA SUMMARY

AVERAGING PERIOD= 20 00 MIN

18 APR 78 17 37 MST

Z[M]	V(W)	V(S)	W	VH	AZ	S	D	T	TD	L
10	6 34	-3 24	0 26	7 12	297	M	M	12 41	-12 94	-287 14
22	7 29	-3 64	0 16	8 15	297	M	M	12 27	-14 18	-258 71
50	7 58	-3 57	0 09	8 38	295	M	M	12 00	-13 83	-415 41
100	8 24	-4 46	0 07	9 37	298	M	M	11 51	-14 52	-292 14
150	8 49	-4 93	-0 28	9 82	300	M	M	11 07	-15 24	********
200	8 11	-5 17	0 22	9 62	300	M	M	10 57	-14 49	********
250	8 49	-5 58	-0 25	10 16	300	M	M	10 08	-14 32	********
300	8 94	-4 98	0 42	10 24	299	M	M	9 59	-14 57	********

Z[M]	UU	VV	WW	TT	UV	VW	UT	VT	UW	WT
10	1 5966	1 3640	0 2895	0 0382	0 4739	0 0805	0 1288	0 1477	-0 1099	0 0106
22	1 4305	1 4449	0 3279	0 0206	0 4685	0 1173	0 0675	0 1224	-0 1253	0 0143
50	1 1943	1 3372	0 3529	0 0137	0 3293	0 0445	0 0255	0 0931	-0 1937	0 0170
100	1 1912	1 1026	0 4137	0 0115	0 2483	0 0324	0 0124	0 0681	-0 1637	0 0188
150	1 1069	1 0820	0 4758	0 0103	0 3073	-0 2524	0 0193	0 0587	-0 4081	-0 0113
200	1 1327	1 0155	0 5022	0 0100	0 2157	-0 0541	0 0234	0 0624	-0 1801	-0 0030
250	1 2926	1 2074	0 5653	0 0092	0 4618	-0 2615	0 0393	0 0637	-0 4373	-0 0186
300	1 2021	1 0413	0 5361	0 0085	0 4272	0 0337	0 0491	0 0626	-0 0774	0 0029

Z[M]	UVW	UWW	VWW	UUW	VVW	WWW	UWT	VWT	WWT	WTT
10	0 0012	-0 0184	0 0032	0 0572	0 0317	-0 0047	0 0075	0 0053	0 0028	0 0031
22	0 0175	0 0020	0 0861	0 0054	0 1382	0 0549	0 0019	0 0086	0 0047	0 0012
50	-0 0104	-0 0919	0 0954	0 1605	-0 0056	0 1352	-0 0117	-0 0016	0 0185	0 0015
100	-0 0155	-0 0916	0 1270	0 1143	0 1038	0 0816	-0 0189	0 0097	0 0301	0 0026
150	-0 0797	0 0260	0 0805	-0 0412	-0 0264	-0 0478	-0 0142	0 0060	0 0139	0 0021
200	-0 0505	0 0449	0 2317	0 0556	0 1253	-0 0268	-0 0068	0 0147	0 0262	0 0016
250	0 1183	0 0875	0 1415	0 2869	0 0664	-0 1156	0 0024	0 0076	0 0138	0 0013
300	0 0533	0 1641	0 2269	0 1200	0 2093	0 2132	0 0067	0 0166	0 0251	0 0016

Table 1. Sample of twenty minute summaries; available for all runs.

conditions and minimal synoptic scale baroclinicity. The distribution of runs according to categories of z/L is given in Table 2. In each case the surface heat flux was directed upwards. The mean wind speed varied from nearly 4 m s^{-1} to over 12 m s^{-1} during these daytime runs. Care was taken to avoid the abrupt transition near sunset from an unstable to a stable boundary layer.

A good estimate of z_i, the height of the lowest inversion base, was the primary criterion used in determining the final data set of nine runs. Since aircraft data were not recorded while southeasterly to southerly winds prevailed, episodes where the tower might interfere with data reliability were automatically eliminated. Table 3 lists each run, its date and time, along with several other boundary layer characteristics.

Table 2. Runs separated according to z/L categories. The numbers within the parenthesis corresponds to the height of the levels.

z/L:	< -4.0	-4.0 to -3.0	-3.0 to -2.0	-2.0 to -1.0	-1.0 to -0.5	-0.5 to -0.3	-0.3 to -0.1	-0.1 to 0
	R12 (50-300)	R12 (22)	R17A(250,300)	R7 (250,300)	R7 (150,200)	R7 (100)	R7 (22,50)	R7 (10)
	R14 (150-300)	R14 (100)	R17B(50)	R12 (10)	R14 (22)	R14 (10)	R17A(22)	R17A(10)
Runs:	R15 (100-300)	R15 (50)		R14 (50)	R15 (10)	R17A(50)	R18B(22,50)	R18B(10)
	R17B(100-300)	R18A(100)		R15 (22)	R17A(100)	R17B(10)	R19 (22,50)	R19 (10)
	R18A(150-300)			R17A(150,200)	R17B(22)	R18A(10)		
				R18A(50)	R18A(22)			
				R18B(200-300)	R18B(100,150)			
				R19 (200-300)	R19 (100,150)			

Table 3. List of runs with significant boundary layer parameters.

run	date (1978)	time (MST)	L (m)	z_i (m)	U speed ($m\ s^{-1}$)	U direction (degrees)	T (°C)	Q_o ($K\ m\ s^{-1}$)	u_* ($m\ s^{-1}$)	T_* (K)	w_* ($m\ s^{-1}$)	θ_* (K)
R7	21 April	1611-1711	-212.10	1257.6	11.48	295	14.63	0.0905	0.5382	-0.1294	1.4403	0.0484
R12	25 April	1432-1532	-6.34	1193.6	3.85	312	15.66	0.0780	0.1723	-0.4514	1.4668	0.0532
R14	26 April	1330-1430	-26.43	486.6	4.19	60	18.36	0.1618	0.2710	-0.5972	1.3831	0.1170
R15	26 April	1503-1603	-16.35	486.6	4.63	8	19.87	0.1006	0.1573	-0.6393	1.1779	0.0854
R17A	28 April	0850-0950	-108.29	481.7	12.22	277	14.11	0.1749	0.6217	-0.2813	1.4216	0.1230
R17B	28 April	0950-1050	-21.70	548.0	7.54	280	14.83	0.2144	0.3834	-0.5593	1.5868	0.1351
R18A	28 April	1216-1316	-27.33	1260.0	9.80	278	16.43	0.2729	0.4383	-0.6227	2.2652	0.1205
R18B	28 April	1416-1516	-185.72	1602.8	8.28	283	14.81	0.0610	0.4029	-0.1514	1.7933	0.0590
R19	28 April	1518-1618	-185.76	1602.8	8.91	278	14.42	0.0449	0.4977	-0.0902	1.3488	0.0333

Chapter III

DATA ANALYSIS

3.1 Calculation of Spectra

Spectra were computed for each observational period included in this study. The calculation of spectra uses Fourier transforms to convert from the digital data series in the time domain to the frequency domain

$$X(n) = \int_{-\infty}^{\infty} x(t)\exp(-2\pi int)dt\,. \qquad (1)$$

Here $X(n)$ is the complex Fourier transform of $x(t)$, the original time series, where n, the frequency, and t, the time, are real variables. Multiplying the frequency domain series, $X(n)$, by its complex conjugate, $X^*(n)$, results in the power spectrum, $S_x(n)$,

$$S_x(n) = X(n)X^*(n). \qquad (2)$$

In this case, the fast Fourier transform (FFT) technique was used in computing the power spectrum. This is an algorithm for computing the discrete Fourier transform (DFT) more quickly than the direct method of computing the autocorrelation function and smoothing with a lag window before finally taking the transform. The FFT is a method which sequentially combines progressively larger weighted sums of data samples so as to produce DFT coefficients. Basically this technique joins the DFT's of the individual data samples such that the occurrence times of these samples are taken into accout sequentially and applied to the DFT's of progressively larger mutually exclusive subgroups of data samples. These are subsequently combined to produce the DFT of the complete series of data samples (Cochran et al., 1967). This highly efficient procedure utilizes the fact that the calculation of the

coefficients of the DFT can be carried out iteratively to reduce both the computation time and the round-off errors.

To cut down on computing time, the spectra were computed for two separate, slightly overlapping, bandwidths. The higher range (4.88×10^{-3} to 2.5 Hz) was obtained by dividing the data series into 17 consecutive blocks of 1024 data points. A composite spectrum was then formed by averaging the 17 separate spectra. Finally, this composite spectrum was smoothed by averaging the spectral estimates over frequency bands of increasing bandwidth as shown in Figure 3.

The lower range (2.87×10^{-4} to 1.3×10^{-1} Hz) was obtained by block averaging each set of 17 nonoverlapping data points. This averaging procedure was designed to reduce the number of data points to 1024 and at the same time eliminate high frequencies in the discrete data series. Averaging the spectrum over the increasingly wide frequency bands of Figure 3 produces the low range of Figure 4. Although this spectrum exhibits more scatter than the composite spectrum mentioned above, the agreement within the region where these two ranges overlap was very good. These low and high ranges were designed to cross-over at 0.025 Hz. Finally, minor smoothing by eye, as illustrated in Figure 4, averaged the peaks and valley to produce the spectra of each run, found in Appendix A.

Often distortions of a turbulence spectrum exist. Aliasing and long trends (Kaimal et al., 1968) are the two most common reasons for distortions. Aliasing is caused by a sampling rate less than twice the highest atmospheric frequency present in the boundary layer. As a result of this slow sampling rate, significant quantities of energy will exist at frequencies higher than the Nyquist frequency, n_0, (half

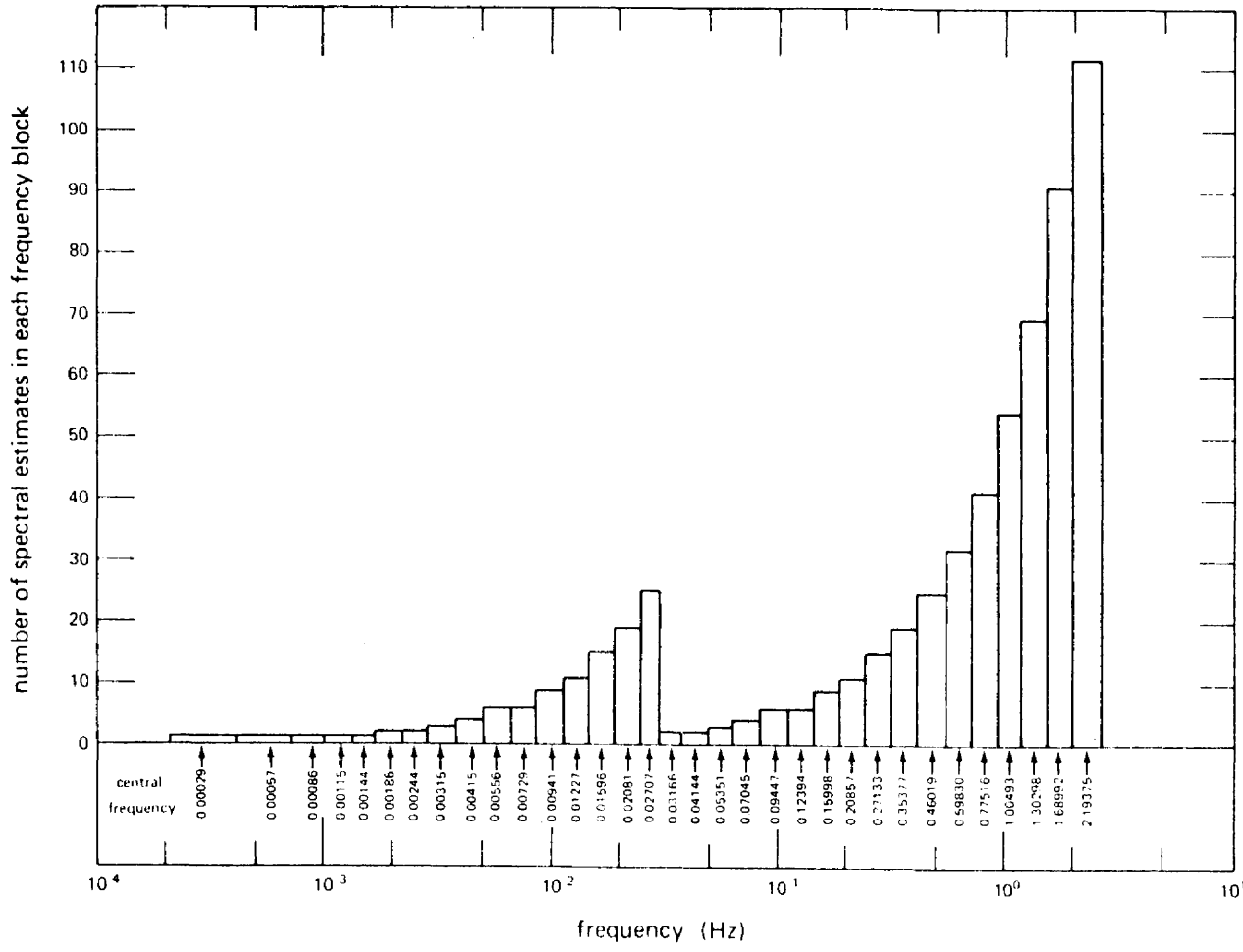

Figure 3. The frequency blocks over which the series of spectral estimates are averaged. The two bandwidths are merged together to form the spectral plot in Figure 4.

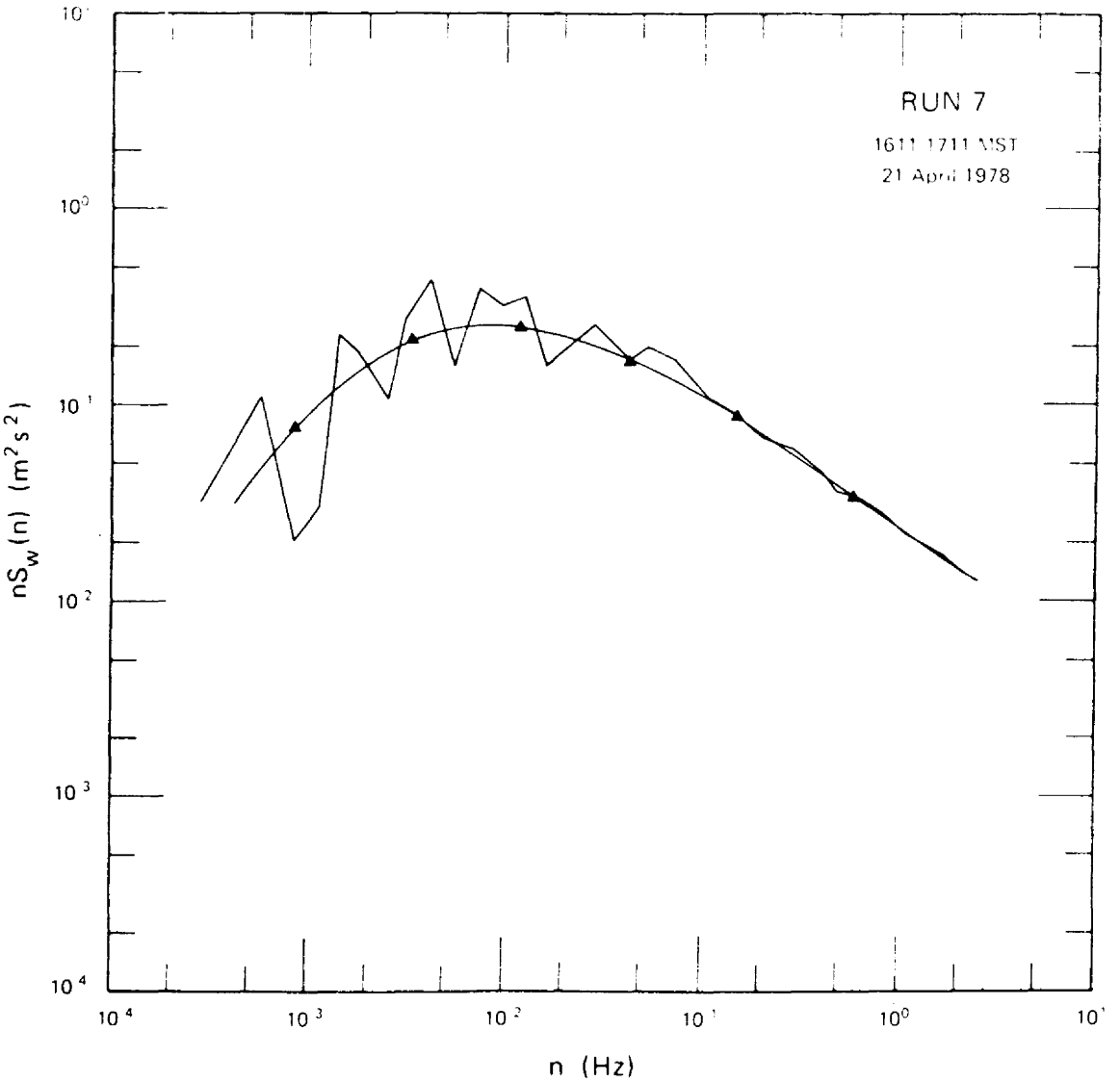

Figure 4. Minor smoothing performed on the spectral plots is illustrated by the curve with solid triangles.

the sampling rate). The excess energy is then folded back into the spectrum at multiple folds over the frequency band: zero Hertz to n_o. Filtering all frequencies greater than the Nyquist frequency before sampling is the ideal method to eliminate the effects of aliasing. However, after data collection the effects of aliasing may be compensated for only if the form of the spectrum above the Nyquist frequency is known. The amount of energy folded back can be estimated and subtracted from the computed spectrum. In April, most of the spectra obeyed the - 5/3 power law in the inertial subrange, extending above the Nyquist frequency. Consequently, corrections for aliasing were obtained by both empirical methods and reconstruction of typical folding.

Long trends are frequently present in any type of geophysical data in such forms as a diurnal variation, a gravity wave, a slow shift in wind direction, or some other type of mesoscale phenomenon. These trends are observed in the low frequency portion of the spectral diagram and will have a slope of -2 if a strictly linear trend exists. A process known as detrending eliminates these trends by continuously removing the running mean of the fluctuating parameter. No detrending operations were performed on the time series used for the spectral computations described here.

3.2 Evaluation of Inertial Subrange Spectral Constants

The logarithmic spectra of the BAO data set exhibited a -2/3 slope within the Kolmogorov universal equilibrium range after compensating for any distortions. According to Kolmogorov's law for the inertial subrange, the one-dimensional wavenumber spectrum, $F_w(\kappa)$, can be expressed in the form

$$F_w(\kappa) = \frac{4}{3}\alpha_1 \varepsilon^{2/3} \kappa^{-5/3}, \qquad (3)$$

where κ is the wavenumber, α_1 is a universal constant equal to 0.5 (Kaimal et al., 1972), and ε is the dissipation rate for the turbulent kinetic energy.

Multiplying both sides of (3) by the wavenumber results in

$$\kappa F_w(\kappa) = \frac{4}{3}\alpha_1 \varepsilon^{2/3} \kappa^{-2/3} \quad . \tag{4}$$

If the turbulence intensity is small, then Taylor's hypothesis (Taylor, 1938) relates one-dimensional wavenumber spectra to single point frequency spectra, $S_w(n)$. This "frozen-turbulence" approximation implies that turbulence patterns are simply advected without any substantial change by the mean wind speed. Using Taylor's hypothesis to convert from wavenumber to frequency spectra

$$\int_0^\infty F_w(\kappa)d\kappa = \int_0^\infty S_w(n)dn = \sigma_w^2 \quad , \tag{5}$$

where $\kappa = \frac{2\pi n}{U}$ (n being the frequency and U the mean horizontal wind speed. Substitute the wavenumber definition into (5)

$$\int_0^\infty F_w\left(\frac{2\pi n}{U}\right) d\left(\frac{2\pi n}{U}\right) = \int^\infty S_w(n)dn \, . \tag{6}$$

Therefore, at one frequency and its corresponding wavenumber

$$\frac{2\pi}{U} F_w\left(\frac{2\pi n}{U}\right) = S_w(n) \, . \tag{7}$$

By multiplying both sides of (7) by the frequency

$$n\left(\frac{2\pi}{U}\right) F_w\left(\frac{2\pi n}{U}\right) = nS_w(n) \, , \tag{8}$$

we arrive at an expression for the "logarithmic" spectra, $nS_w(n)$,

$$\kappa F_w(\kappa) = nS_w(n) \, . \tag{9}$$

Since it is traditional in atmospheric work to plot $nS(n)$, (4) can be written

$$nS_w(n) = \frac{4}{3}\alpha_1 \varepsilon^{2/3}\left(\frac{2\pi n}{U}\right)^{2/3} . \tag{10}$$

Solving for the dissipation rate of turbulent kinetic energy, ε

$$\varepsilon^{2/3} = \frac{nS_w(n)}{\left[\frac{4/3\alpha_1}{(2\pi)^{2/3}}\right] U^{2/3}}\, n^{2/3} = \frac{nS_w(n)}{0.1958\, U^{2/3}}\, n^{2/3} . \tag{11}$$

Applying this expression at $n = 1$ Hz and rearranging we obtain

$$\varepsilon = \frac{11.54}{U}\,[nS_w(n)]^{3/2}_{n=1} . \tag{12}$$

A similar relationship can be derived for the destruction rate of temperature variance, N. Corrsin (1951) developed the following inertial subrange form for the temperature spectra

$$F_\theta(\kappa) = \beta_1 N \varepsilon^{-1/3} \kappa^{-5/3} \tag{13}$$

where β_1 is a universal constant similar to α_1 with a numerical value of 0.8 (Wyngaard and Coté, 1971). If Taylor's hypothesis is assumed and both sides of (13) are multiplied by the wavenumber, then

$$nS_\theta(n) = \beta_1 N \varepsilon^{-1/3}\left(\frac{2\pi n}{U}\right)^{-2/3} . \tag{14}$$

Solving for N and applying at $n = 1$ Hz we acquire an expression for the dissipation rate of $\overline{\theta^2}/2$, the temperature variance

$$N = 4.26\left(\frac{\varepsilon}{U^2}\right)^{1/3}[nS_\theta(n)]_{n=1} . \tag{15}$$

3.3 Determination of z_i

The vertical temperature soundings obtained by aircraft were utilized to determine the height of the lowest inversion base, z_i. The time and position (latitude and longitude) of the aircraft when it passed through the inversion base was required to specify the height of the aircraft above sea level and the elevation of the ground beneath the aircraft, respectively. The value of z_i is simply the difference of these two quantities.

Note that z_i was estimated for runs R17A, R17B, and R18A by using a linear extrapolation between the soundings begun at 1010 MST, 28 April 1978 and 1359 MST, 28 April 1978. It has been assumed that the inversion base increases linearly with time, as observed by Kaimal et al. (1976).

Rising convective plumes and entrainment of warm stable air downward causes the height of the lowest inversion base to vary as much as 50 m over a short period of time. A comparison of z_i measurements obtained from several remote sensors and the in situ sensors of the aircraft was conducted during the Phoenix experiment in September 1978 at BAO. The aircraft z_i values were within 20 m of the z_i observed by the remote sensors. To reduce the variability of the height of the lowest inversion base, the values of z_i obtained during the aircraft's ascent and descent were averaged together to acheive the z_i values used in this study.

Chapter IV

GENERAL CHARACTERISTICS OF THE UNSTABLE BOUNDARY LAYER

4.1 Boundary Layer Structure

The planetary boundary layer is the portion of the atmosphere directly affected by the diurnal heating and cooling of the earth's surface. In this layer, turbulent transfer is the primary mechanism that transports the atmospheric properties through the depth of the boundary layer. The unstable boundary layer may be further stratified into three layers: surface layer, matching layer, and mixed layer. The surface layer, only a few tens of meters thick, is often referred to as the shear layer, since in this stratum wind shear plays an important role in the production of turbulence. Strong vertical mixing produced by convection causes the near adiabatic lapse rate and negligible mean wind shear typical of the mixed layer. This stratum corresponds to the upper 9/10 of the planetary boundary layer and over land often extends to a couple of kilometers by midafternoon. A capping inversion defines the upper limit of the mixed layer. Between the surface layer and the mixed layer, a transition from the strong gradients near the ground to the nearly constant distribution of wind speed and potential temperature above occurs within the matching layer.

4.2 Similarity Laws and Scaling Rules

An approach to atmospheric turbulence analysis which has gained considerable success in recent years is the similarity theory, originally proposed by Obukhov (1946) and first supported by data in a paper by Monin and Obukhov (1954). According to this theory, atmospheric properties such as vertical gradients, variances, and length scales when normalized by the appropriate scaling parameters will show

universal behavior. The similarity approach allows factors such as wind, thermal stability, and height above ground to be considered when developing the universal forms. The systematic trends that often emerge in these plots clearly demonstrate that order does preside in nature, even with seemingly random turbulence data collected under a wide range of conditions.

The variables which control turbulence in each layer are used to form the scaling parameters associated with each portion of the planetary boundary layer. Starting with the surface layer, the controlling variables of each layer will be discussed below and are summarized in Table 4 at the end of this section.

In the surface layer, Monin-Obukhov similarity holds. The surface shear stress, τ_o, and the height above the ground, z, are important parameters along with the surface kinematic heat flux, $Q_o = (\overline{w\theta})_{surface}$, and the buoyancy parameter, g/T. These four constants combine to form the four scaling parameters: u_*, T_*, z, and L. The Obukhov length, $L = -u_*^3/[kQ_o(g/T)]$, is an independent length scale formed from the variables and its ratio with z is now a stability parameter, z/L, in place of the Richardson number. The scaling parameter for velocity, u_*, is defined as $(\tau_o/\rho)^{1/2}$ which under conditions of stationarity and horizontal homogeneity can be approximated by the square root of the kinematic momentum flux, $(\overline{uw})^{1/2}$. The scaling parameter for temperature, T_*, is then defined as $-Q_o/u_*$. According to Monin-Obukhov similarity, dimensionless ratios of atmospheric properties formed by using u_* and T_* become universal functions of z/L.

In the matching or transition layer, the mixed layer similarity laws must coincide with the Monin-Obukhov similarity laws. This layer

extends from L to a height equivalent to $z_i/10$. Here τ_o exerts little if any influence on turbulence, and the controlling parameters reduce to three variables: z, Q_o, and g/T. These variables are combined to form a scaling velocity, $u_f = [Q_o z(g/T)]^{1/3}$, and a scaling temperature, $T_f = Q_o/u_f$ for the layer. Under conditions of local free convection, Wyngaard et al. (1971) predicted that the dimensionless ratios formed by these scaling parameters are constants. The above prediction has also been supported by the April boundary layer experiment.

Turbulence in the mixed layer is no longer sensitive to z and depends on the depth of the convective region. Consequently, the height of the lowest inversion base, z_i, serves as the significant length scale along with the other controlling variables, Q_o and g/T, to define the turbulent processes in this stratum. Under steady state conditions, the dimensionless groups formed with the scaling velocity, $w_* = [Q_o z_i(g/T)]^{1/3}$, and the scaling temperature, $\theta_* = Q_o/w_*$, should be functions of z/z_i only.

Table 4. Important variables which describe turbulence in each stratum of an unstable boundary layer.

	Controlling variables	Scaling parameters
Surface layer:	τ_o	u_*
	z	T_*
	g/T	L
	Q_o	
Matching layer:	z	u_f
	g/T	T_f
	Q_o	
Mixed layer:	z_i	w_*
	g/T	θ_*
	Q_o	

Chapter V

SPECTRA OF THE VELOCITY COMPONENTS

5.1 Normalizing

Normalizing logarithmic spectral intensities with similarity parameters removes much of the run-to-run variability observed in atmospheric spectra. With the proper choice of normalizing parameters the spectra from different heights and stabilities can be combined to form universal curves. The approach used here is to force the inertial subranges of all spectra into a single curve; and to observe the spectral behavior at the low frequency end, as a function of z/L in the surface layer or z/z_i in the mixed layer.

As shown in (10), Kolmogorov's Law for the inertial subrange of the u spectrum can be expressed in the form

$$nS_u(n) = \alpha_1 \varepsilon^{2/3} \left(\frac{2\pi n}{U}\right)^{-2/3} . \qquad (16)$$

By normalizing the spectral intensity with u_*^2 and rearranging the terms on the right-hand side, (16) becomes

$$\frac{nS_u(n)}{u_*^2} = \frac{\alpha_1}{(2\pi k)^{2/3}} \frac{(\varepsilon k z)^{2/3}}{u_*^2} \left(\frac{nz}{U}\right)^{-2/3} , \qquad (17)$$

where k is von Kármán's constant with a value of 0.35 (Businger et al., 1971). Using the surface layer definitions of the dimensionless dissipation rate, $\phi_\varepsilon = (kz\varepsilon)/u_*^3$, and the dimensionless frequency, $f = nz/U$, (17) may be rewritten as

$$\frac{nS_u(n)}{u_*^2} = \frac{\alpha_1}{(2\pi k)^{2/3}} \phi_\varepsilon^{2/3} f^{-2/3} . \qquad (18)$$

The dependence on the stability parameter, z/L, must be removed to collapse the one-dimensional velocity spectra into a single curve in

the inertial subrange. To obtain the universal curve, both sides are divided by $\phi_\varepsilon^{2/3}$. The new form of (18) becomes

$$\frac{nS_u(n)}{u_*^2 \phi_\varepsilon^{2/3}} = 0.3\ f^{-2/3} . \tag{19}$$

As a consequence of local isotropy, the spectral forms for the transverse velocity components, v and w, differ from (19) by a factor of 4/3, resulting in

$$\frac{nS_v(n)}{u_*^2 \phi_\varepsilon^{2/3}} = \frac{nS_w(n)}{u_*^2 \phi_\varepsilon^{2/3}} = 0.4\ f^{-2/3} . \tag{20}$$

The analogous expression for the u component in the mixed layer (Kaimal et al., 1976) is

$$\frac{nS_u(n)}{W_*^2 \psi_\varepsilon^{2/3}} = 0.15\ f_i^{-2/3} ,$$

where $f_i = nz_i/U$ and $\psi_\varepsilon = \varepsilon/[Q_0(g/T)]$ is the dimensionless dissipation rate of turbulent kinetic energy in the mixed layer. Under isotropic conditions, the one-dimensional transverse velocity spectra assumes the form

$$\frac{nS_v(n)}{W_*^2 \psi_\varepsilon^{2/3}} = \frac{nS_w(n)}{W_*^2 \psi_\varepsilon^{2/3}} = 0.2\ f_i^{-2/3} . \tag{21}$$

5.2 Longitudinal Velocity Component

The normalized unstable u spectra observed at the BAO do not exhibit any systematic behavior at low frequences (Figure 5) when plotted against the dimensionless frequency, $f = nz/U$. This apparent independence of the stability parameter, z/L was also displayed by the

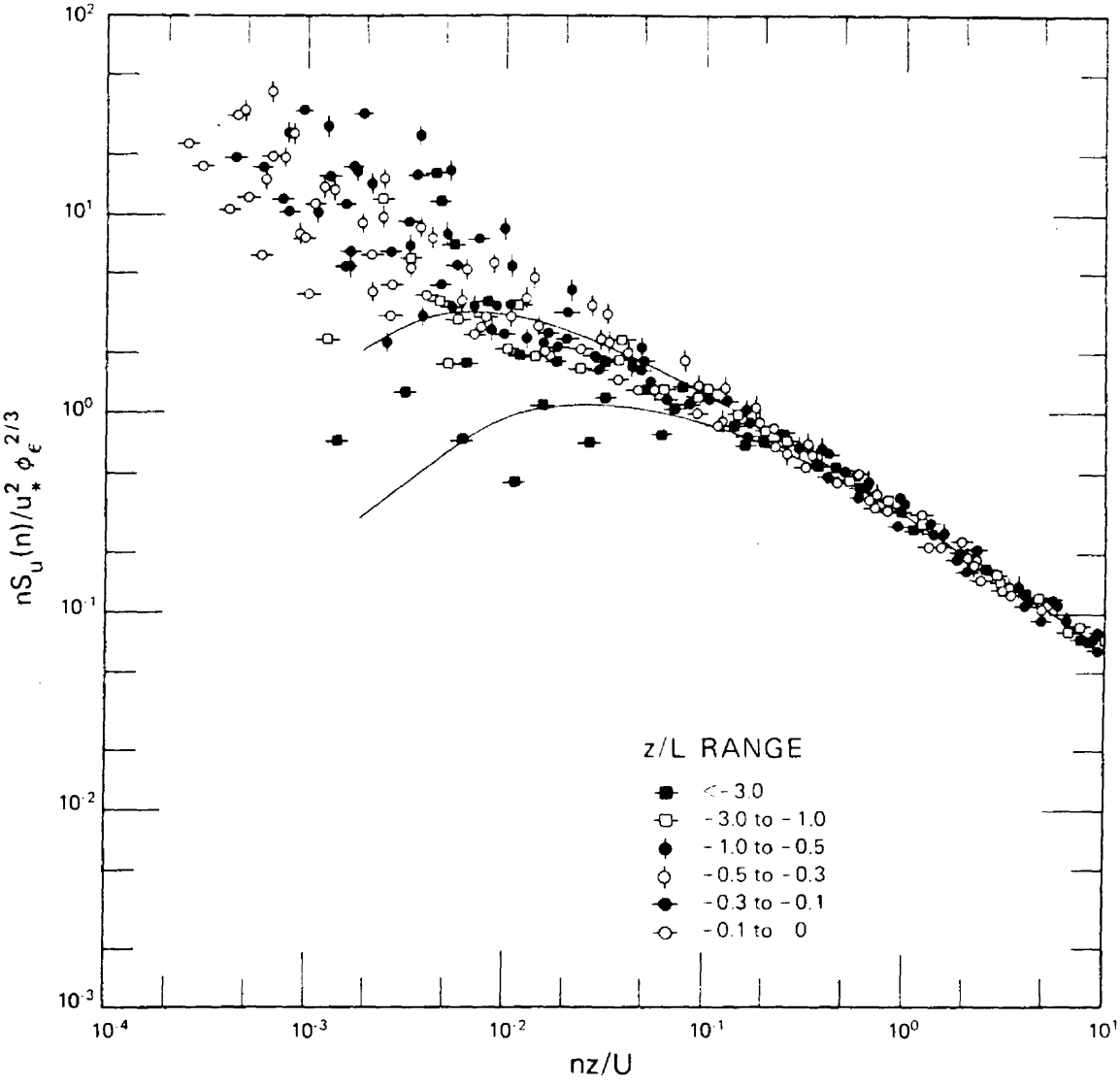

Figure 5. Normalized logarithmic u spectra plotted against dimensionless frequency for various z/L values in the surface layer. The envelope, defined by the solid curves, was developed from the Kansas data (Kaimal et al., 1972).

Kansas spectra (Kaimal et al., 1972). However, the low frequency roll-off of spectral intensity observed in Kansas, defined by the solid curves, is not present in the April 1978 BAO data set. In actuality, during the majority of runs the normalized spectral estimates continued to increase as frequency decreased. This behavior indicates the presence of a trend which has a time scale greater than the typical turbulence time scale of a few minutes. One example of a trend in the u component is shown in Figure 6. The corresponding discrete digital time series, plotted in Figure 7, shows a significant increase in u at the beginning of the record. Since no detrending has been performed on the original time series, this large initial increase, present at all levels of the tower, causes the logarithmic u spectrum to continue increasing in intensity at the low end of the spectral bandwidth. This low frequency increase present in other runs can also be explained by the time series displaying behavior similar to Figure 7.

Within the mixed layer, the longitudinal spectra converge to a -2/3 line at the high frequencies, but behave in a random fashion at the lower frequencies (Figure 8). Even the open circles, which represent cases without a trend, do not show any clear separation according to z/z_i; as was seen with Minnesota spectra (Kaimal et al., 1976)--possibly a consequence of the uneven terrain. Nonetheless, the effect of the trend in the other runs (solid circles) makes a comparison with the Minnesota data even more difficult.

As seen in Figure 8, the BAO u spectral peak coincides with a longer wavelength than the Minnesota spectral peak (compare the open circles with the envelope defined by the solid curves). A BAO maximum wavelength greater than the $(\lambda_m)_u = 1.5\ z_i$ observed at Minnesota may

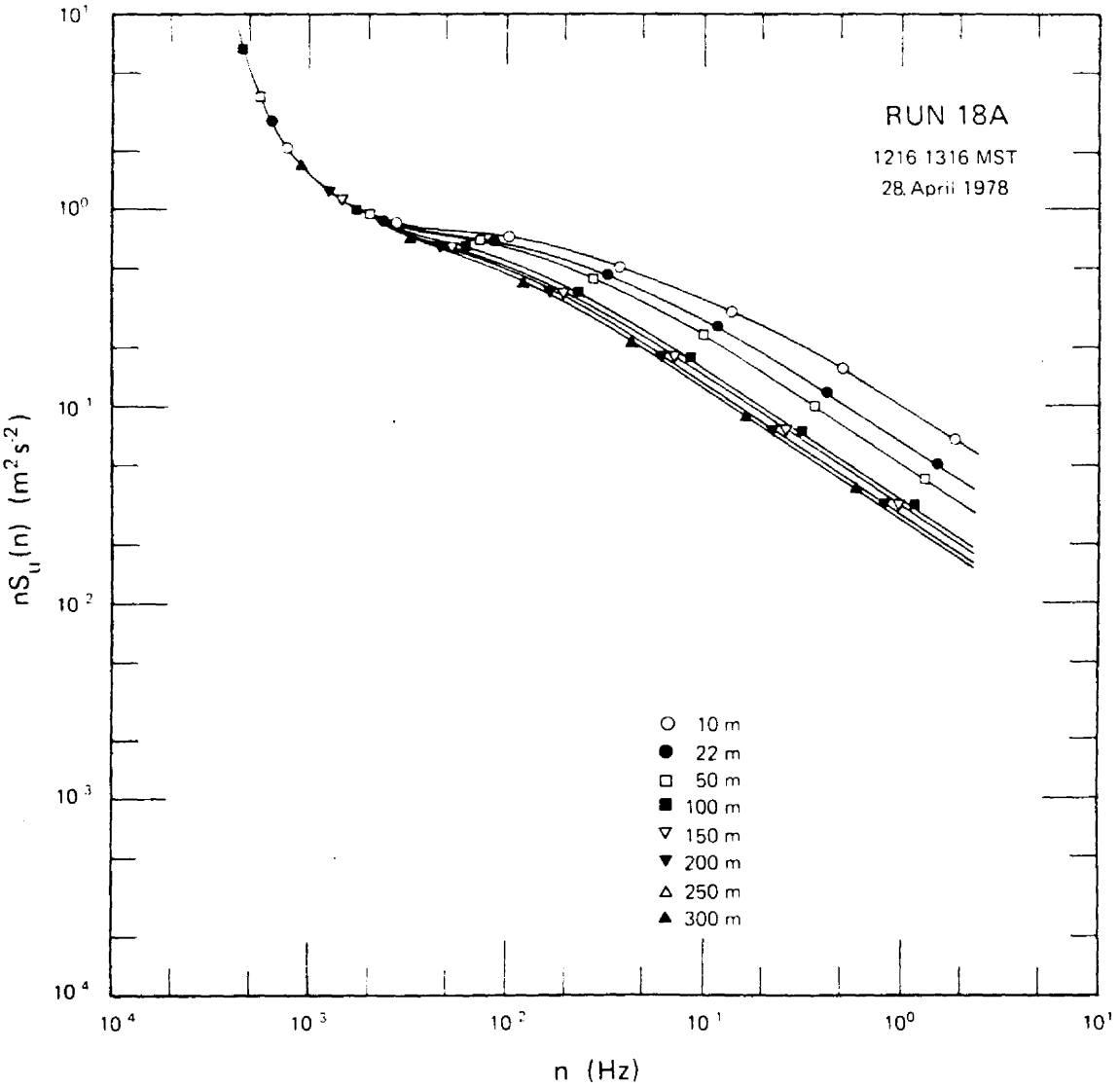

Figure 6. Longitudinal velocity spectra for all levels of the BAO tower. Note the increasing spectral values corresponding to the low frequencies.

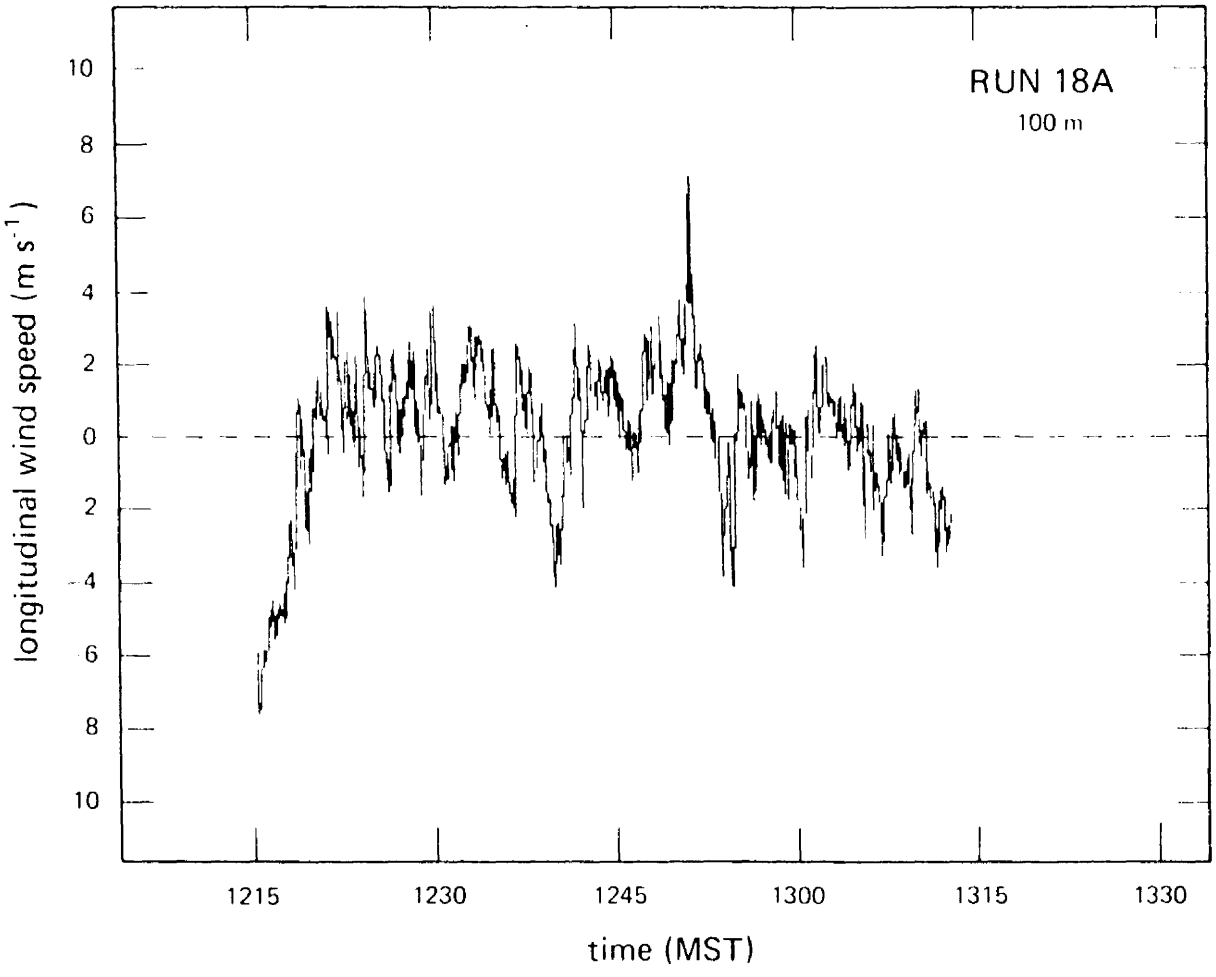

Figure 7. Time series of the longitudinal wind speed coinciding with the u spectral curve of the 100 m level in Figure 6.

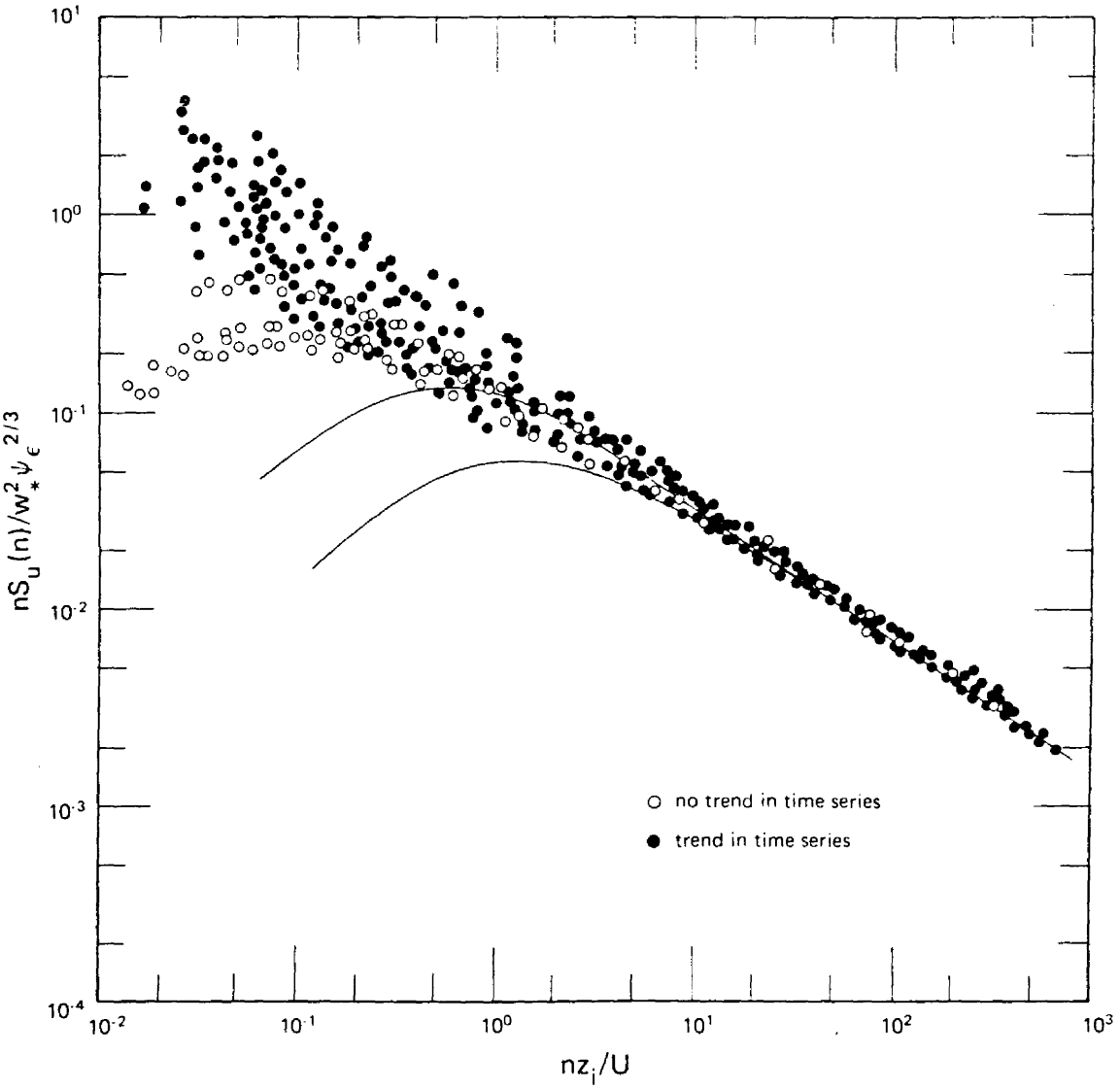

Figure 8. Normalized logarithmic u spectra plotted against dimensionless frequency in the mixed layer. The solid curves defines the envelope obtained from the Minnesota data (Kaimal et al., 1976).

be caused by the irregular terrain surrounding the tower; however, the quantity of data is insufficient to be conclusive.

Prior to normalizing the logarithmic u spectra, a decrease of the spectral intensities in the inertial subrange with an increase in height, z, in the surface layer is present in all cases. An example of the inertial subrange behavior with height is displayed in Figure 9 where all tower levels, except 200 m and 250 m, of Run 17B are illustrated. In Run 17B the height of the lowest inversion base, z_i, is 548 m; consequently, the mixed layer extends from approximately 55 m to about 550 m. The spectral intensities of the inertial subrange within the mixed layer approaches a constant value at all heights in the mixed layer. The same inertial subrange spectral behavior was observed in Kansas and Minnesota.

5.3 Lateral Velocity Component

The scatter representing the generalized spectrum for the lateral velocity component, v, in the surface layer is shown in Figure 10. The unstable normalized spectra from the BAO experiment predominantly lies within the envelope, defined by the solid lines on Figure 10, established from the Kansas spectra (Kaimal et al., 1972). In several runs of the BAO data the value of z/L extended to less than -4.0, but no functional dependence on the stability parameter is apparent.

Different spectral behavior is exhibited in the scatter representing the universal spectral curve for v in the mixed layer as illustrated in Figure 11. The normalized spectra of this transverse velocity component does not conform to the single spectral shape of the Minnesota spectra, defined by the solid curves. As indicated by the solid circles in Figure 11, the v spectra of a few runs include a

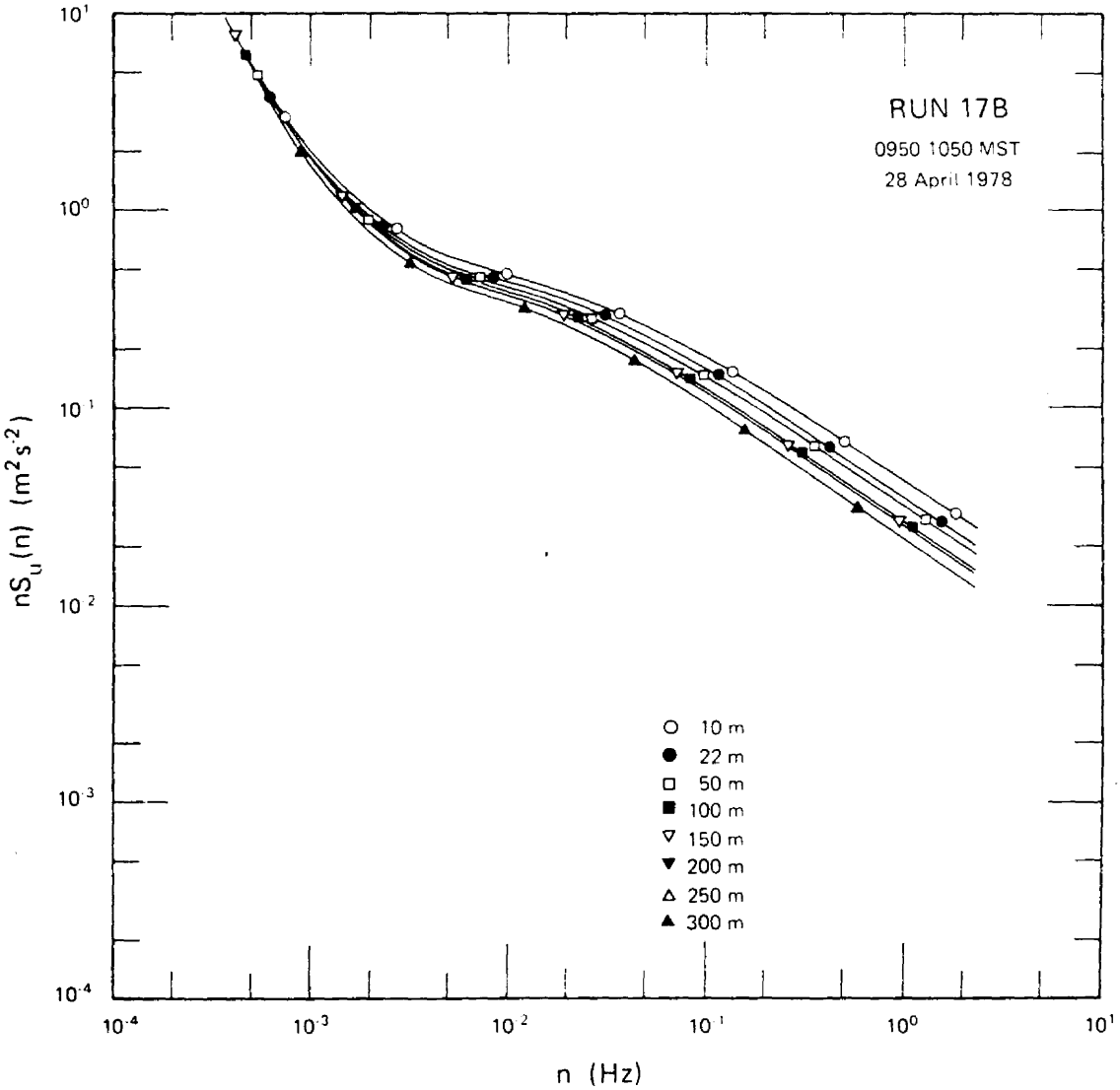

Figure 9. Longitudinal spectral curves for Run 17B. Notice the rapidly decreasing inertial subrange spectral intensities with increasing height, passing upward from the surface layer into the mixed layer.

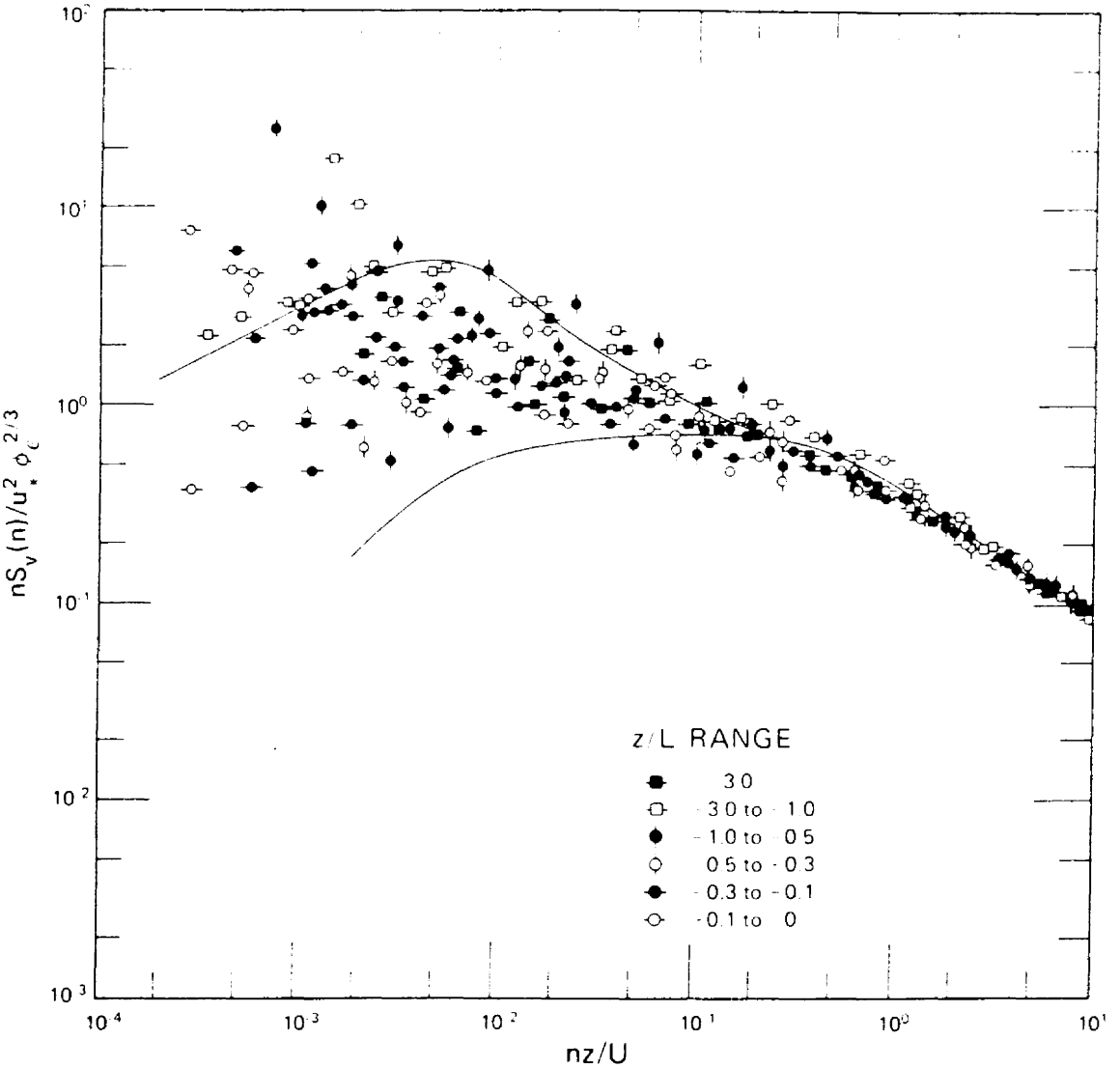

Figure 10. Generalized lateral spectra in the surface layer plotted against dimensionless frequency. The BAO data agrees well with Kansas observations as defined by the envelope (Kaimal et al., 1972).

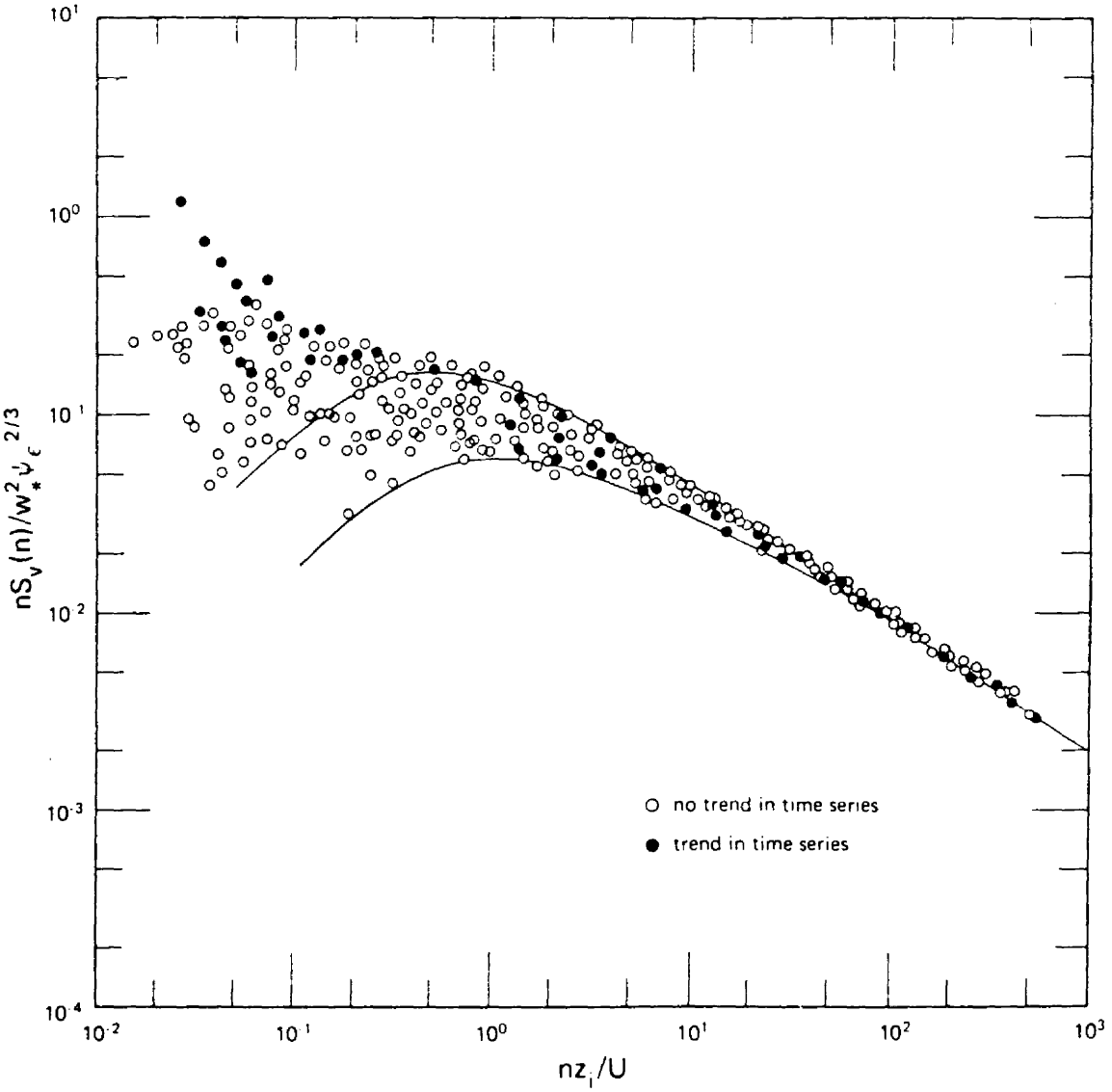

Figure 11. Generalized lateral spectra plotted against dimensionless frequency for the mixed layer. The envelope, represented by the lines, correspond to observations from Minnesota (Kaimal et al., 1976).

trend with a long-time scale indicating the influence of mesoscale and synoptic scale phenomena. The long-term trend may represent a sharp increase in the time series trace as in Figure 7 or a time series with a very long period of oscillation as in Figure 12. Figure 13 shows the smoothed spectral plots corresponding to the time series of Figure 12. More frequently, however, the v spectral behavior exhibits a low frequency roll-off. This roll-off is not as steep in the Minnesota spectra; consequently the energy containing region is spread over a wider range of frequencies. The undulating terrain may result in the larger span of eddy sizes associated with this region.

In several runs the lateral velocity spectra appear to straddle the longitudinal and vertical velocity spectra. The relationship of the u and w spectra to the v spectrum in these runs supports the spectral behavior observed by Kaimal (1978). As in Figure 14 the vertical velocity spectral peak coincides with the inflection point of the lateral velocity spectrum which occurs at the intermediate frequencies. In accordance to local isotropy requirements the v spectrum matches the w spectrum in the inertial subrange with a spectral intensity 4/3 greater than the u spectrum.

Isotropy describes the condition in which the statistical properties of the fluctuating velocity components show no dependence on the direction; in other words, are unaffected by the rotation or reflection of the axes defining the velocity components. In order for local isotropy to exist in the inertial subrange: the velocity spectra must obey the -5/3 power law, a 4/3 ratio present between the spectral intensities of transverse and longitudinal velocity components, and a vanishing cospectra are required. Both the lateral and vertical

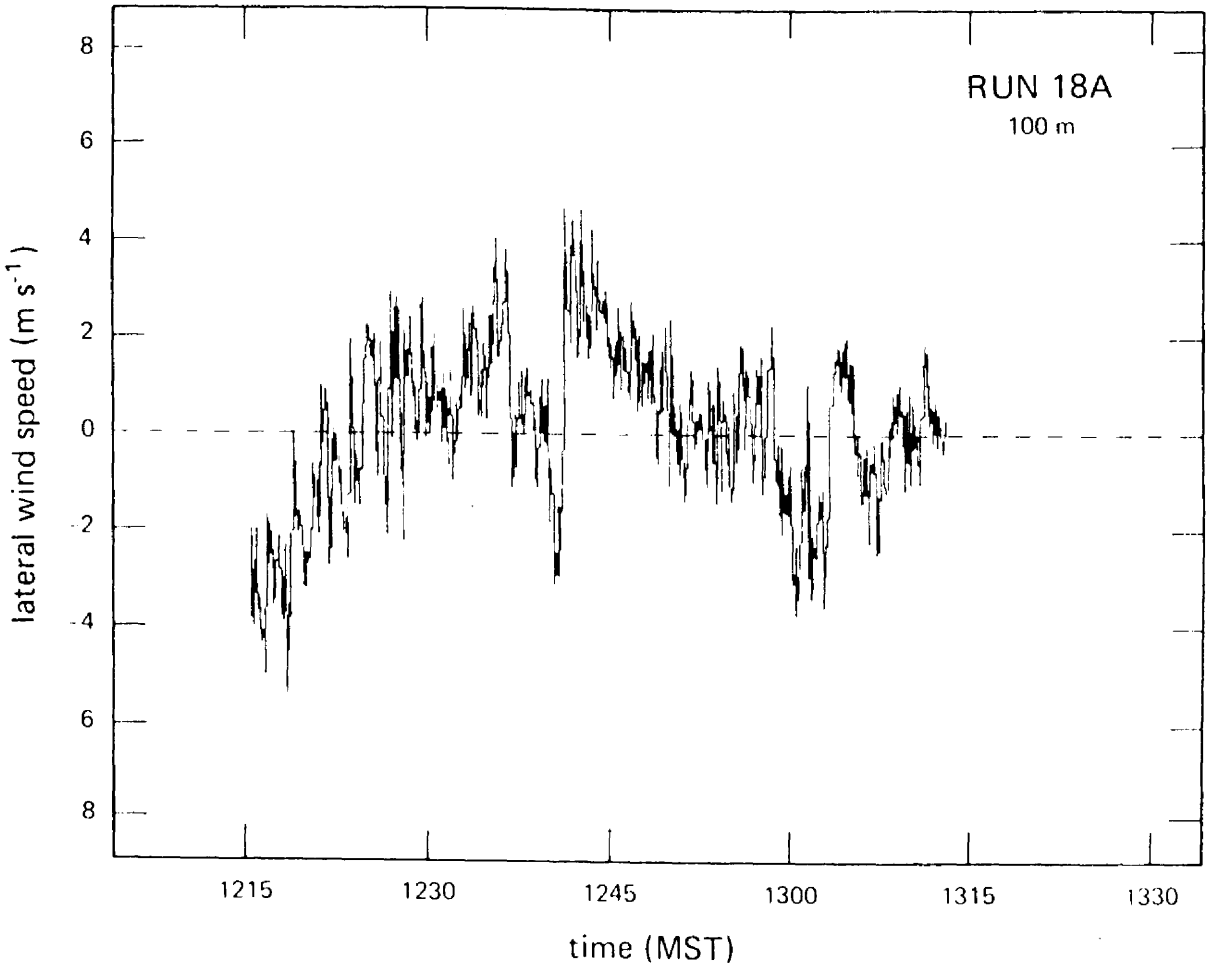

Figure 12. Time series plot of the lateral wind speed for Run 18A.

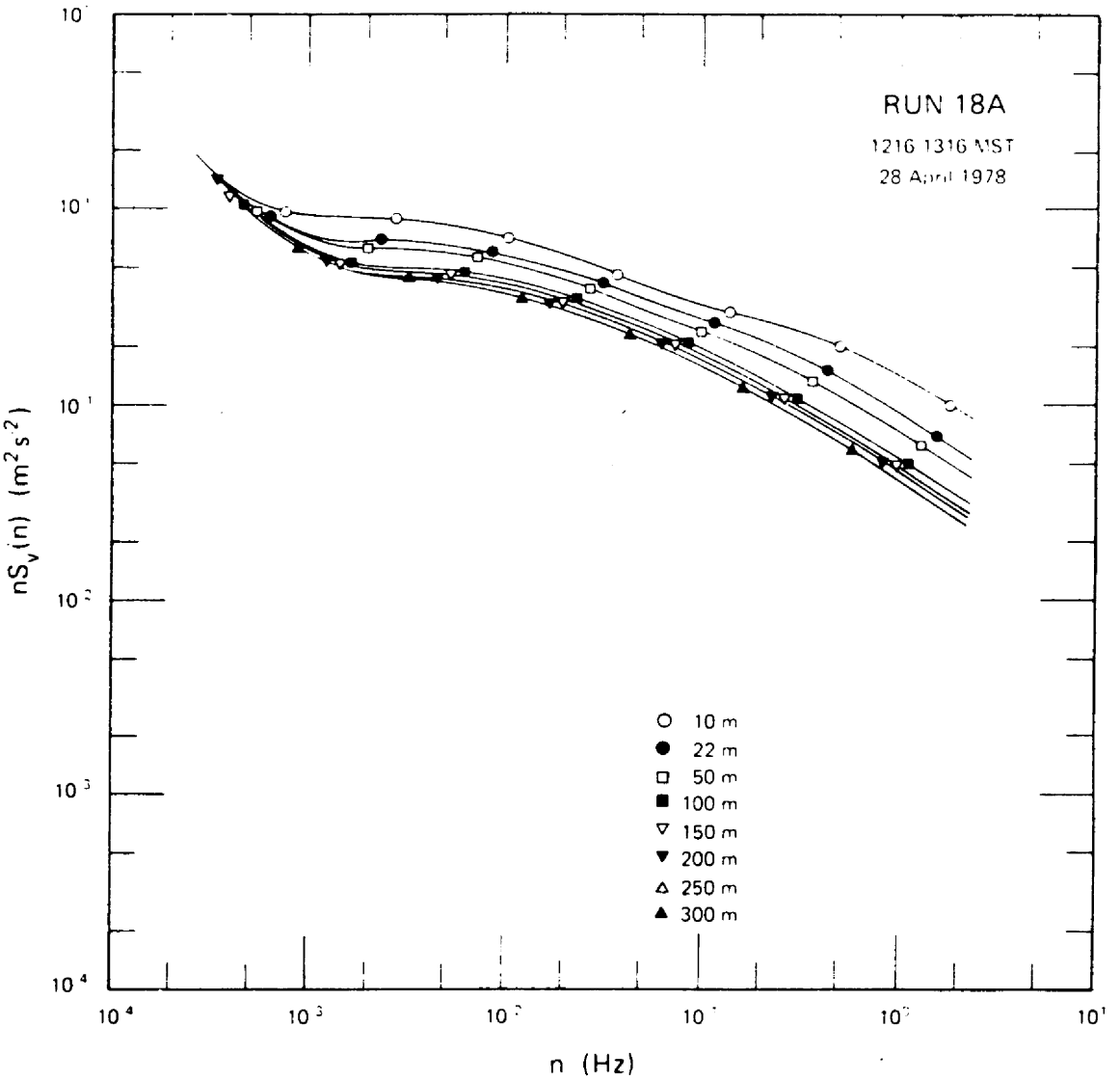

Figure 13. Spectral curves for the v velocity component calculated from the time series in Figure 12.

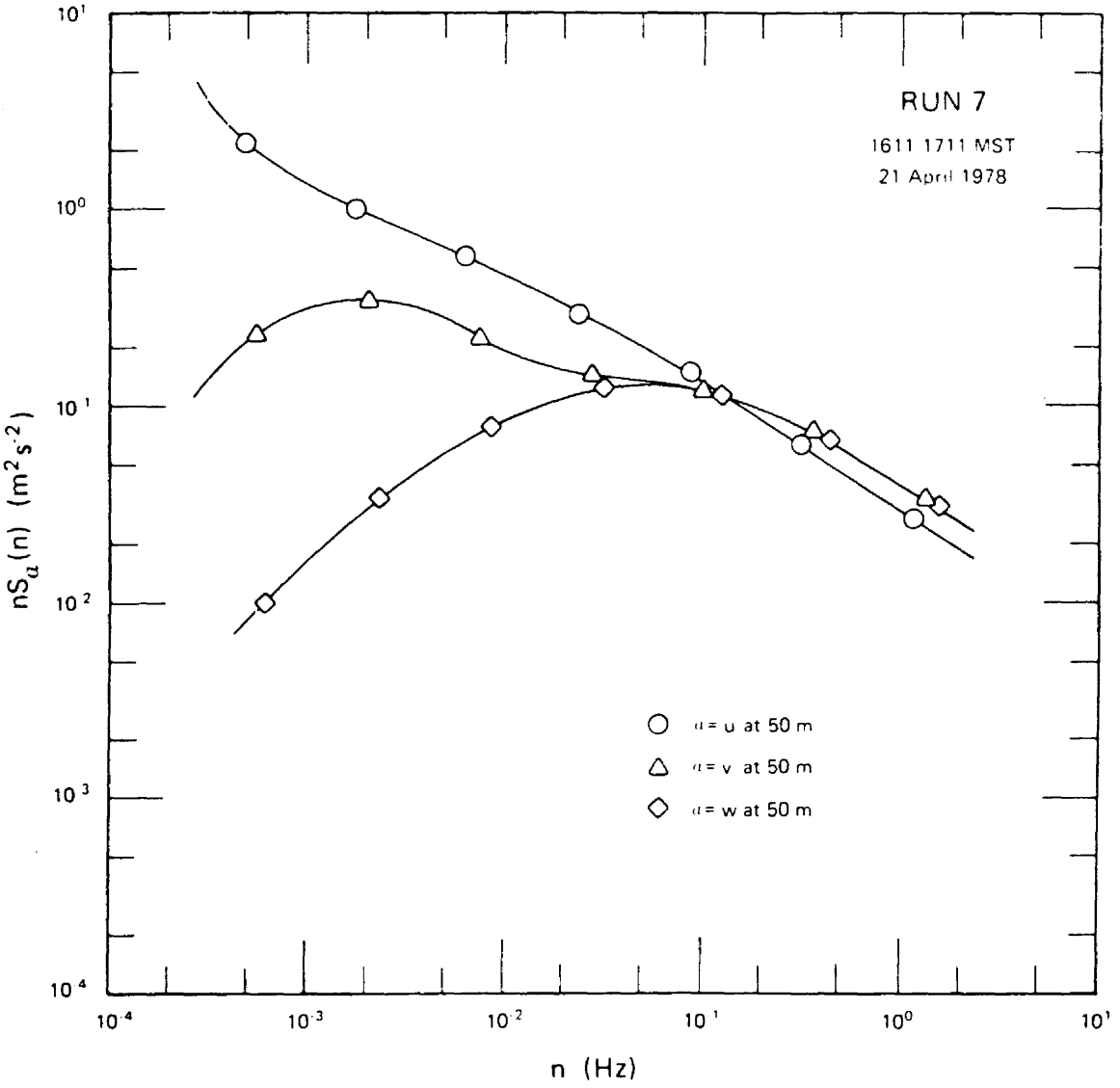

Figure 14. Spectral curves for the velocity components at 50 m. Note the inertial subrange behavior corresponding to the local isotropy predictions.

components are normal to the mean wind--the longitudinal velocity component. As seen in Figure 14 the first two requirements for isotropy are satisfied. Upon inspecting the cospectra between the transverse and longitudinal velocity components the third requirement is also satisfied.

5.4 Vertical Velocity Component

The nondimensional plot for vertical velocity, w, (Figure 15) shows partitioning according to z/L for the slightly unstable cases. Similar to the Kansas surface layer spectra, w spectra independent of z/L dominate under the more unstable conditions ($z/L < -0.3$) in the BAO boundary layer. The scatter of the normalized April spectra is restricted to a smaller region than the area enclosed in the envelope (solid lines of Figure 15) defined by the Kansas spectra.

The individual BAO vertical velocity spectra displayed various characteristics common to w spectra observed during previous surface layer experiments conducted under homogeneous conditions. Common to all w spectra in the surface layer, as the height, z, increases, the following decreases (as seen in Figure 16): the spectral intensities at the high frequencies, the frequency corresponding to the spectral peak, and the frequency at which the onset of the inertial subrange occurs. The influence of the surface layer depth at the high frequencies of the vertical velocity spectra is illustrated in Figure 17. The shallow surface layer present during Run 15 ($L = -16.35$ m) forces the spectral intensities of the inertial subrange to become squeezed together as the constant spectral intensity associated with the mixed layer is approached. In contrast, Run 7 has a fairly deep surface layer ($L = -212.10$ m) causing a fairly wide spread of spectral intensities at the high frequency end.

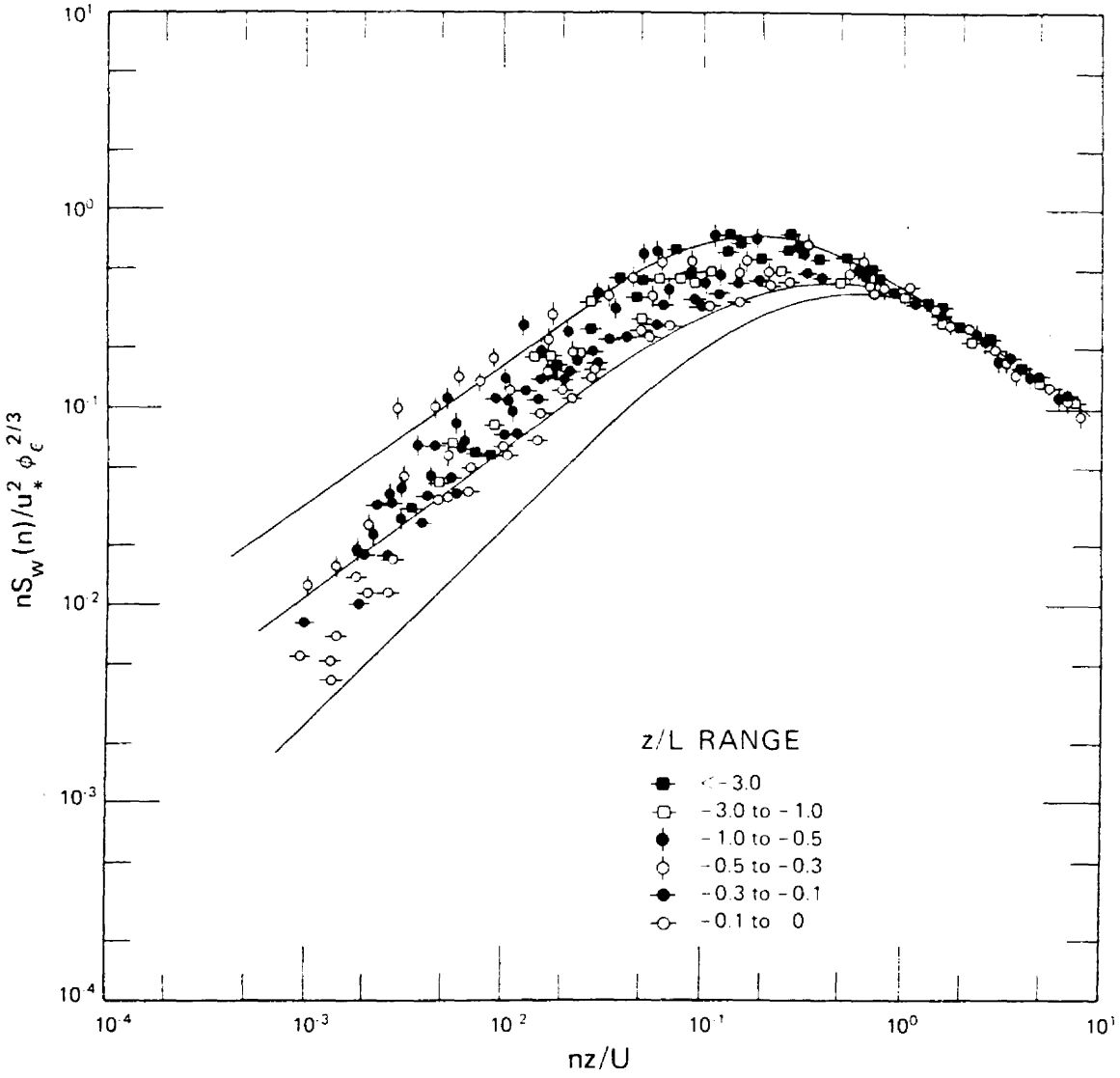

Figure 15. Normalized vertical velocity spectra in the surface layer plotted against dimensionless frequency. The lower envelope represents z/L values ranging from 0 to -0.3 during the Kansas experiment; the upper envelope corresponds to z/L values which ranged from -0.3 to -2.0 (Kaimal et al., 1972).

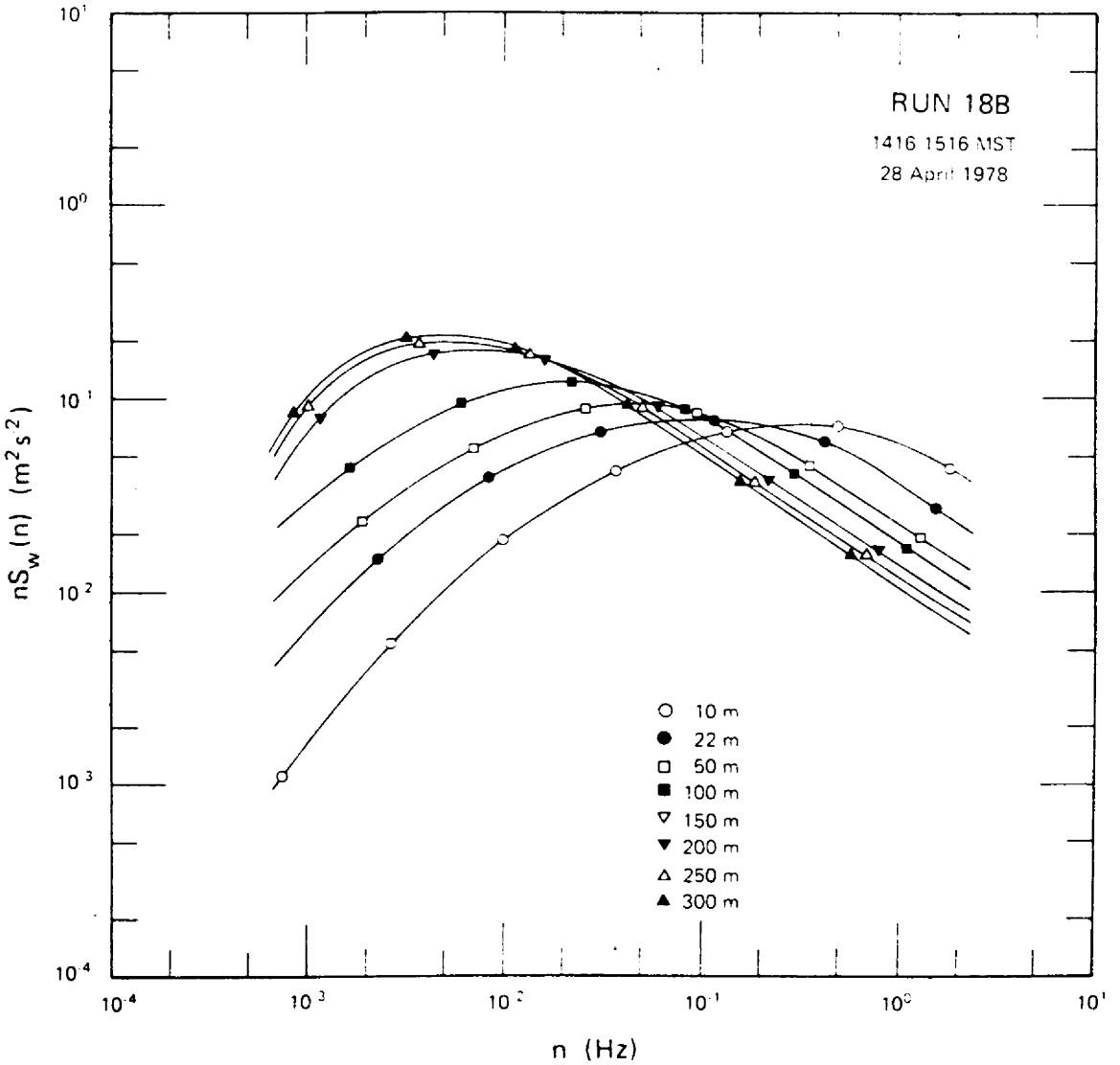

Figure 16. Vertical velocity spectra for Run 18B representing the characteristic changes in spectral shape with increasing height.

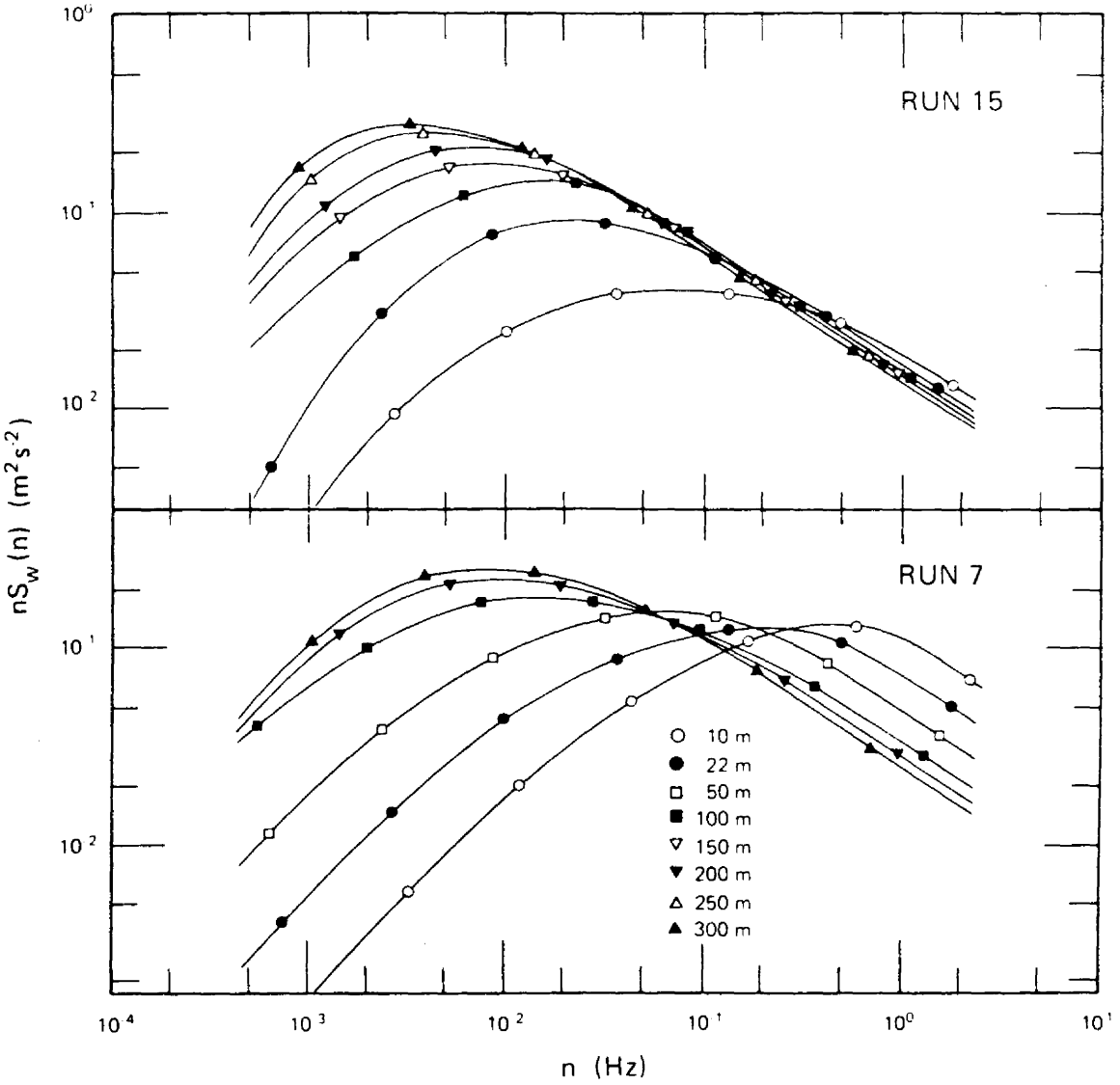

Figure 17. Comparison of spectral behavior in the inertial subrange with a shallow surface layer (Run 15) caused by light winds ($U = 4.63\ m\ s^{-1}$) and a deep surface layer (Run 7) associated with strong winds ($U = 11.48\ m\ s^{-1}$).

The dimensionless dissipation rate of turbulent kinetic energy, $\phi_\varepsilon = 0.35\ z\varepsilon/u_*^3$, which appears in the normalization of the spectral estimates, increases (slowly at first) with increasing instability in the surface layer. As seen in Figure 18, the scatter resulting from the April BAO data agrees well with the dissipation rate observed in Minnesota (Kaimal, 1978),

$$\phi_\varepsilon^{2/3} = 1 + 0.75\ \left|\frac{z}{L}\right|^{2/3}. \tag{23}$$

For comparison, the curve describing the dissipation rate in Kansas (Wyngaard and Coté, 1971),

$$\phi_\varepsilon^{2/3} = 1 + 0.5\ \left|\frac{z}{L}\right|^{2/3}, \tag{24}$$

has been included in the figure. The smaller coefficient in (24) may perhaps be a consequence of the limited stability range in the Kansas data compared to the Minnesota and BAO data.

If the dimensionless standard deviation of the vertical velocity fluctuations, σ_w/u_*, is defined as a function of the stability parameter, z/L, then the shear stresses can be calculated from the vertical velocity measurements for any given stability. Wyngaard et al. (1971) found that σ_w/u_* increased linearly with decreasing stability in an unstable atmosphere. The observed dependence of σ_w/u_* on stability was found to be

$$\frac{\sigma_w}{u_*} = 1.9\left(-\frac{z}{L}\right)^{1/3}. \tag{25}$$

As displayed in Figure 19, the BAO vertical velocity fluctuations exhibit only minimal scatter from the predicted expression.

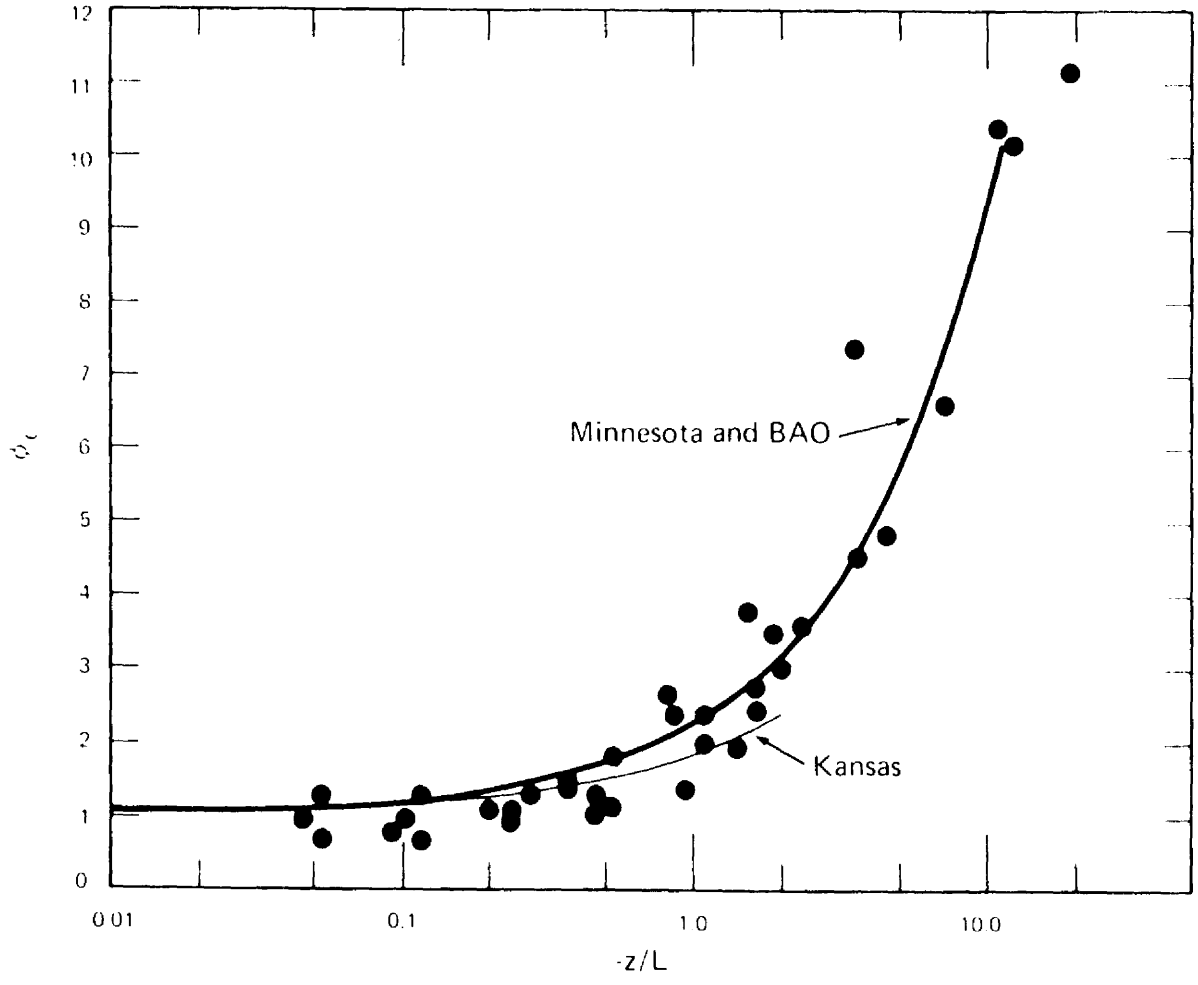

Figure 18. Dimensionless dissipation rate of turbulent kinetic energy within the surface layer plotted against z/L.

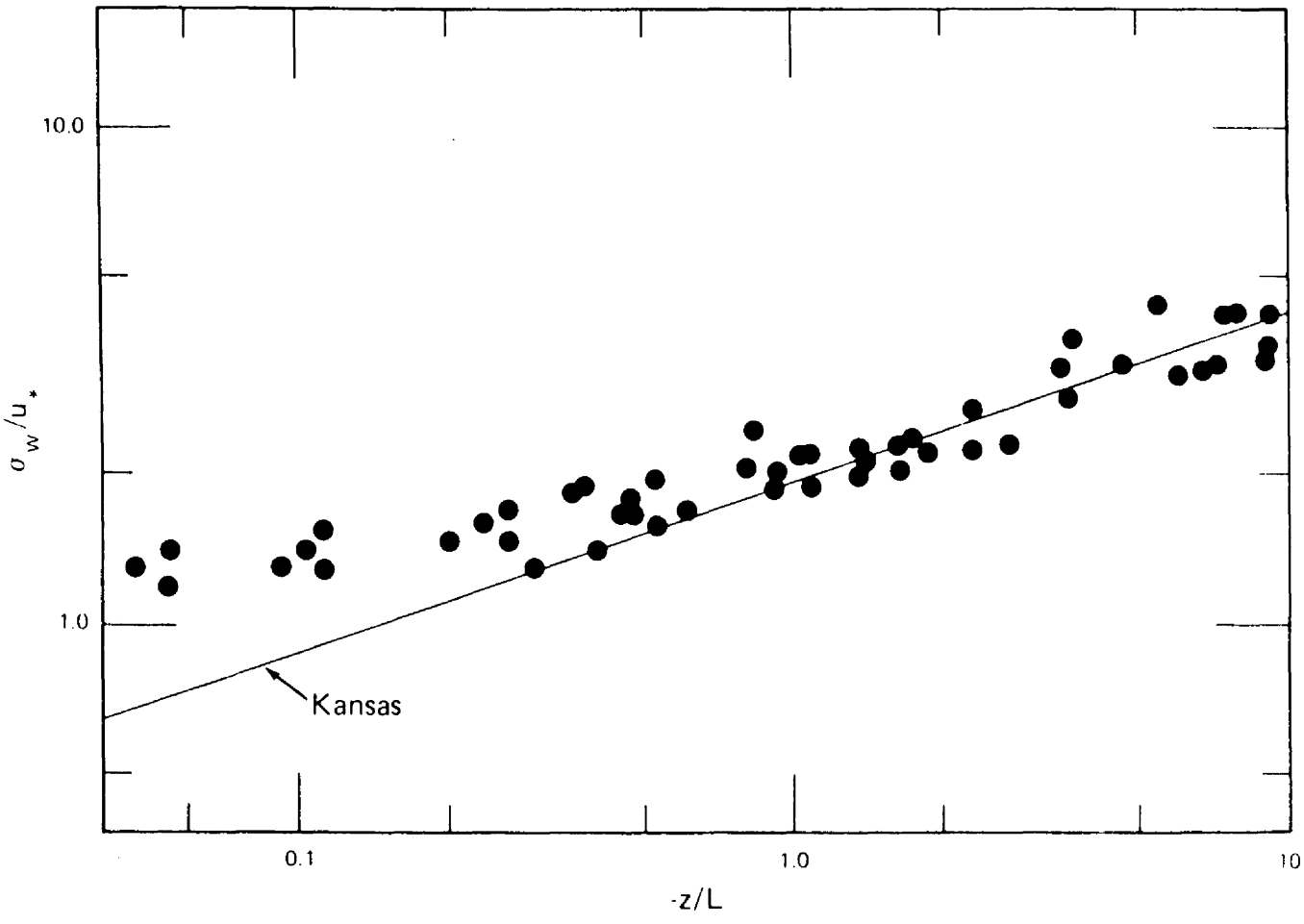

Figure 19. Normalized standard deviation of the vertical velocity for varying z/L values.

In the mixed layer, the w spectra do not systematically vary with z/z_i--or height (Figure 20). Instead, the scatter defines a wider region with a sharper low frequency roll-off of spectral intensity than the area defined by the Minnesota spectra over flat terrain, denoted by the solid lines in Figure 20. Consequently, the energy containing region of the April BAO w spectra is restricted to a smaller range of frequencies.

Slightly different spectral behavior characterizes the individual vertical velocity spectra in the mixed layer, than in the surface layer. The mixed layer is a region with near-constant distributions of atmospheric parameters, such as wind speed and potential temperature; the spectral intensities associated with the inertial subrange also approach a constant for all levels in the mixed layer. The frequency of the w spectral peak is also invariant in the mixed layer, as in Figure 21.

Within the mixed layer, the dimensionless dissipation rate of turbulent kinetic energy, $\psi_\varepsilon = \varepsilon/[Q_0(g/T)]$, represents the ratio of the dissipation and the buoyant production rates. Theoretically in a convectively unstable boundary layer ψ_ε should have a constant value of 0.5, assuming a linearly decreasing heat flux profile and a negligible wind shear across the capping inversion (Kaimal et al., 1976). The data set used in this investigation exhibits values of ψ_ε greater than 0.5 (Figure 22) implying that more energy was lost through dissipation than gained by production processes; however, energy must be conserved. The high dissipation rates cannot be attributed to the undulating terrain, since similar behavior was observed over flat terrain in Minnesota. Although the wind shear across the inversion was not

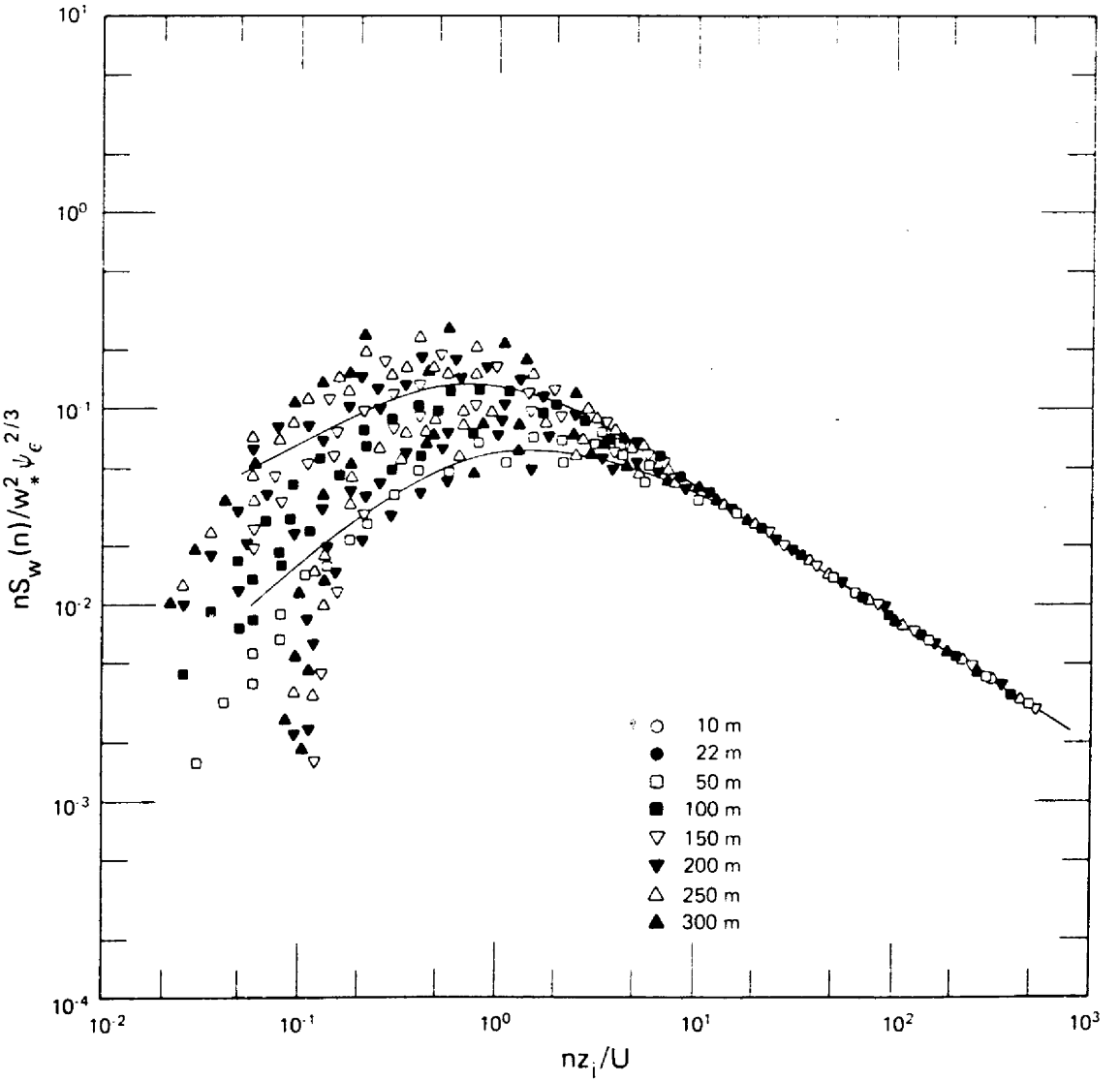

Figure 20. Normalized w spectra compared with the Minnesota envelope (Kaimal et al., 1976) for varying heights in the mixed layer.

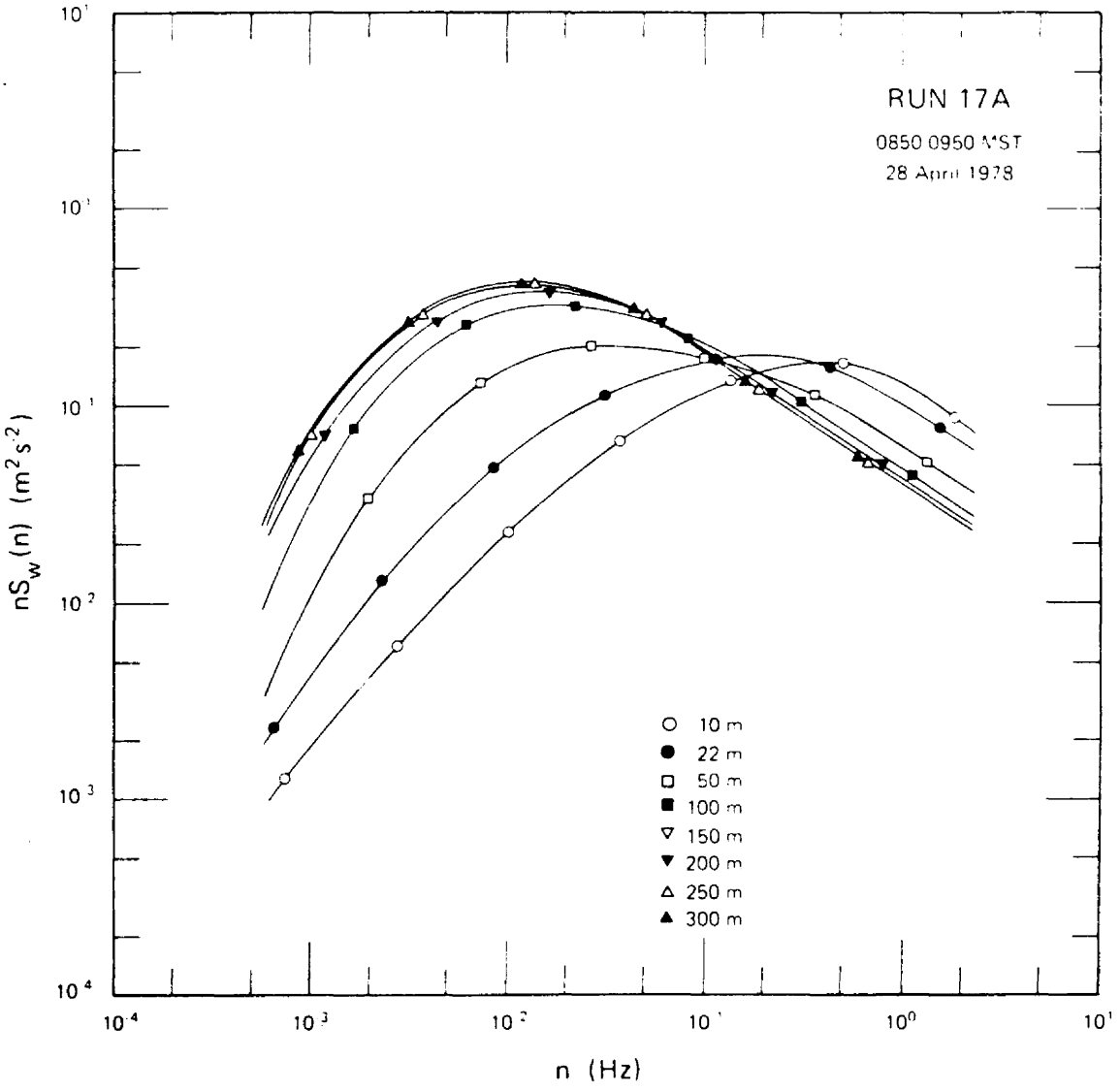

Figure 21. Vertical velocity spectral curves for Run 17A. Note the tendency for the spectral intensities within the inertial subrange and the frequency of the spectral peak to become invariant with height.

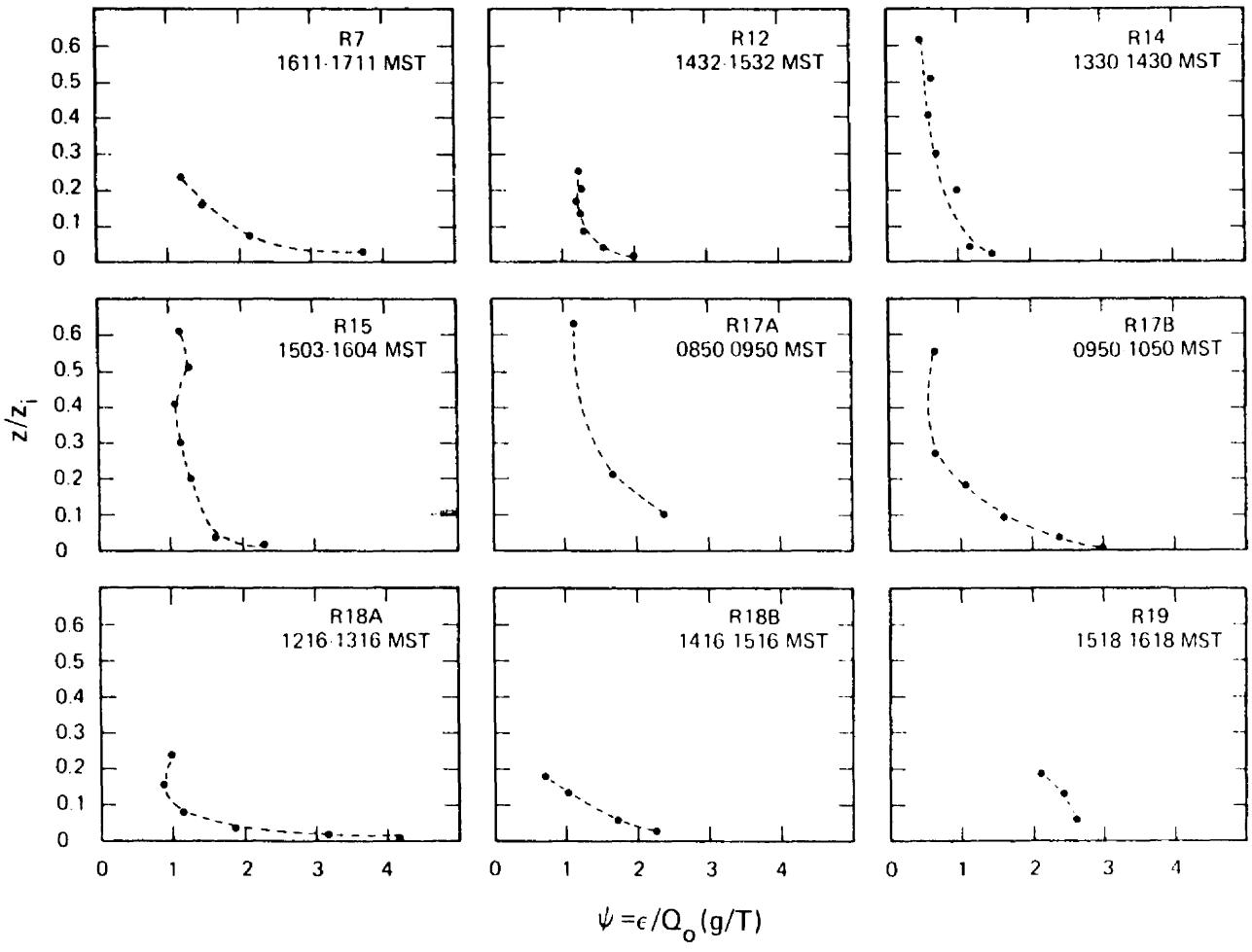

Figure 22. Vertical profiles of the dimensionless dissipation rate of turbulent kinetic energy in the mixed layer.

consistently negligible, as assumed, this is not the sole cause for the high ψ_ε values. Consequently further research is required to obtain a more complete understanding of the turbulent kinetic energy processes in the mixed layer.

5.5 Peak Wavelength

The horizontal velocity components cannot be examined for the behavior of the peak spectral estimates due to the run-to-run variations of the low frequency end of the spectra. Since the vertical velocity spectra did not include any long-term trends, the frequency corresponding to the maximum value of the w spectra is examined in this section.

In the April BAO vertical velocity spectra, the frequency corresponding to the peak spectral value, $f_m = z/(\lambda_m)_w$, decreased with increasing instability, as shown in Figure 23; supporting the results of the Kansas experiment (Kaimal et al., 1972). Eventually a constant, 0.13, is achieved in the matching layer ($|z/L| > 1.0$). The matching layer has been defined as a transition layer. It is in this layer that a double limit exists where the atmospheric quantities as seen from the surface layer below must also coincide with the value of the atmospheric parameter in the mixed layer above. In the Kansas, Minnesota and April BAO experiments, f_m becomes a constant in the matching layer (0.17 at Kansas and Minnesota as compared to 0.13 at BAO). The difference in the size of the energy containing eddy in the matching layer may be due to the different terrain types at the experiment sites.

The normalized frequency associated with the spectral peak, $f_m=z/(\lambda_m)_w$, may also be expressed as a normalized wavelength, $(\lambda_m)_w/z$. The behavior of $(\lambda_m)_w/z$ as it varies with z/L in the surface layer and z/z_i in the mixed layer is illustrated in Figure 24. The single

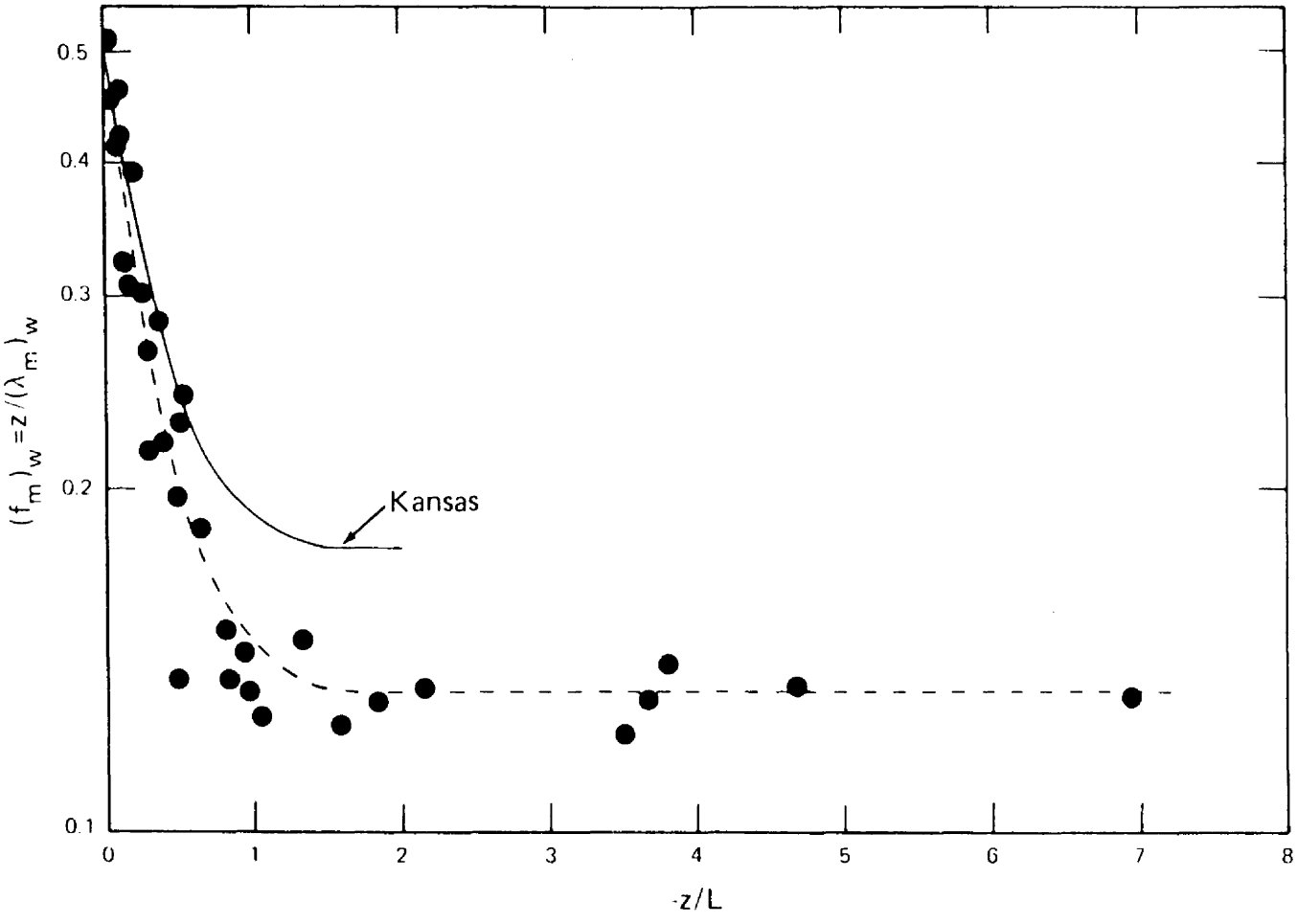

Figure 23. Logarithmic spectral peak for the vertical velocity component plotted against z/L. The dashed curve is the visual best fit.

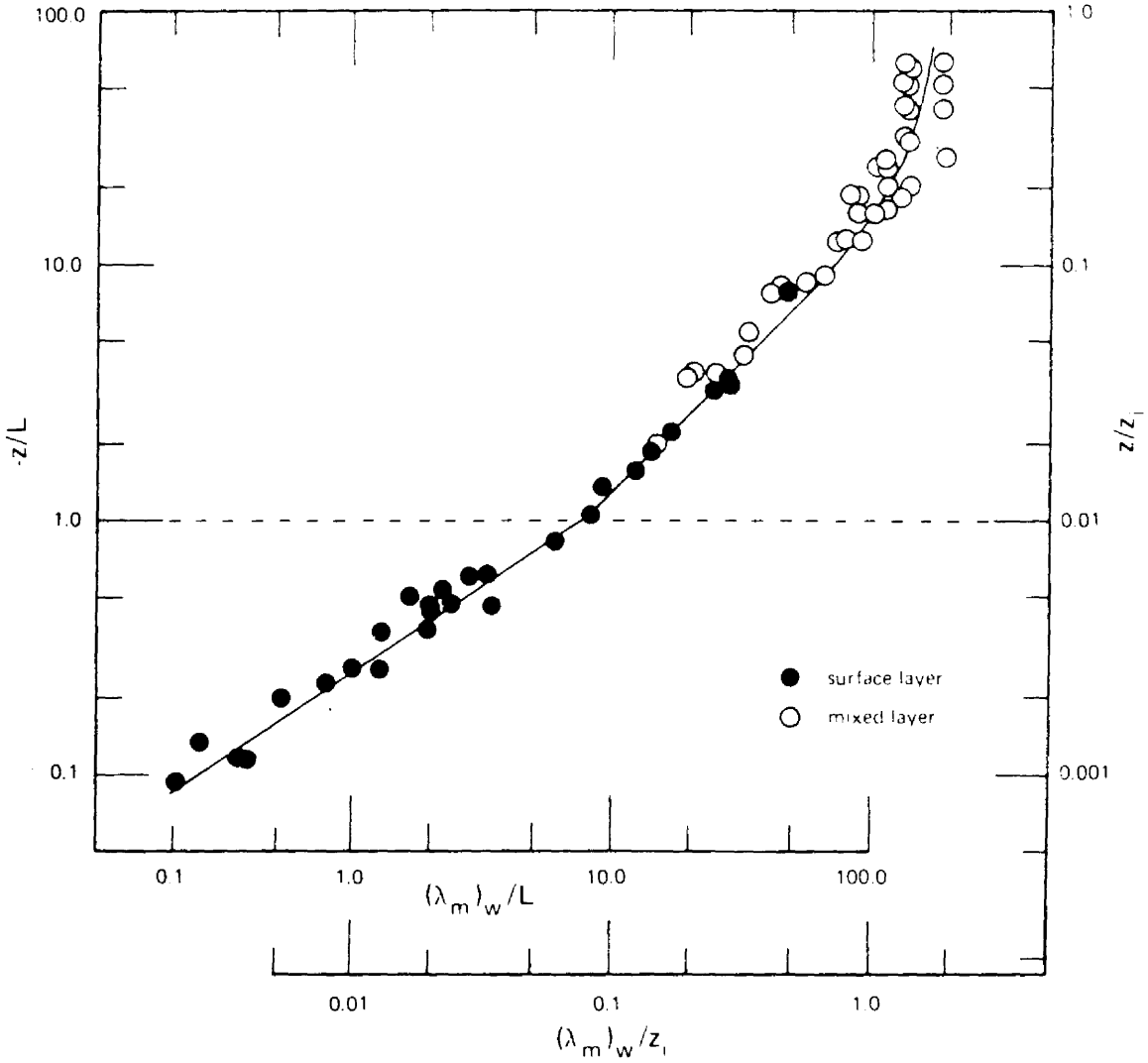

Figure 24. Dimensionless peak wavelength for the vertical velocity component as a function of z/L in the surface layer and z/z_i in the mixed layer.

curve describing the wavelength associated with the vertical velocity spectral peak through the depth of the unstable boundary layer is accomplished by changing the normalizing length scale from the Obukhov length, L, to the mixed layer length scale, z_i, within the matching layer. In Figure 24, the peak wavelength linearly increases with increasing values of z/L. At the top of the surface layer, where z = L, a value of 7.7 is achieved; this constant corresponds to the $f_m = z/(\lambda_m)_w = 0.13$ observed in Figure 23. Once within the mixed layer, $(\lambda_m)_w$ gradually increases with height asymptotically approaching 1.7 in the upper half of this layer ($z > z_i/2$); suggesting an exponential relationship. A peak wavelength of 1.7 z_i is larger than the 1.5 z_i that the Minnesota spectra revealed--the rolling terrain might cause these larger eddies. Summarizing the observed dependence of the vertical velocity peak wavelength on the length scale in a convectively unstable boundary layer:

$$(\lambda_m)_w \approx \begin{cases} 7.7\ L\left|\frac{z}{L}\right|^{3/2} & 0 < z \leq |L| \\ 7.7z & |L| \leq z \leq 0.1\ z_i \\ 1.7\ z_i[1-\exp(-6.1\ z/z_i] & 0.1\ z_i \leq z \leq z_i \end{cases} \quad (26)$$

Chapter VI

SPECTRUM OF TEMPERATURE

6.1 Normalizing

The inertial subrange of the temperature, θ, spectrum may also be expressed in nondimensional form by applying the surface layer and mixed layer similarity rules to Corrsin's (1951) relationship for the inertial subrange. As shown in (14) the inertial subrange spectrum for temperature can be expressed in the form

$$nS_\theta(n) = \beta_1 N_\varepsilon^{-1/3}\left(\frac{2\pi n}{U}\right)^{-2/3} . \tag{27}$$

Using Monin-Obukhov similarity theory in the surface layer, the following normalization results

$$\frac{nS_\theta(n)}{T_*^2} = 0.47\ \phi_N\phi_\varepsilon^{-1/3}\ f^{-2/3} , \tag{28}$$

where $T_*^2\phi_N\phi_\varepsilon^{-1/3} \equiv z^{2/3}N\varepsilon^{-1/3}$. The inclusion of $\phi_N\phi_\varepsilon^{-1/3}$ in the left-hand side of (28) forces the inertial subrange of all spectra into a single line with a -2/3 slope,

$$\frac{nS_\theta(n)}{T_*^2\phi_N\phi_\varepsilon^{-1/3}} = 0.47\ f^{-2/3} . \tag{29}$$

Using mixed layer similarity theory, a comparable normalization is achieved

$$\frac{nS_\theta(n)}{\theta_*^2\psi_N\psi_\varepsilon^{-1/3}} = 0.24\ f_i^{-2/3} , \tag{30}$$

where $\theta_*^2\psi_N\psi_\varepsilon^{-1/3} \equiv z_i^{2/3}N\varepsilon^{-1/3}$. Consistent with similarity theory, the low frequency portion of (29) varies with z/L in the surface

layer and the low frequencies of (30) depend only on z/z_i in the mixed layer.

6.2 Universal Spectrum of Temperature

Plotting the normalized, surface layer, logarithmic spectral intensities against the dimensionless frequency, $f = nz/U$, produces Figure 25. The θ spectra, representing convectively unstable conditions, crowd into a relatively narrow band, previously defined by the Kansas data (Kaimal et al., 1972), with no apparent dependence on the stability parameter, z/L.

Only broad generalizations have ever been made of the fluctuating temperature spectrum within the mixed layer. The entrainment of warm air through the inversion capping the convectively unstable boundary layer, affecting the upper portion of the mixed layer, has resulted in run-to-run variations in the low frequency portion of θ spectra. The θ spectra at the low frequencies experience either an increase (Figure 26) or a decrease (Figure 27) of the spectral intensity. The spectral gap in Figure 26, lies between the rise at the low frequency end, caused by the diurnal temperature trend and the peak representing temperature turbulence. The diurnal trend causes the spectral curves of all heights to converge to a single upward extending curve. In the absence of a trend, a low frequency roll-off of θ spectral intensity, as in Figure 27, is observed.

Due to these low frequency fluctuations of the θ spectra, Kaimal, et al. (1976) felt that the thermal turbulent behavior, unlike velocity turbulence, could not be generalized within mixed layer similarity rules. Deardorff (1978), on the other hand, developed a universal plot based on the idealized curves presented by Kaimal et al.

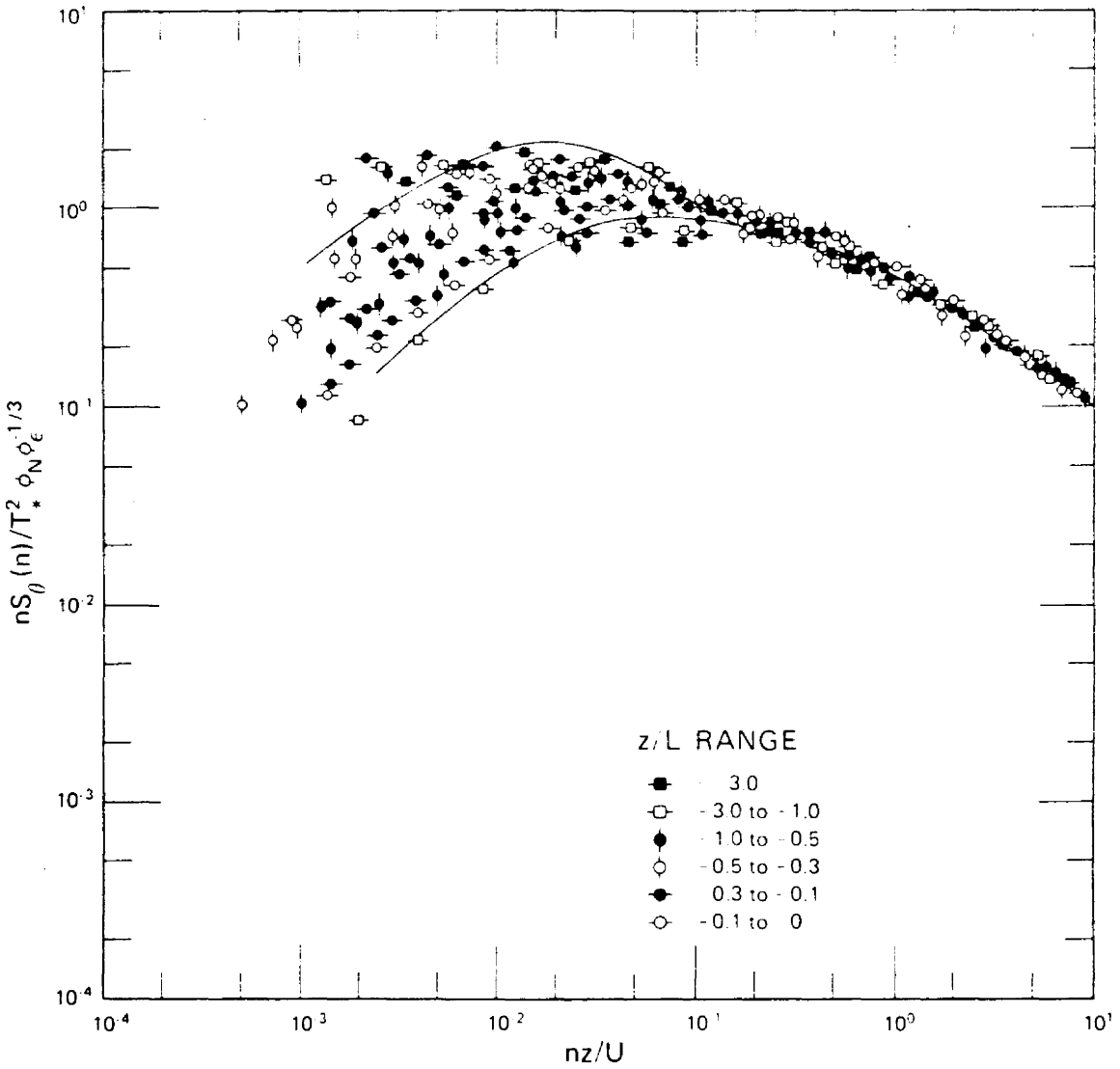

Figure 25. Normalized temperature spectra in the surface layer at BAO compared to the Kansas data, represented by the envelope, (Kaimal et al., 1972).

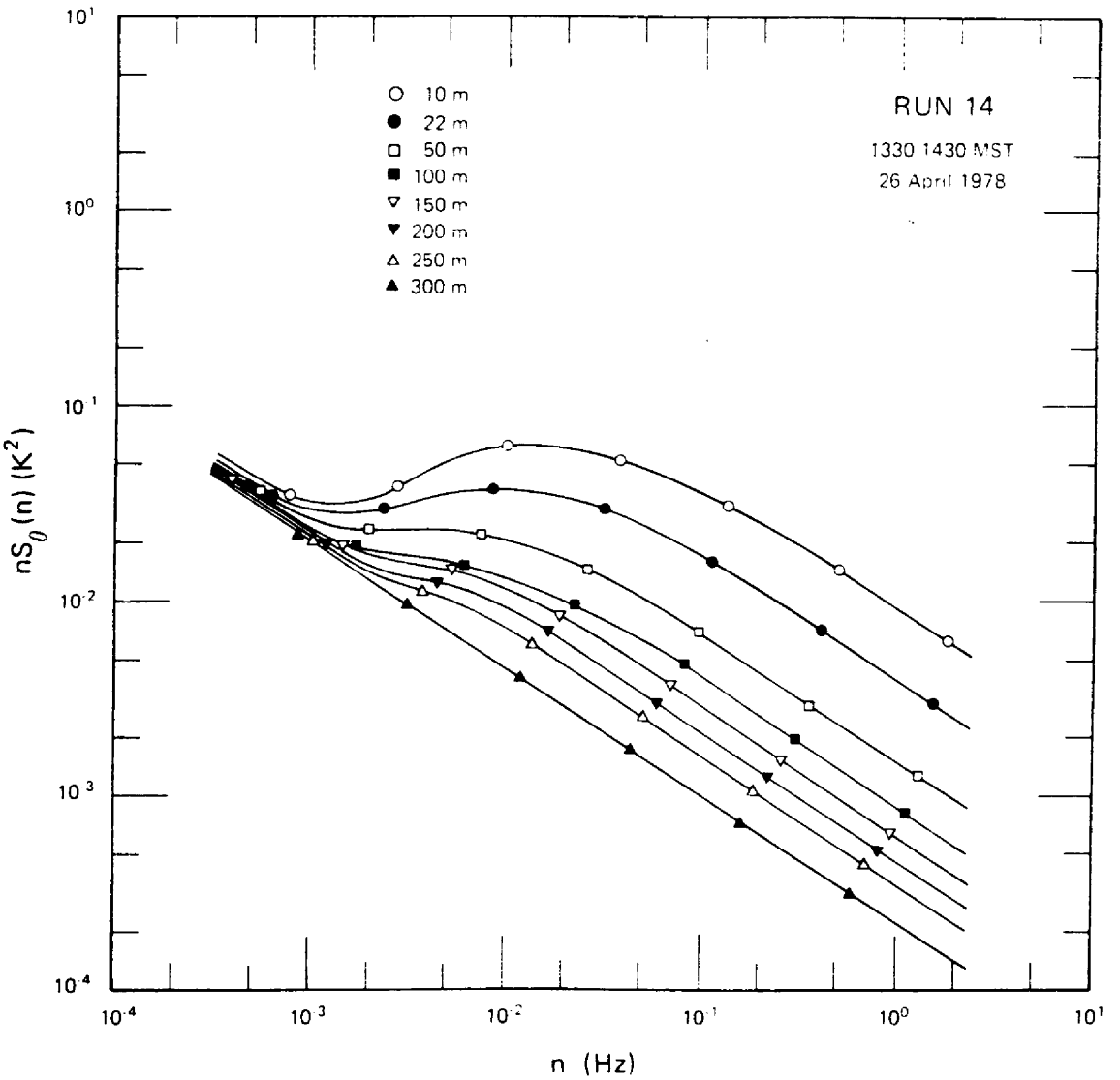

Figure 26. Temperature spectra for Run 14. Note the spectral gap present at the low frequencies.

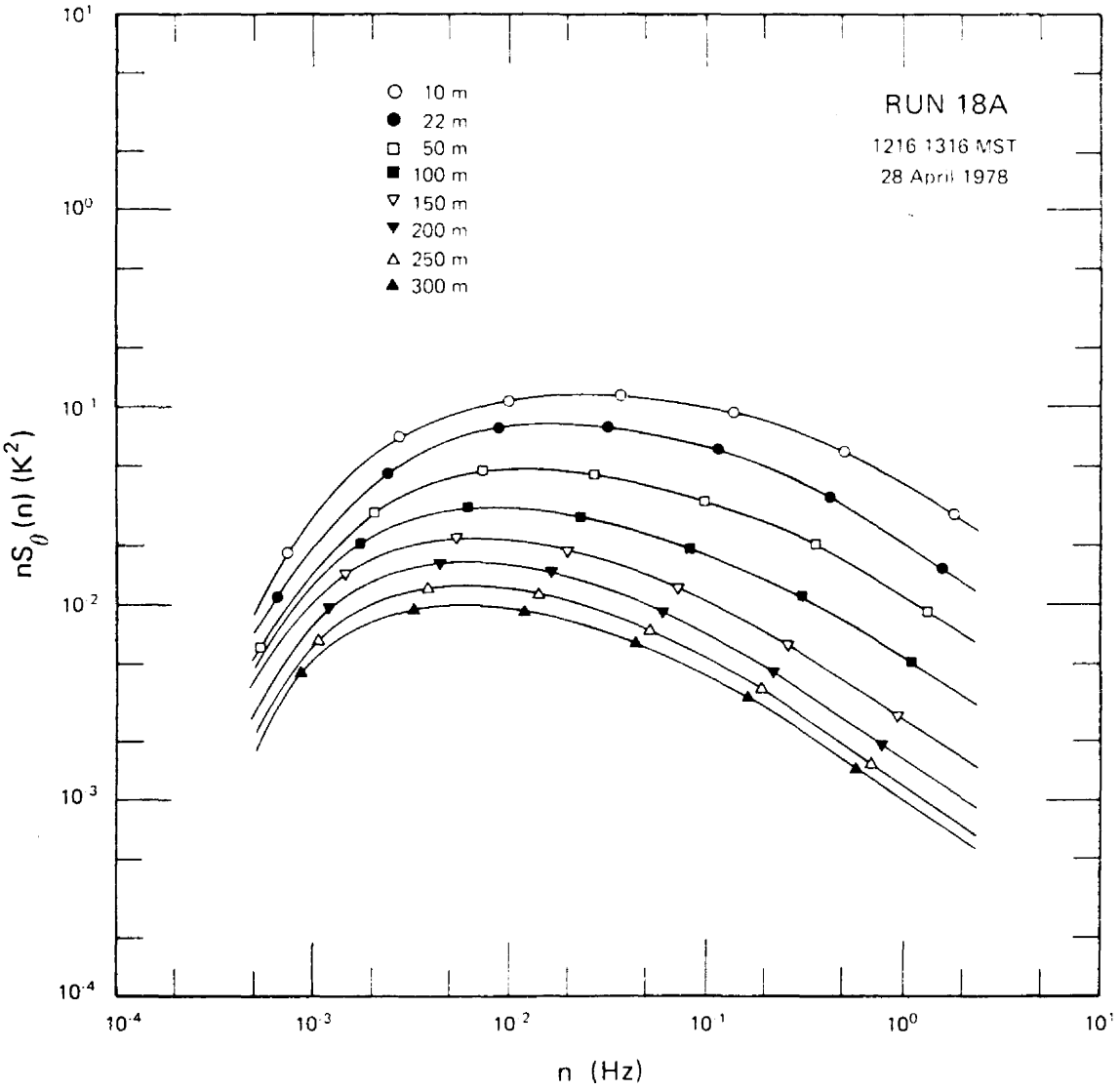

Figure 27. Temperature spectra for Run 18A. Note the low frequency roll-off of spectral intensity.

(1976). He found a rapid increase of the wavelength corresponding to the spectral peak within the matching layer; gradually shifting to non-distinct spectral peaks in the mid-portion of the mixed layer, where thermal variance is minimal. The spectral behavior in the upper third of the mixed layer is not understood, since the effect of entrainment on the boundary layer is unknown. Figure 28 compares Deardorff's universal spectral curves, solid lines on the figure, to the mixed layer spectra from BAO, the agreement is good except for a shift in spectral peak to lower frequencies which may be caused by the rolling terrain. The BAO data did not extend into the upper third of the mixed layer; consequently the effect of warm air entrained from above the boundary layer was not a complication.

The dimensionless, normalized standard deviation of temperature, σ_θ/T_*, decreases linearly with increasing instability, shown in Figure 29. Wyngaard et al. (1971) observed the functional dependence of σ_θ/T_* on the stability parameter to be

$$\frac{\sigma_\theta}{T_*} = 0.95\left(-\frac{z}{L}\right)^{-1/3}, \qquad (31)$$

indicated on Figure 29 by the solid curve. The predicted form fits the BAO data reasonably well.

6.3 Peak Frequency

The frequency of the maximum spectral value of θ, $(f_m)_\theta$, in the unstable surface layer increased with increasing instability (Figure 30). Within the matching layer a constant value of 0.13 is achieved. The Kansas θ spectra (Kaimal et al., 1972) displayed a similar increase with instability before approaching a constant, 0.05, in the matching layer.

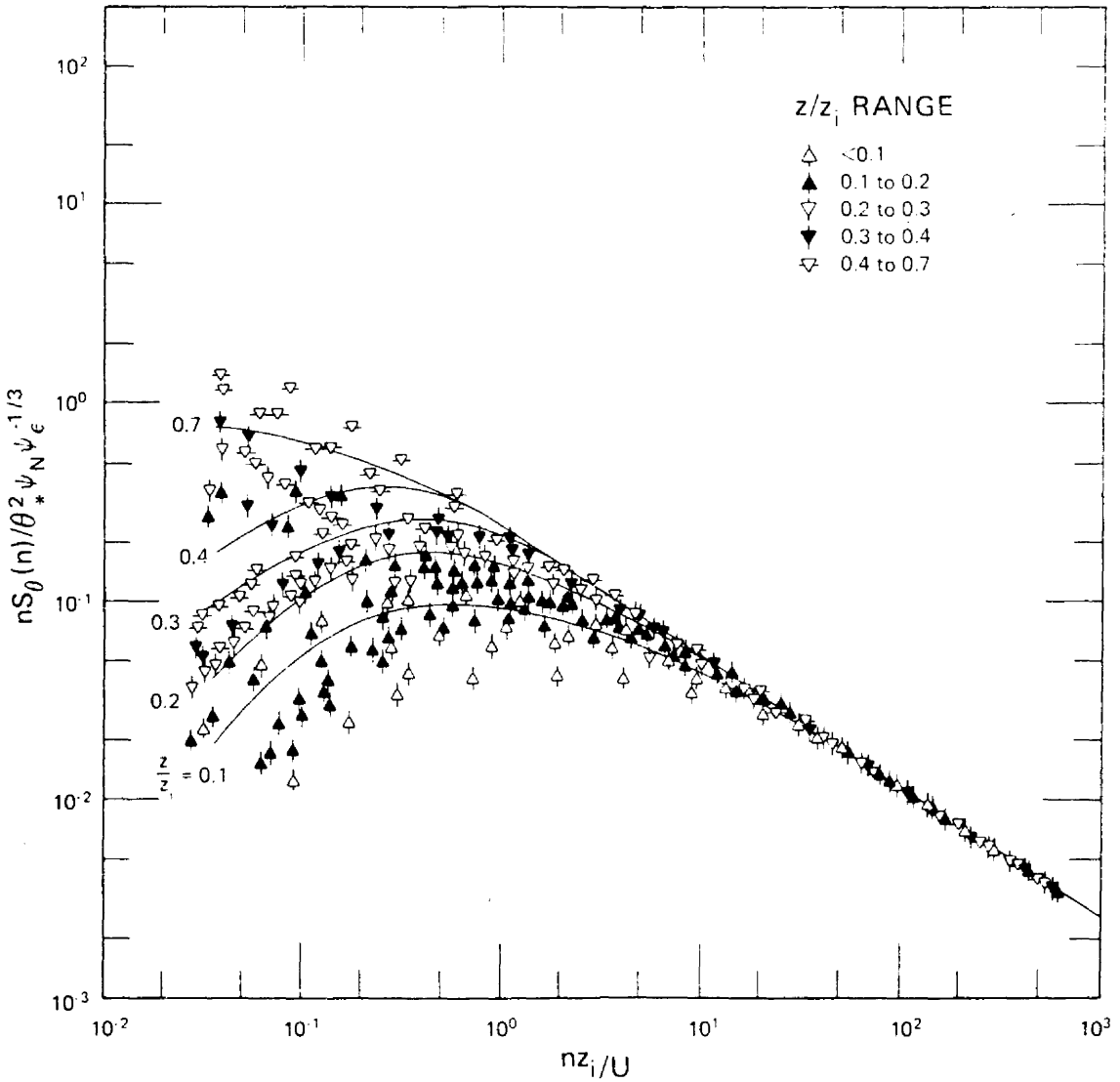

Figure 28. Normalized θ spectra plotted against dimensionless frequency in the mixed layer for values of z/z_i ranging from 0 to 0.7. The solid curves correspond to the idealized universal curves developed by Deardorff (1978).

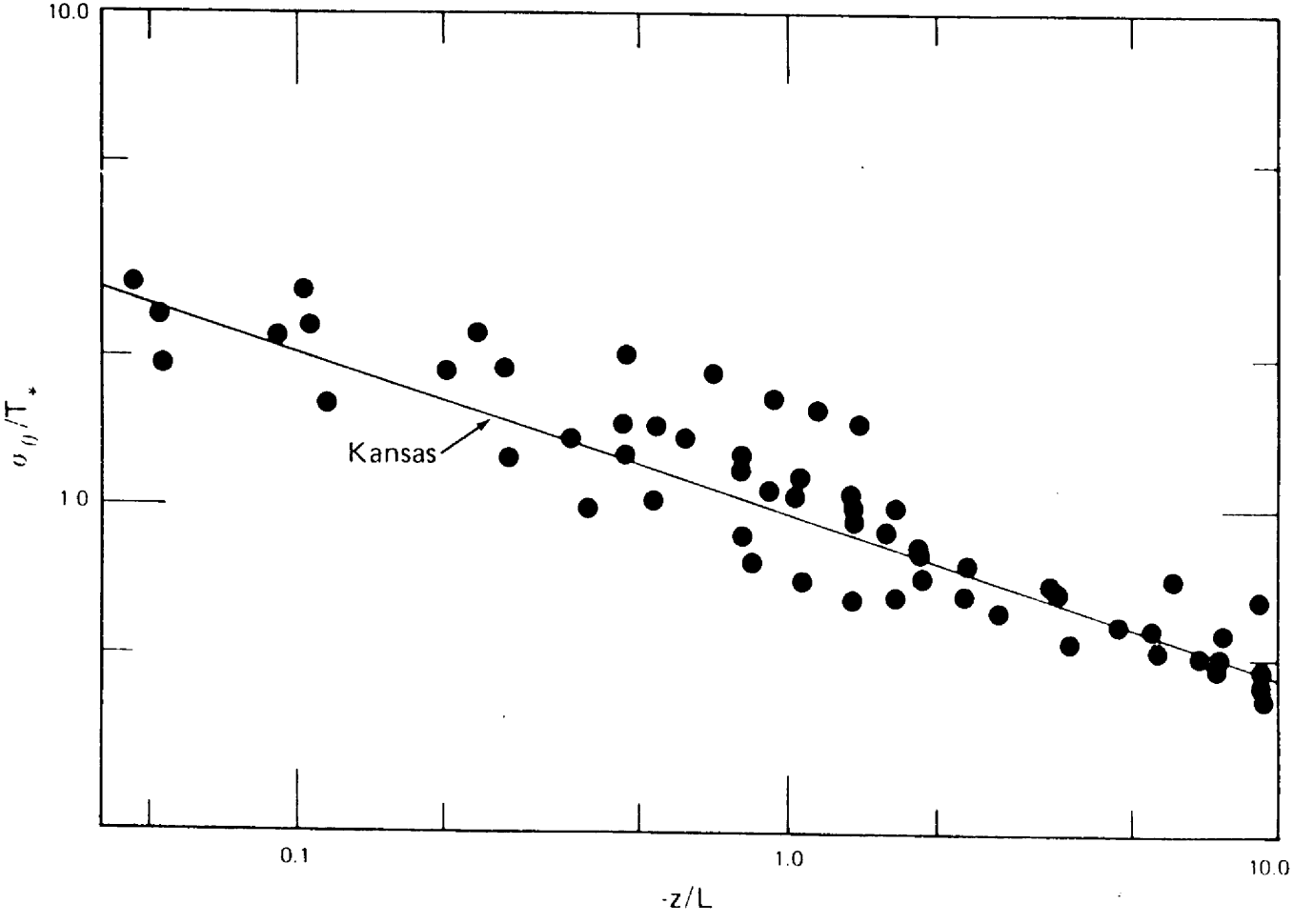

Figure 29. Normalized standard deviation of θ over a wide range of z/L values.

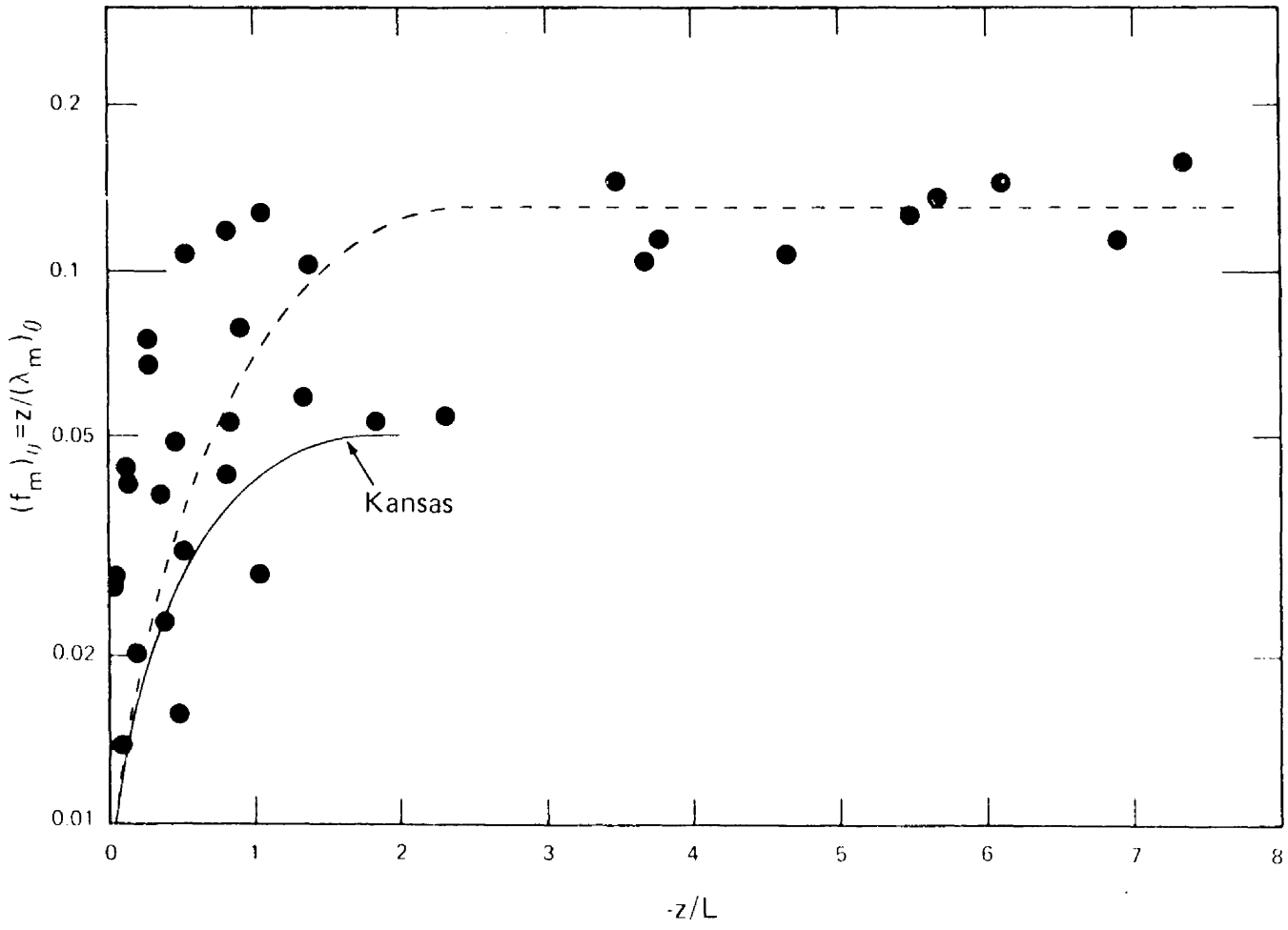

Figure 30. Logarithmic spectral peak frequency for the fluctuating temperature plotted against z/L. The dashed curve is the best fit visually.

The constant value of 0.13 associated with April BAO θ spectra for $(f_m)_\theta$ in the matching is much greater than the equivalent quantity obtained from the Kansas spectra. At the same time, the April BAO $(f_m)_\theta$ is equivalent to the BAO $(f_m)_w$ (see Figure 23), suggesting comparable convective scales of temperature and vertical velocity. Possibly, the Kansas spectra did not exhibit a similar value of $(f_m)_\theta$ since data was collected to only 22 m as compared to collection throughout the entire surface and matching layer depths at BAO. Another explanation may be related to the different types of terrain--flat at the Kansas field site and uneven around the BAO tower as seen in Figure 1.

Chapter VII

SUMMARY, CONCLUSIONS, SUGGESTIONS FOR FURTHER RESEARCH

7.1 Summary

The objective of this research was to observe and compare the behavior of the temperature and velocity spectra obtained from an inhomogeneous boundary layer (BAO) with the homogeneous boundary layers at Kansas and Minnesota. Therefore, this investigation attempted to determine whether the empirical relations developed from data over flat terrain remain valid in a boundary layer which overlies an irregular terrain.

To understand the spectral behavior of the convectively unstable boundary layer, the facilities of the Boulder Atmospheric Observatory (BAO) were used. The 300 m instrumented tower surrounded by a gently rolling terrain provided the primary data base collected during the latter part of April 1978. Instrumented aircraft and a surface network which recorded various atmospheric parameters supported the tower data. Limiting the study to only well mixed, convectively unstable, daytime conditions assured a well-defined boundary layer which was easily stratified into the surface, matching, and mixed layers. The time series of the fluctuating velocity and temperature fields were obtained from the sonic anemometers and resistance thermometers mounted at each of the eight standard levels (10 m, 22 m, 50 m, 100 m, 150 m, 200 m, 250 m, 300 m) of the tower. Time series of one hour were reduced, by using fast Fourier transform (FFT) techniques, to obtain turbulence spectra at the various levels within the lowest 300 m of a daytime boundary layer.

The velocity spectra (longitudinal, lateral, and vertical components) and the temperature spectra exhibited run-to-run variations at the low frequencies. Broad generalizations were still made for each set of universal spectral curves over the irregular terrain which surrounded the BAO site. Although the velocity and temperature spectra displayed a variety of spectral shapes, the $n^{-5/3}$ power law was consistently observed at the high frequencies. In general, with increasing height above the ground the spectral intensities in the -5/3 region decreased within the surface layer and became constant in the mixed layer. Often the horizontal spectra represented a long-term trend in the low frequency region caused the spectra at all levels to merge into a single curve. At the opposite end of the spectrum, local isotropy existed at the high frequencies, since the three criteria (vanishing cospectra, -5/3 power for the logarithmic spectra, and a 4/3 ratio between the transverse and longitudinal velocity components) were observed.

The characteristics of vertical velocity spectral behavior: the decrease in the spectral intensity with frequency in the inertial subrange; the decrease in the frequency corresponding to the onset of the inertial subrange with height; and the low frequency roll-off of energy were observed in each of the nine runs chosen. The spectra representing the temperature fluctuations was characterized by two shapes, either a spectral gap caused by a strong diurnal temperature trend or a low frequency roll-off of spectral intensity when that diurnal trend was not pronounced.

The frequency corresponding to the maximum spectral value for vertical velocity, $(f_m)_w$, and temperature, $(f_m)_\theta$, were found to be equivalent within the matching layer. Consequently, the turbulent

thermal eddies within a boundary layer overlying an irregular terrain are comparable in size to the one-dimensional vertical velocity eddies. Although the rate of dissipation of turbulent kinetic energy within the surface layer agrees well with previous results obtained over smooth terrain, the mixed layer dissipation rate did not agree--more energy appeared to be lost than gained.

The spectra representing the fluctuations of the velocity and the temperature fields obeyed the surface layer and mixed layer similarity laws which were developed from and supported by data collected under homogeneous conditions. Within the surface layer no systematic behavior, as a function of z/L, was observed for the normalized u (Figure 5), v (Figure 10), or θ (Figure 25) spectra, but was evident in the normalized w spectra (Figure 15). None of the universal plots formed with mixed layer similarity rules (Figures 8, 10, 20, and 28) displayed any systematic behavior according to z/z_i. Except for the long-term trend present in the horizontal velocity spectra, the universal spectral curves representing temperature and velocity generally agreed with the spectral shapes previously found in unstable boundary layers over flat terrain. As an exception, the scatter corresponding to April's BAO normalized vertical velocity spectra in the surface layer was less than the area defined by Kansas w spectra.

7.2 Conclusions

The conclusions resulting from this study are summarized below:

1. From comparing the spectral behavior over flat terrain with the spectra representing the velocity and temperature fluctuations in an unstable boundary layer overlying an irregular terrain, one may conclude that the complications, introduced by an irregular terrain,

on spectral behavior are minimal. This is especially true with the vertical velocity spectra.

2. Unlike homogeneous boundary layers, the turbulent eddies represented by vertical velocity and temperature fluctuations were found to be of comparable size in the matching layer at the Boulder Atmospheric Observatory.

3. During convectively unstable conditions, the wavelength corresponding to the w spectral peak increases with increasing height. This investigation showed that a smooth transition could be made in the matching layer by changing the length scale used in normalizing $(\lambda_m)_w$--the Obukhov length, L, in the surface layer and the height of the lowest inversion base, z_i, in the mixed layer. Therefore, the terrain does not appear to affect the transition from surface layer to mixed layer scaling.

4. The April BAO θ spectra support Deardorff's idealized universal curves for θ within the first half of the mixed layer.

7.3 Suggestions for Further Research

This investigative study was the first of many boundary layer experiments to be conducted at the Boulder Atmospheric Observatory. The following suggestions for future research deal with both specific and general questions regarding the boundary layer over irregular terrain.

Among the specific problems, the dissipation rate of turbulent kinetic energy within the mixed layer, ψ_ε, indicated that more energy was lost than the amount of energy gained. Since this may be a consequence of an incomplete understanding of the turbulent kinetic energy processes in a mixed layer situated over an irregular terrain, further research is necessary. Another specific research problem is to study

the physical cause for the long-term trends or variations which were present in many of the horizontal velocity spectra (see Appendix A).

In general, future research should be directed to determining whether the deviations the April BAO spectra exhibited from the previously defined universal curves are consistent with all inhomogeneous unstable boundary layers--at BAO and elsewhere. What effect the uneven terrain has on a stable boundary layer is unknown and also needs investigation. A model study by Brost and Wyngaard (1978) indicates that even a slightly sloping terrain will strongly influence the stable boundary layer. The universal spectral curves from previous stable boundary layer studies (Kaimal et al., 1972; Kaimal et al., 1976) have displayed systematic behavior as a function of z/L in the surface layer and z/z_i in the mixed layer. We need to determine if this is also present in stable boundary layers overlying an irregular terrain. Finally, since the tower provides only the temporal changes in spectral behavior, the spatial variations in the spectral behavior of this type of boundary layer must be investigated. Augmenting the tower with remote sensors, instrumented aircraft, and the Portable Automatic Mesonet (PAM) allows this type of investigation to be undertaken.

REFERENCES

Brost, R. A. and Wyngaard, J. C., 1978. "A Model Study of the Stably-stratified Planetary Boundary Layer." J. Atmos. Sci., 35, 1427-1440.

Businger, J. A., Wyngaard, J. C., Izumi, Y, and Bradley, E. F., 1971. "Flux-profile Relationship in the Atmospheric Surface Layer." J. Atmos. Sci., 28, 181-189.

Busch, N. E. and Panofsky, H. A., 1968. "Recent Spectra of Atmospheric Turbulence." Quart. J. Roy. Meteor. Soc., 94, 132-148.

Cochran, W. T., Cooley, J. W., Favin, D. L., Helms, H. D., Kaenel, R. A., Lang, W. W., Maling, G. C., Nelson, D. E., Rader, C. M., and Welch, P. D., 1967. "What is the Fast Fourier Transform?" IEEE Transactions on Audio and Electracoustics, AU-15, 45-55.

Corrsin, S., 1951. "On the Spectrum of Isotropic Temperature Fluctuations in an Isotropic Turbulence." J. Appl. Physics, 22, 469-473.

Deardorff, J. W., 1978. Notes from Short Course on the Planetary Boundary Layer. Amer. Meteor. Soc., to be published as textbook.

Haugen, D. A., Kaimal, J. C., and Bradley, E. F., 1971. "An Experimental Study of Reynolds Stress and Heat Flux in the Atmospheric Surface Layer." Quart. J. Roy. Meteor. Soc., 97, 168-180.

Kaimal, J. C., 1978. "Horizontal Velocity Spectra in an Unstable Surface Layer." J. Atmos. Sci., 35, 18-24.

Kaimal, J. C., Newman, J. T., Bisberg, A., and Cole, K., 1974. "An Improved Three-component Sonic Anemometer for Investigation of Atmospheric Turbulence. Flow: its Measurement and Control in Science and Industry, Instr. Soc. of Amer., 349-359.

Kaimal, J. C., Wyngaard, J. C., and Haugen, D. A., 1968. "Deriving Power Spectra from a Three-component Sonic Anemometer." J. Appl. Meteor., 7, 827-837.

Kaimal, J. C., Wyngaard, J. C., Haugen, D. A., Coté, O. R., Izumi, Y., Caughey, S. J., and Readings, C. J., 1976. "Turbulence Structure in the Convective Boundary Layer." J. Atmos. Sci., 33, 2152-2169.

Kaimal, J. C., Wyngaard, J. C., Izumi, Y., and Coté, O. R., 1972. "Spectral Characteristics of Surface-layer Turbulence." Quart. J. Roy. Meteor. Soc., 98, 563-589.

Monin, A. S. and Obukhov, A. M., 1954. "Basic Laws of Turbulent Mixing in the Ground Layer of the Atmosphere." Tr. Geofiz. Inst. Akad. Nauk. SSSR, 151, 163-187.

Obukhov, A. M., 1946. "Turbulence in the Atmosphere with Inhomogeneous Temperature." Tr. Geofiz. Inst. Akad. Nauk. SSSR, 1, 95-115.

Panofsky, H. A., 1969. "The Spectrum of Temperature." Radio Sci., 4, 1143-1146.

Panofsky, H. A., 1978. "Matching in the Convective Planetary Boundary Layer." J. Atmos. Sci., 35, 272-276.

Panofsky, H. A. and McCormick, R. A., 1960. "The Spectrum of Vertical Velocity near the Surface." Quart. J. Roy. Meteor. Soc., 86, 495-503.

Taylor, G. I., 1938. "The Spectrum of Turbulence." Proc. Roy. Soc., A164, 476-490.

Wyngaard, J. C. and Coté, O. R., 1971. "The Budgets of Turbulent Kinetic Energy and Temperature Variance in the Atmospheric Surface Layer." J. Atmos. Sci., 28, 190-121.

Wyngaard, J. C., Coté, O. R., and Izumi, Y., 1971. "Local Free Convection, Similarity, and the Budgets of Shear Stress and Heat Flux." J. Atmos. Sci., 28, 1171-1182.

APPENDIX A

SPECTRAL PLOTS OF RUNS CHOSEN FOR ANALYSIS

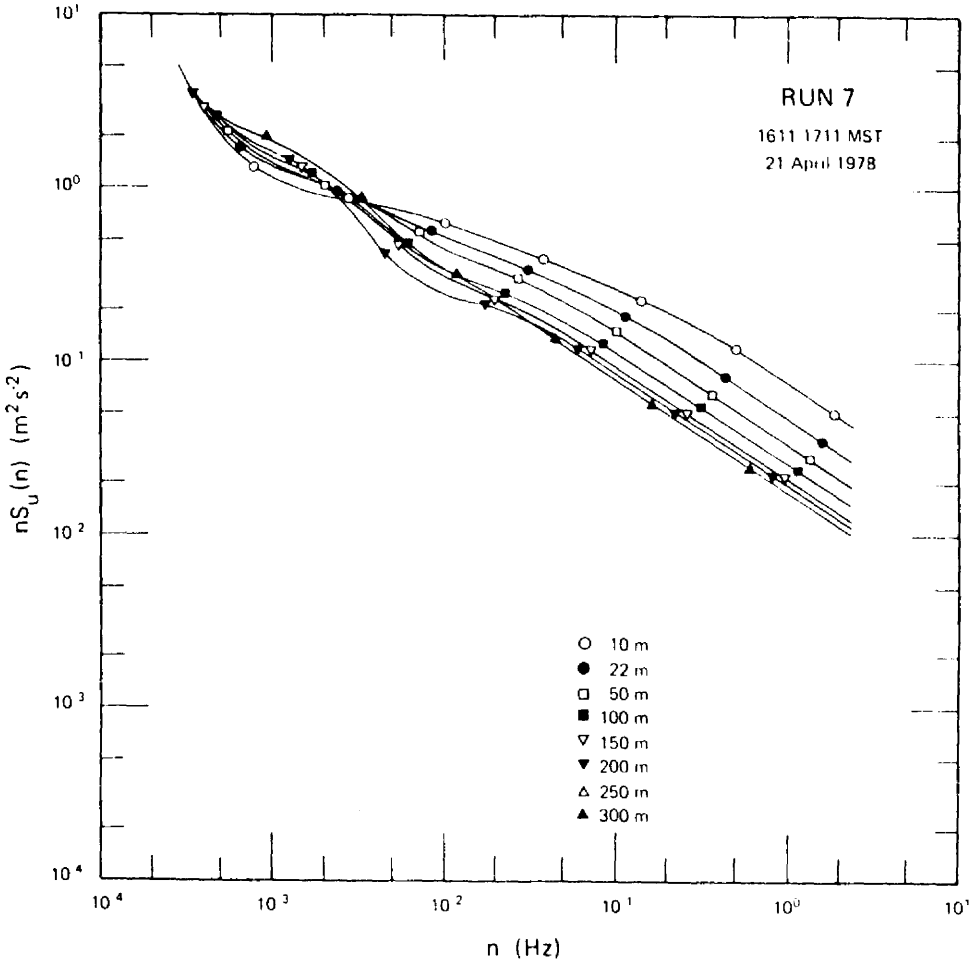

Figure 31. Longitudinal velocity spectra for Run 7.

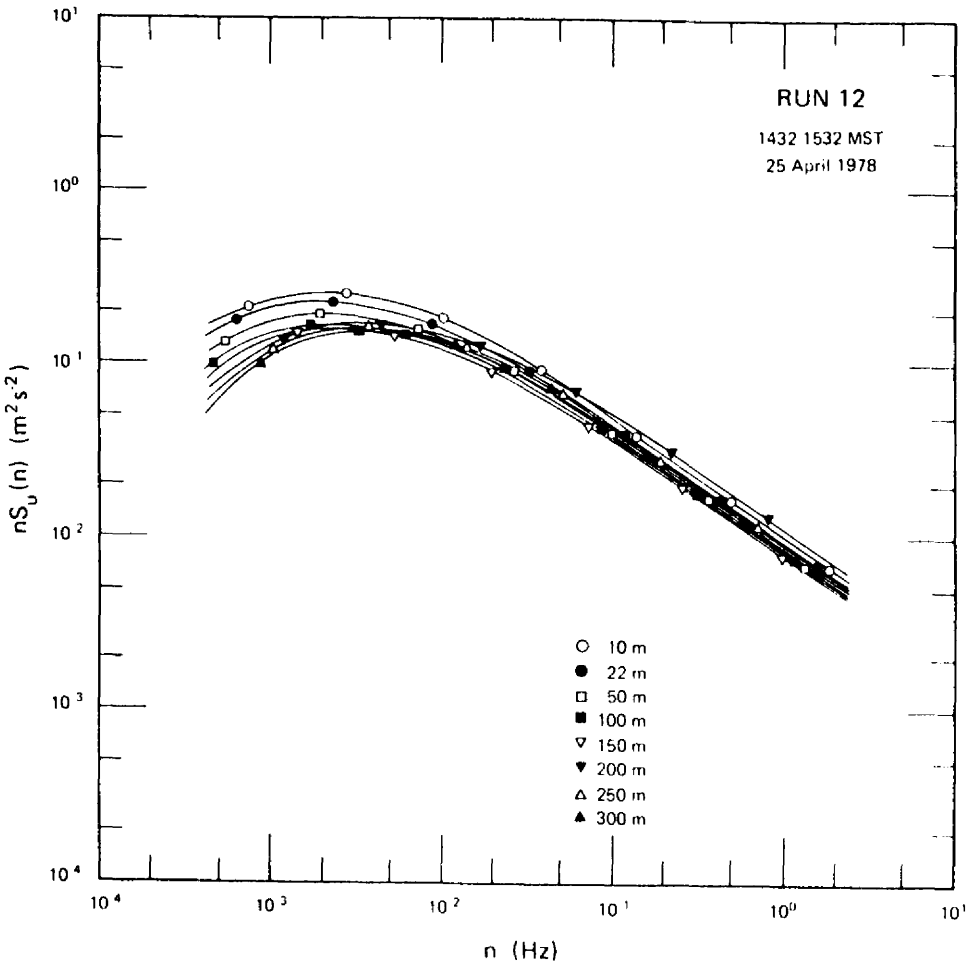

Figure 32. Longitudinal velocity spectra for Run 12.

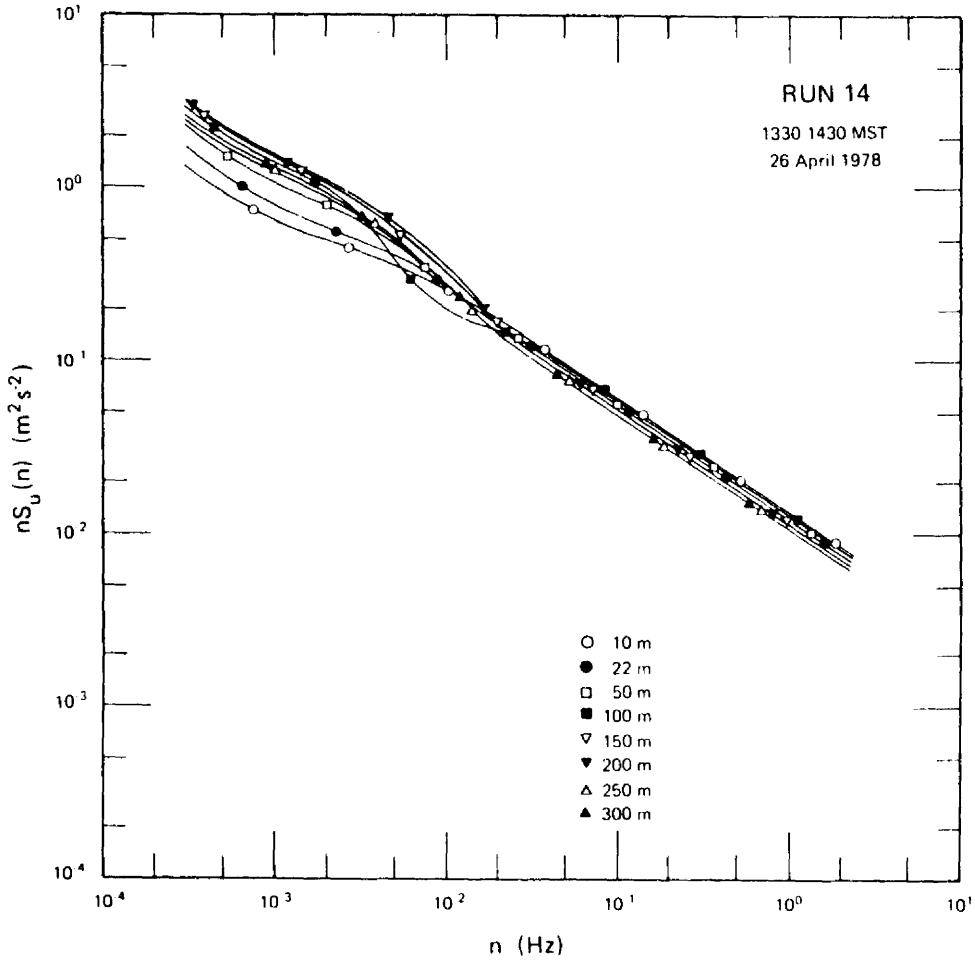

Figure 33. Longitudinal velocity spectra for Run 14.

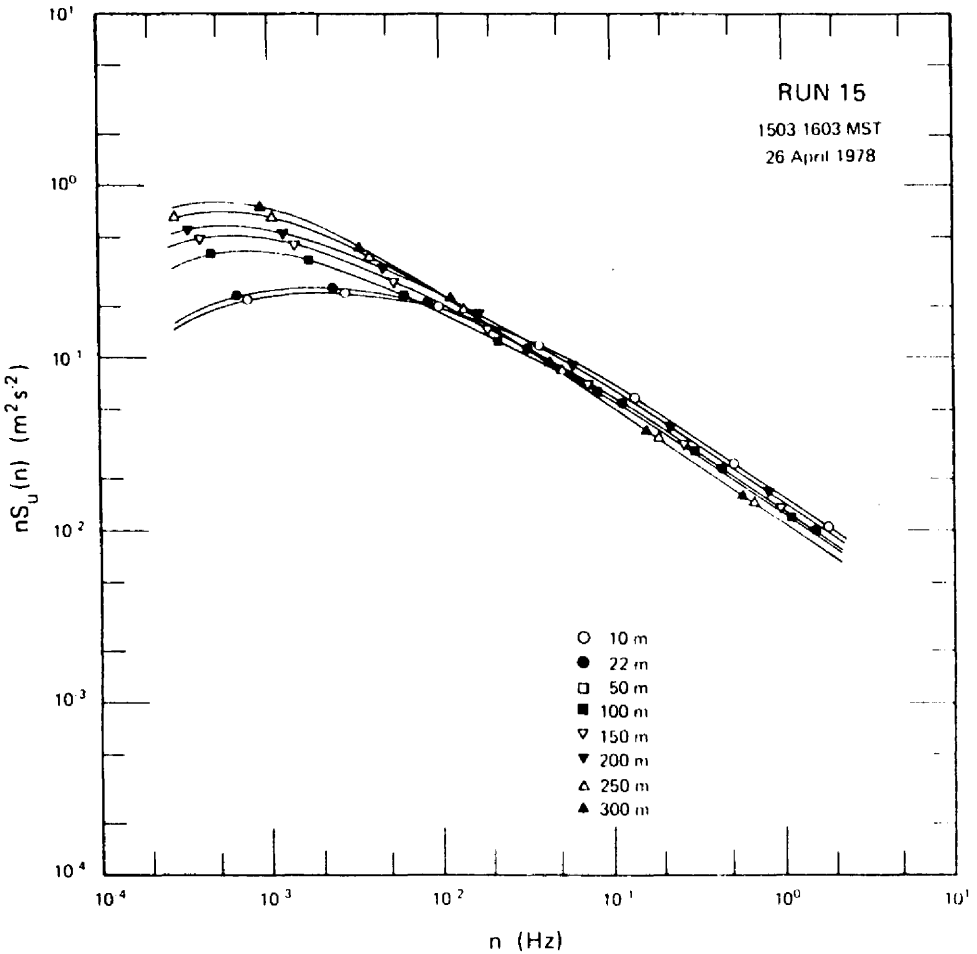

Figure 34. Longitudinal velocity spectra for Run 15.

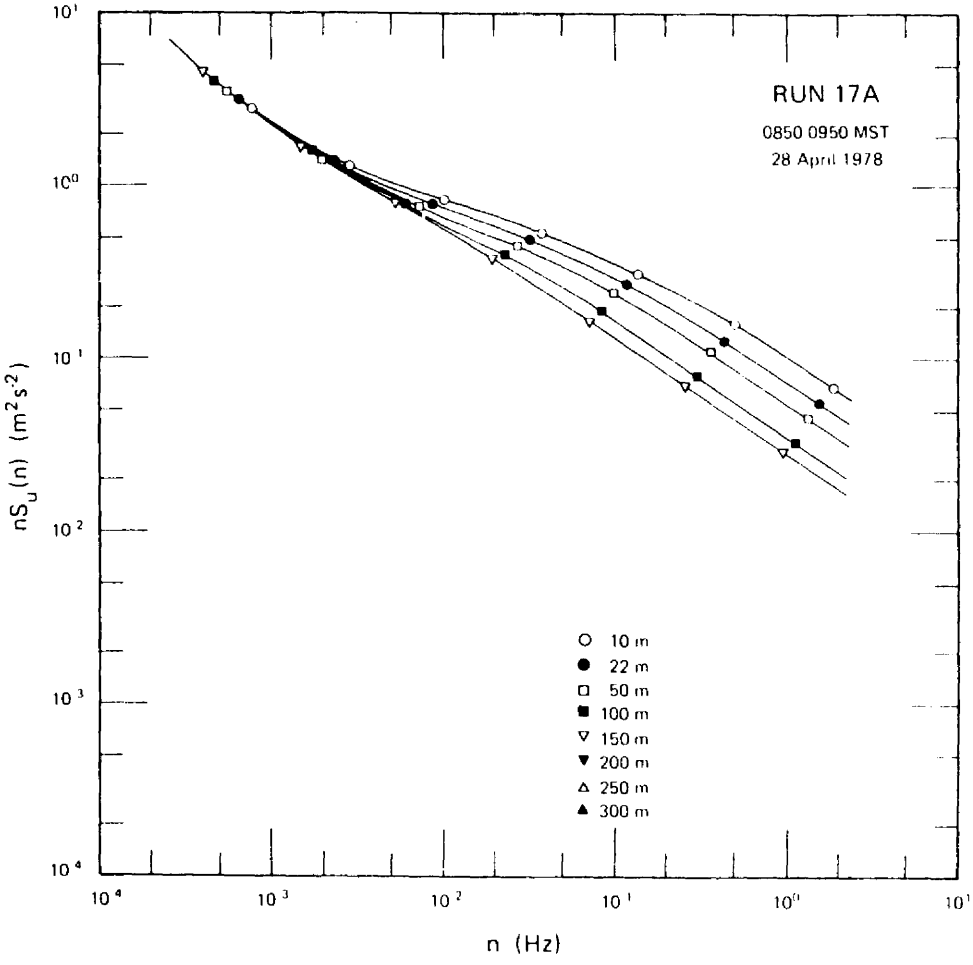

Figure 35. Longitudinal velocity spectra for Run 17A.

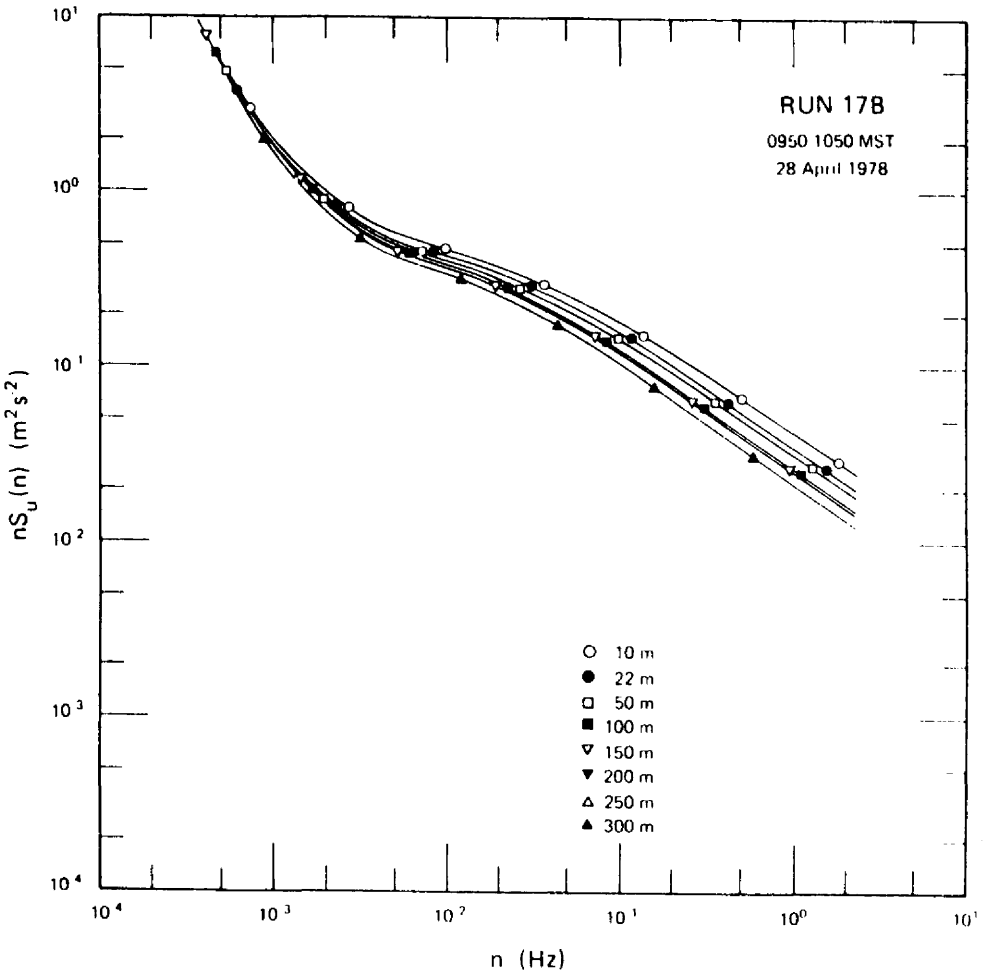

Figure 36. Longitudinal velocity spectra for Run 17B.

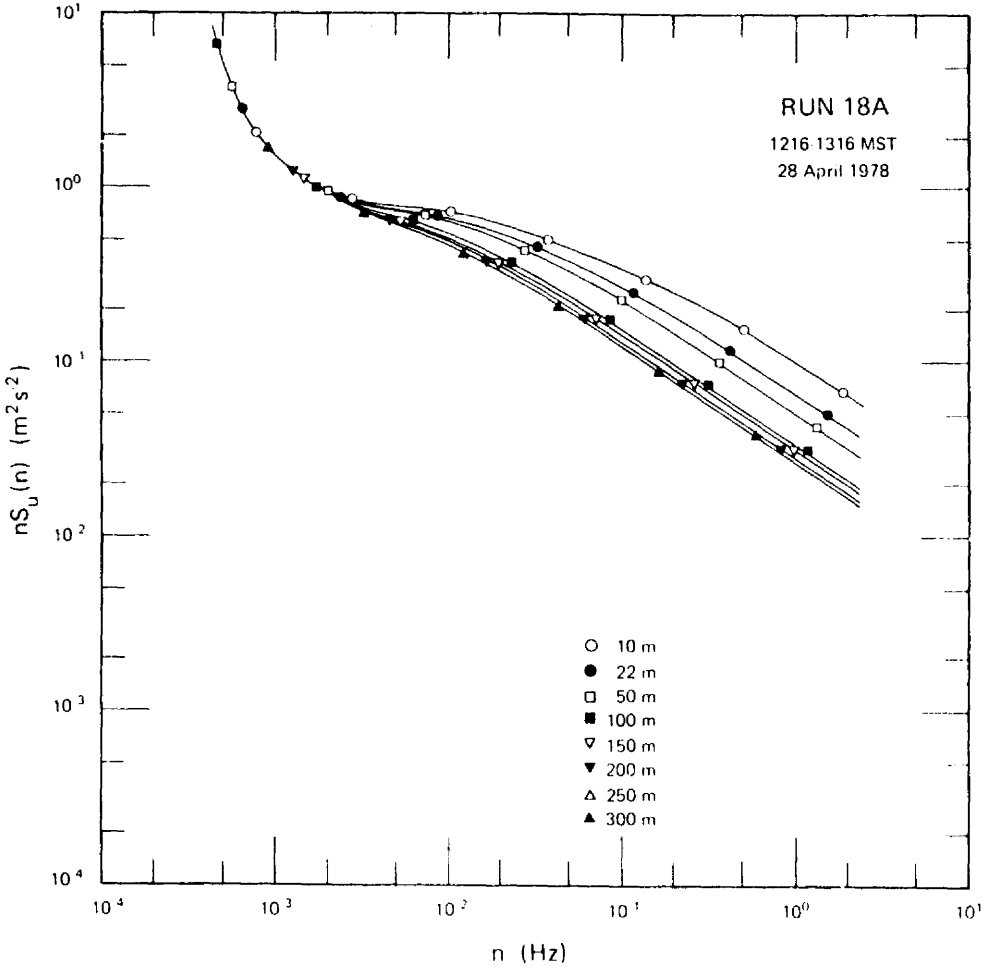

Figure 37. Longitudinal velocity spectra for Run 18A.

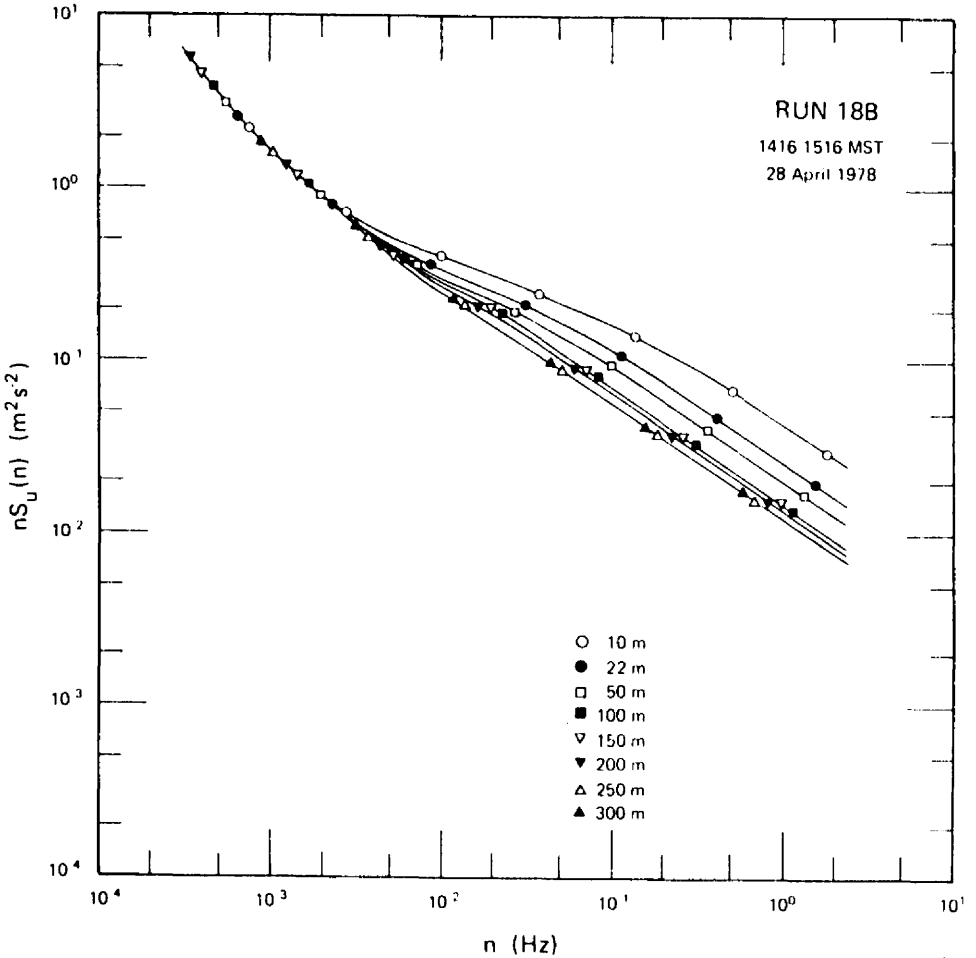

Figure 38. Longitudinal velocity spectra for Run 18B.

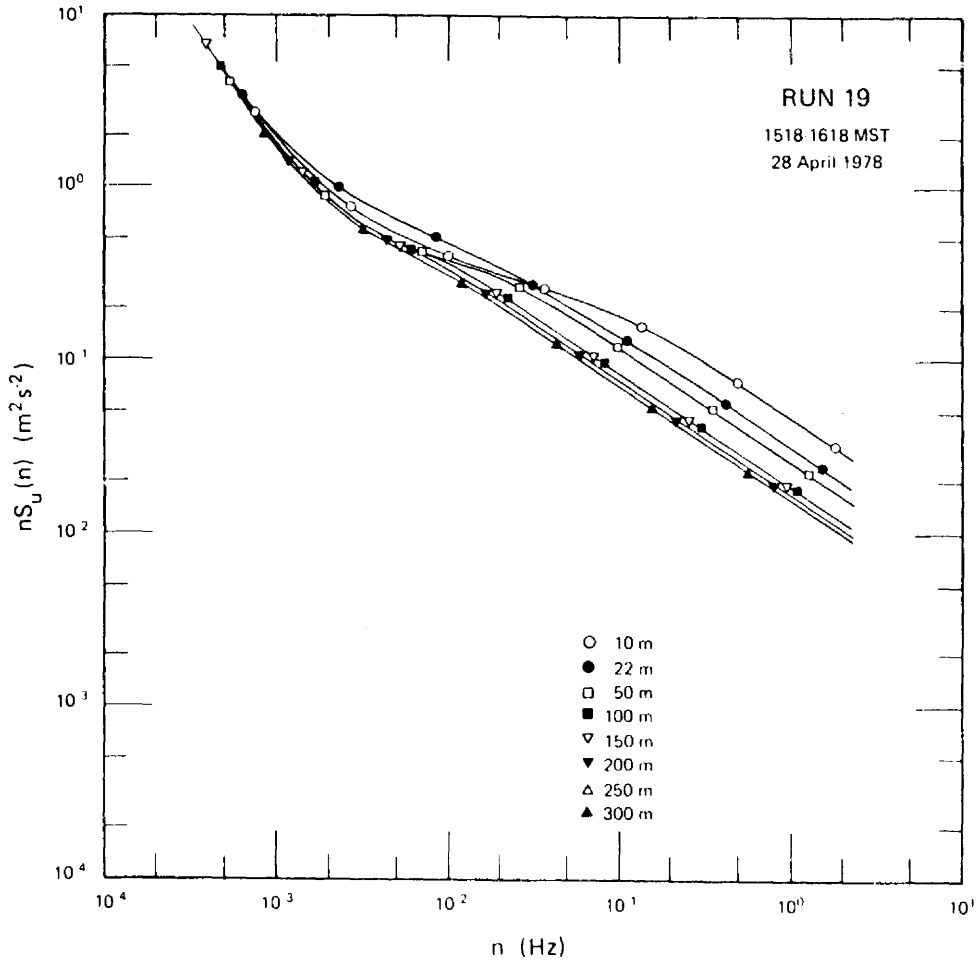

Figure 39. Longitudinal velocity spectra for Run 19.

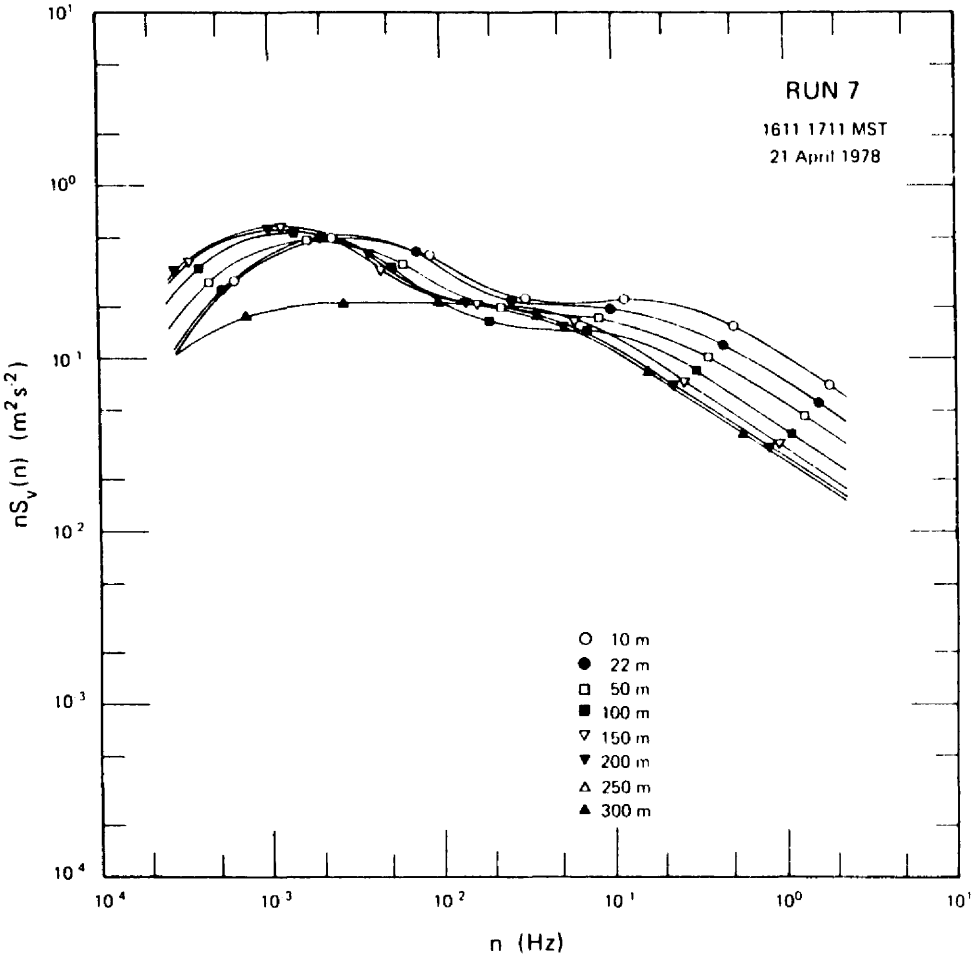

Figure 40. Lateral velocity spectra for Run 7.

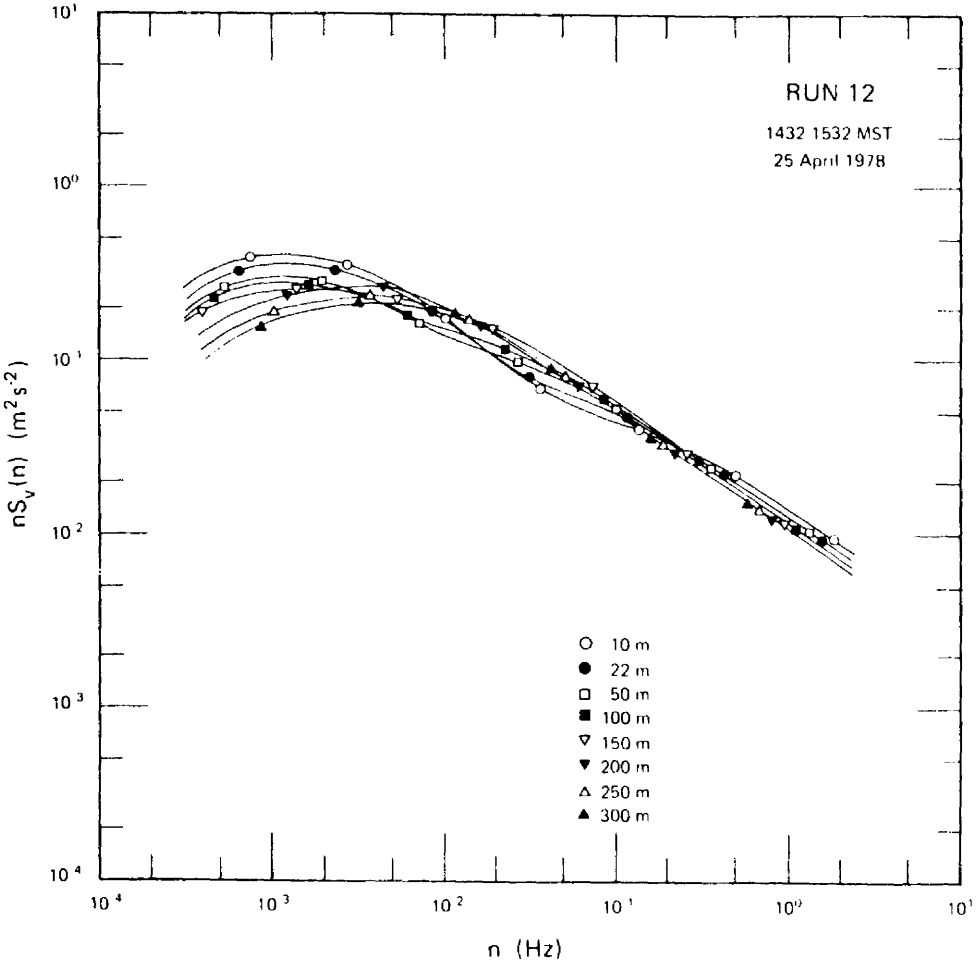

Figure 41. Lateral velocity spectra for Run 12.

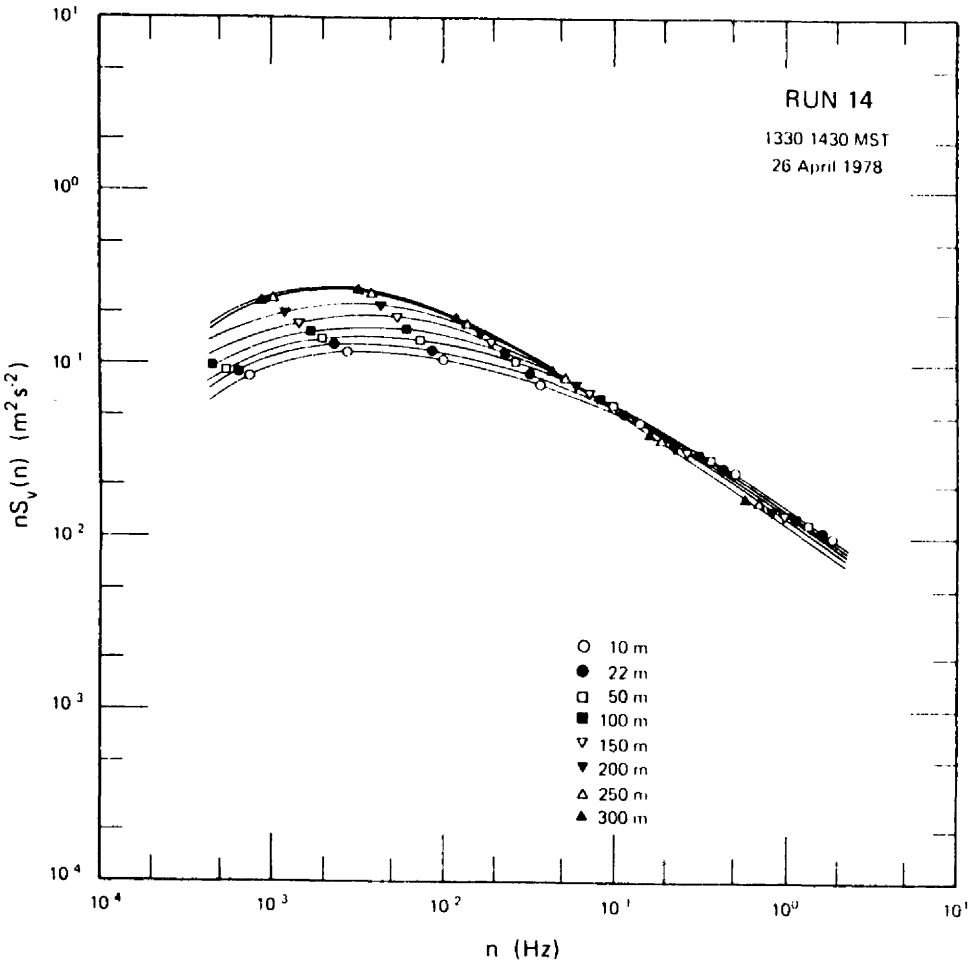

Figure 42. Lateral velocity spectra for Run 14.

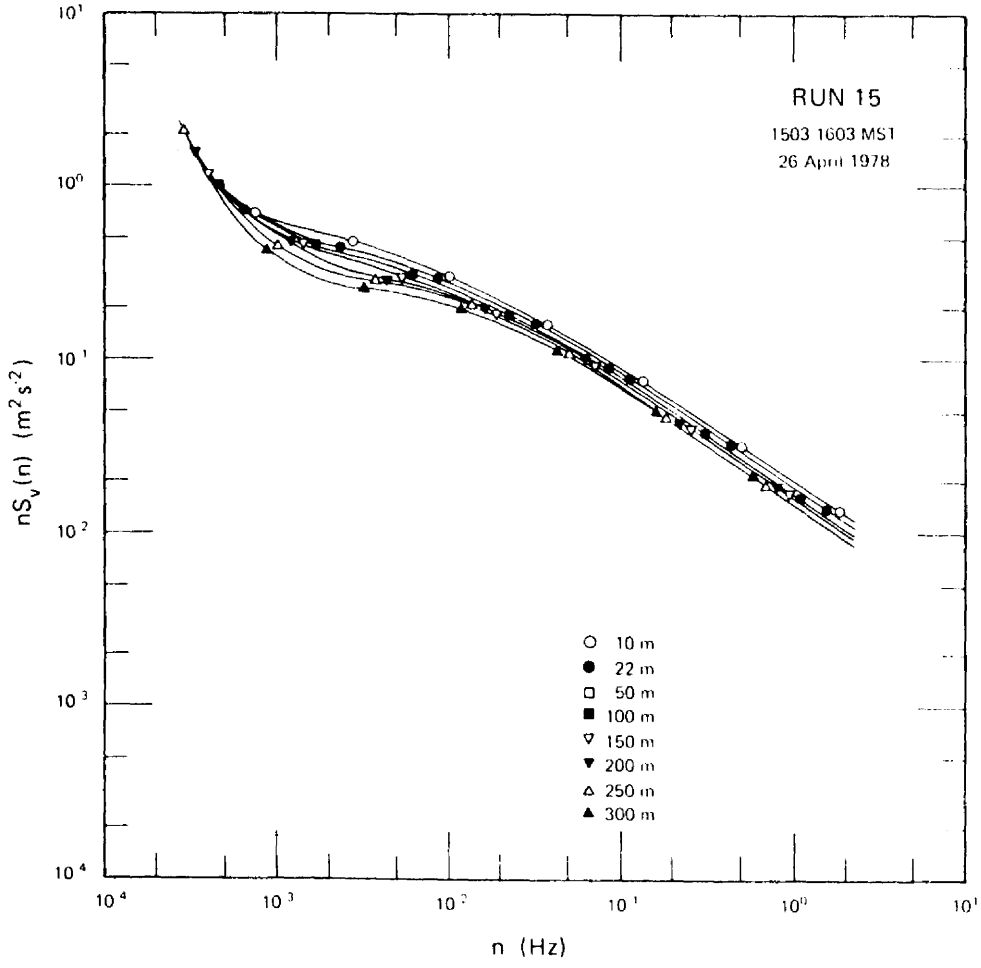

Figure 43. Lateral velocity spectra for Run 15.

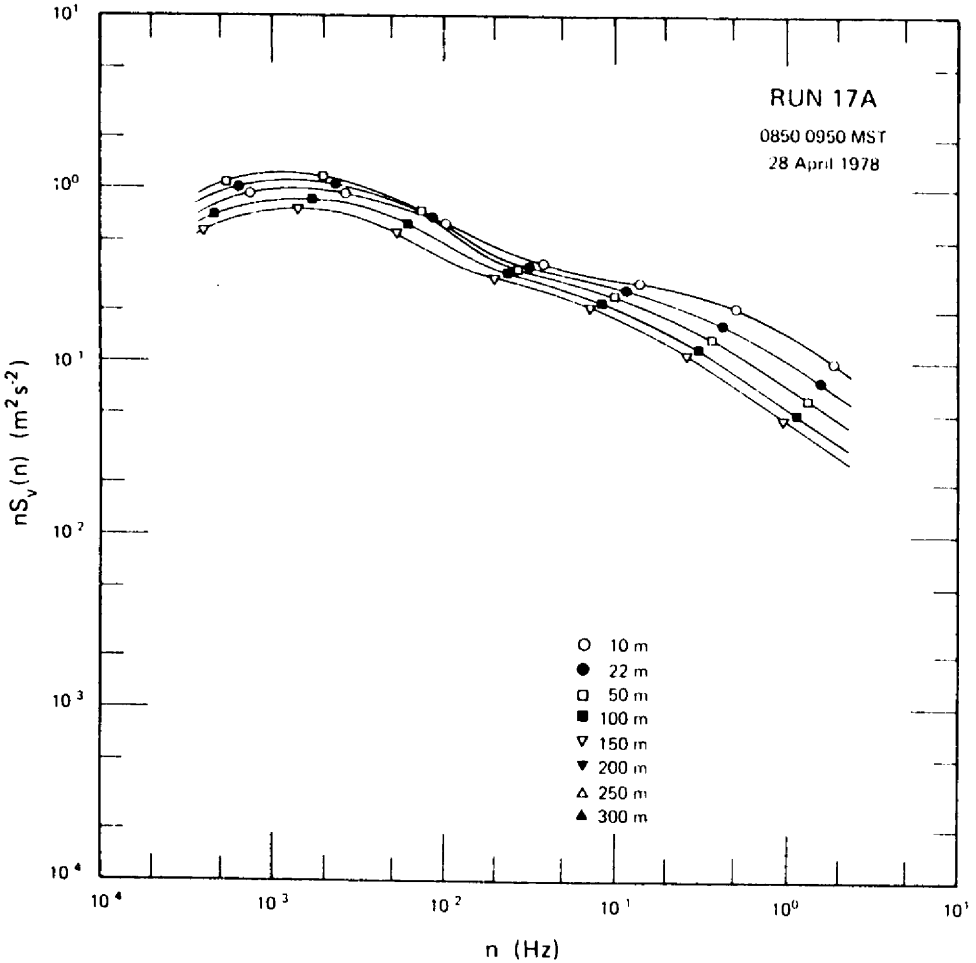

Figure 44. Lateral velocity spectra for Run 17A.

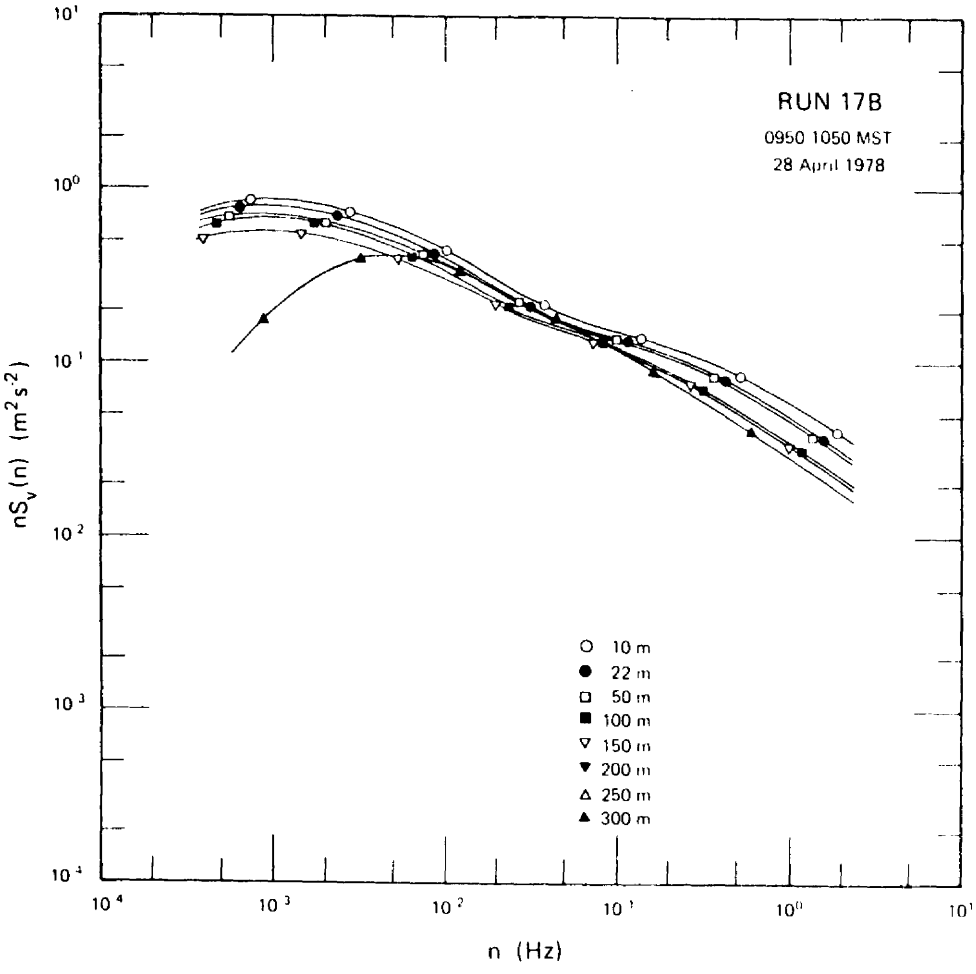

Figure 45. Lateral velocity spectra for Run 17B.

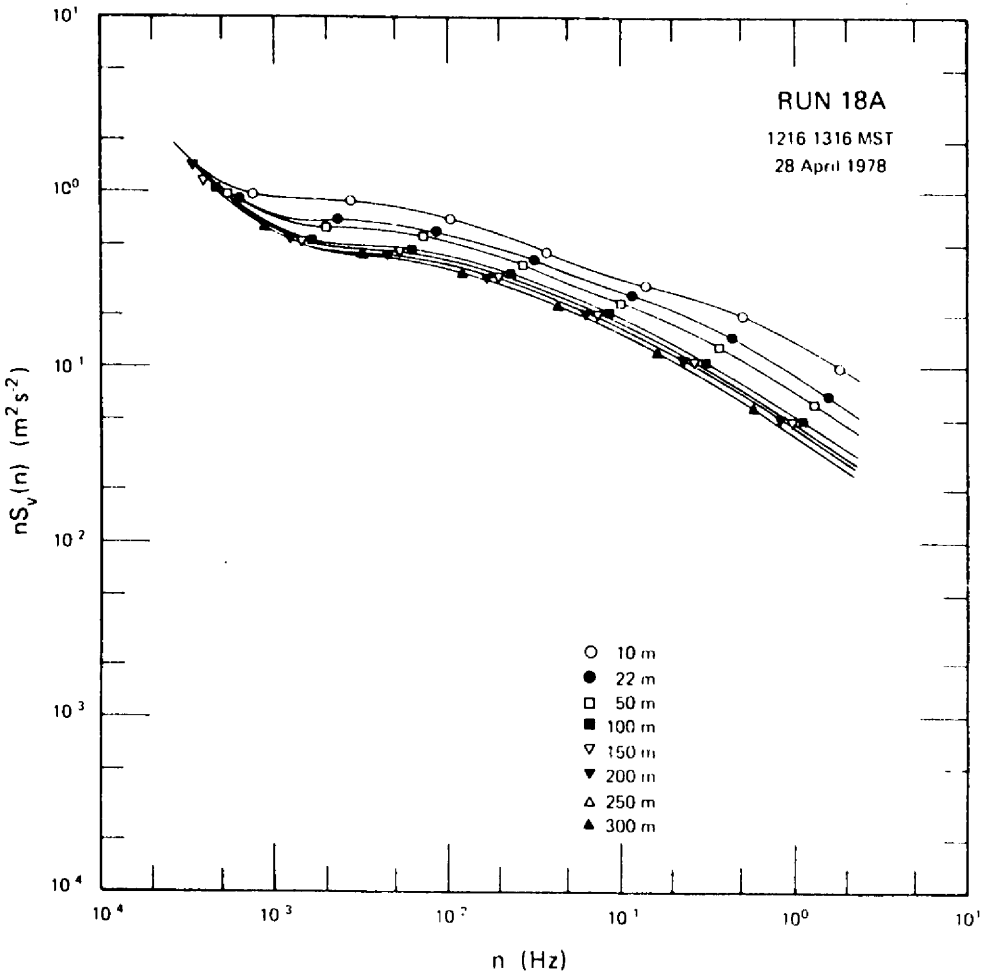

Figure 46. Lateral velocity spectra for Run 18A.

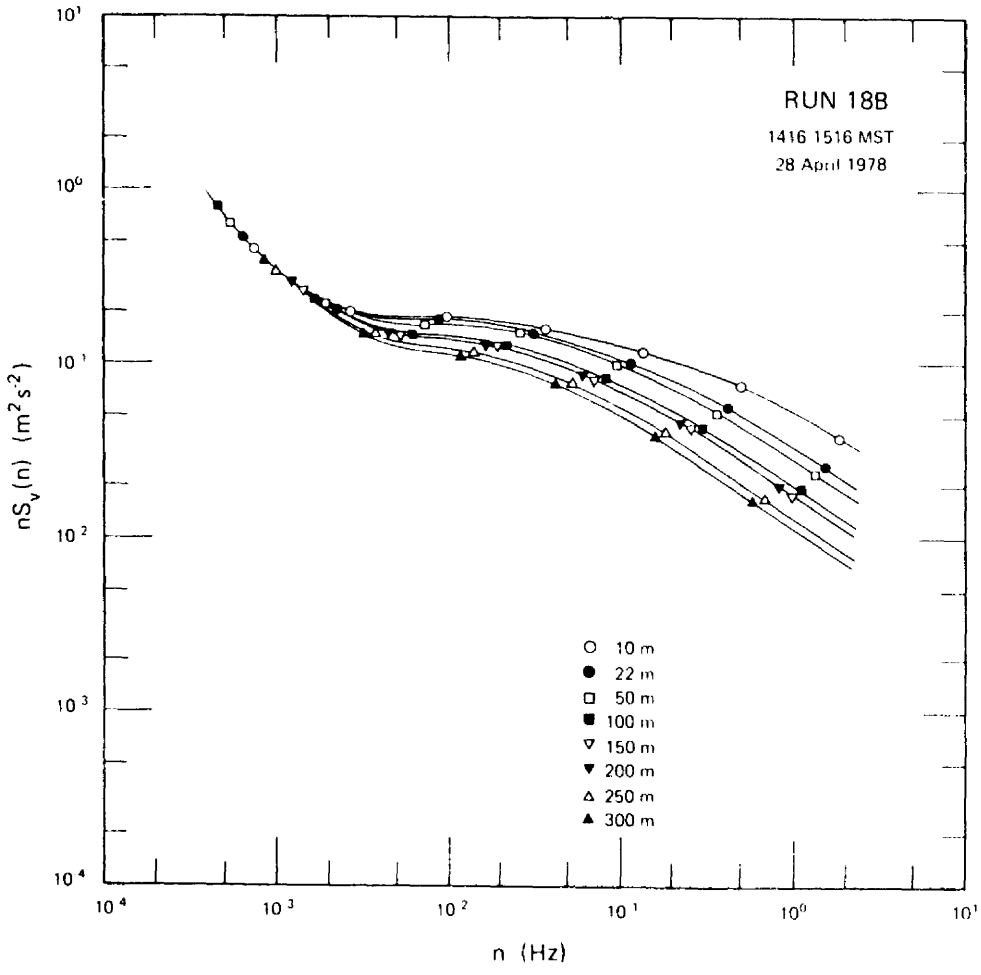

Figure 47. Lateral velocity spectra for Run 18B.

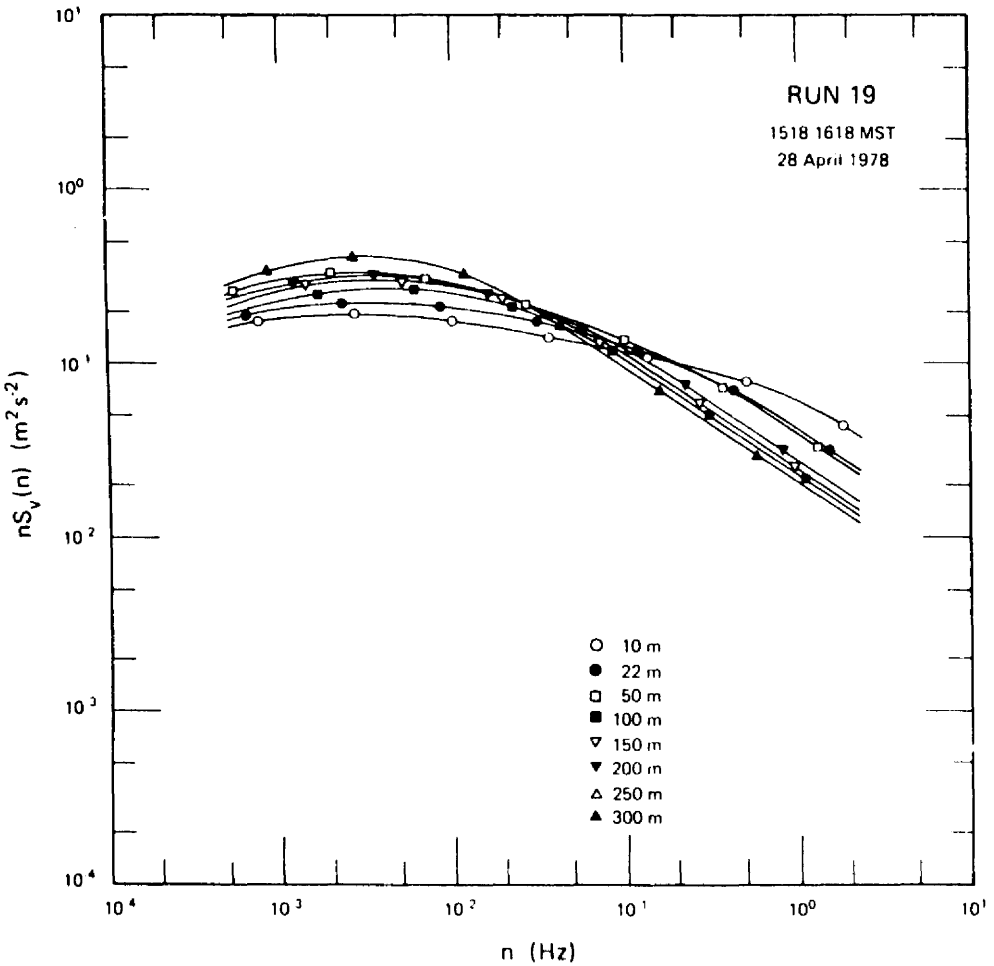

Figure 48. Lateral velocity spectra for Run 19.

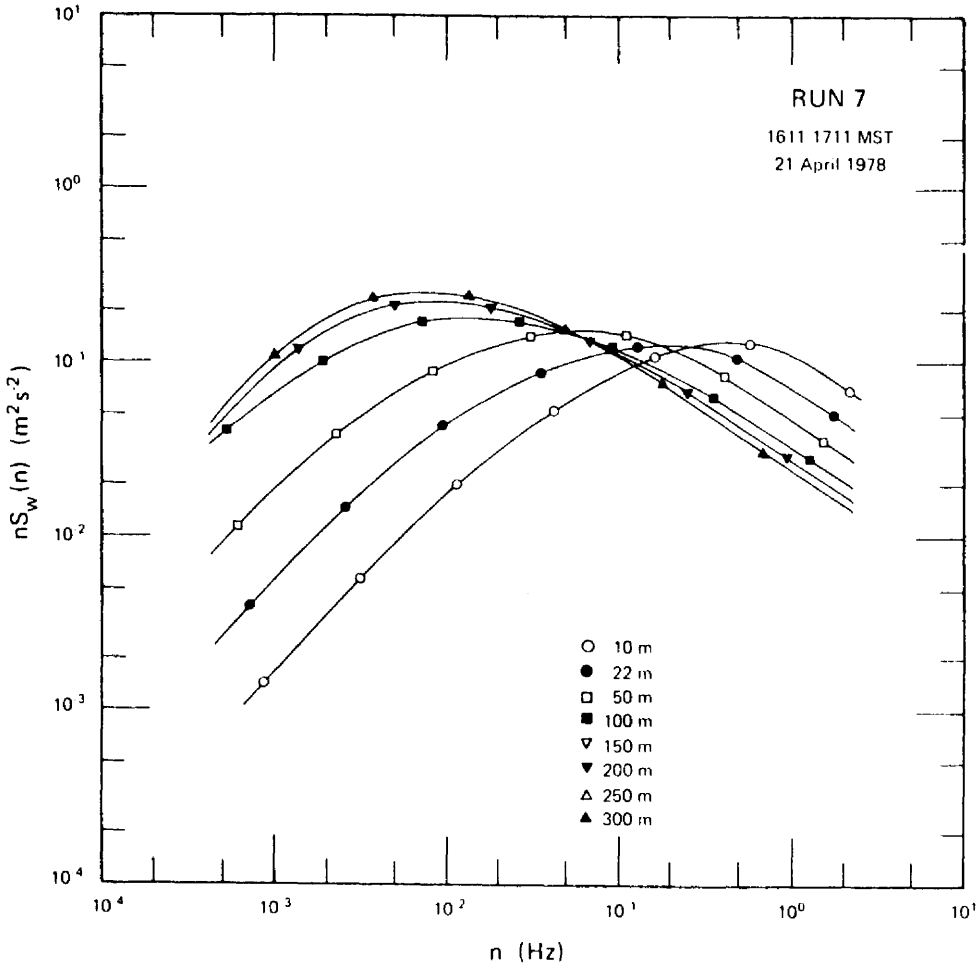

Figure 49. Vertical velocity spectra for Run 7.

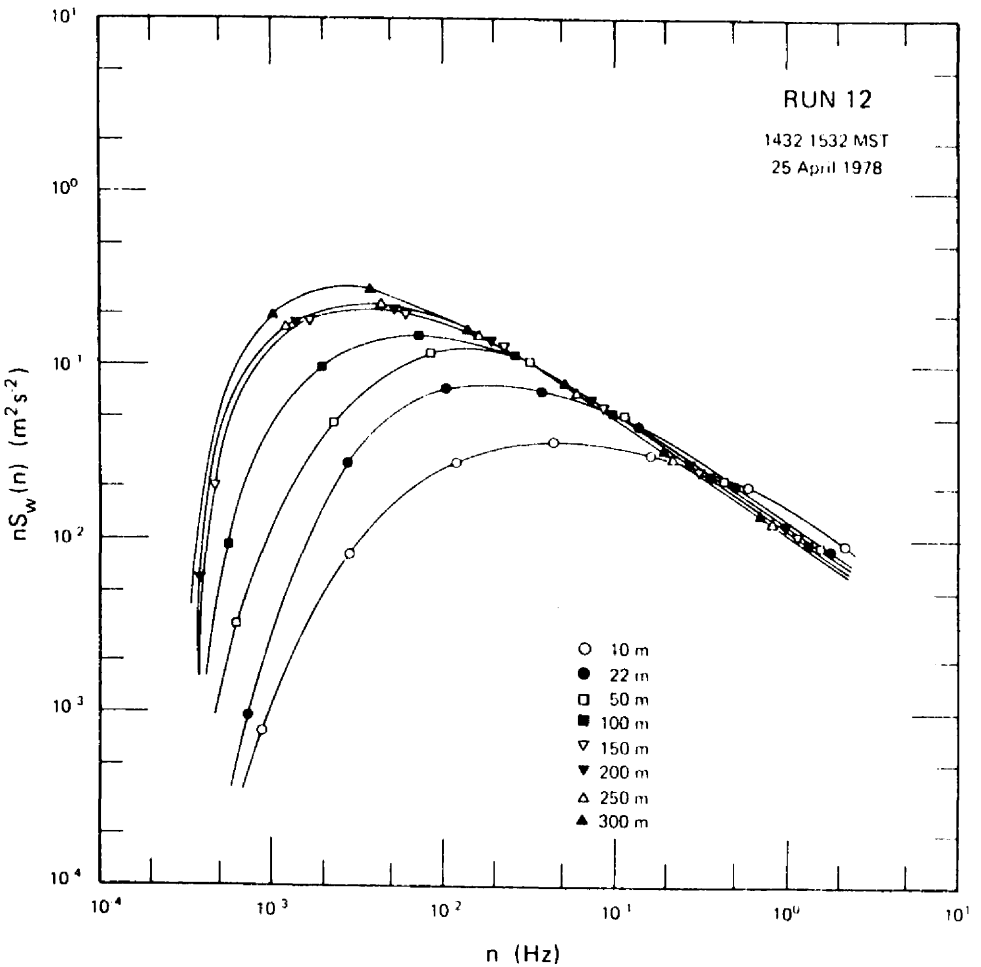

Figure 50. Vertical velocity spectra for Run 12.

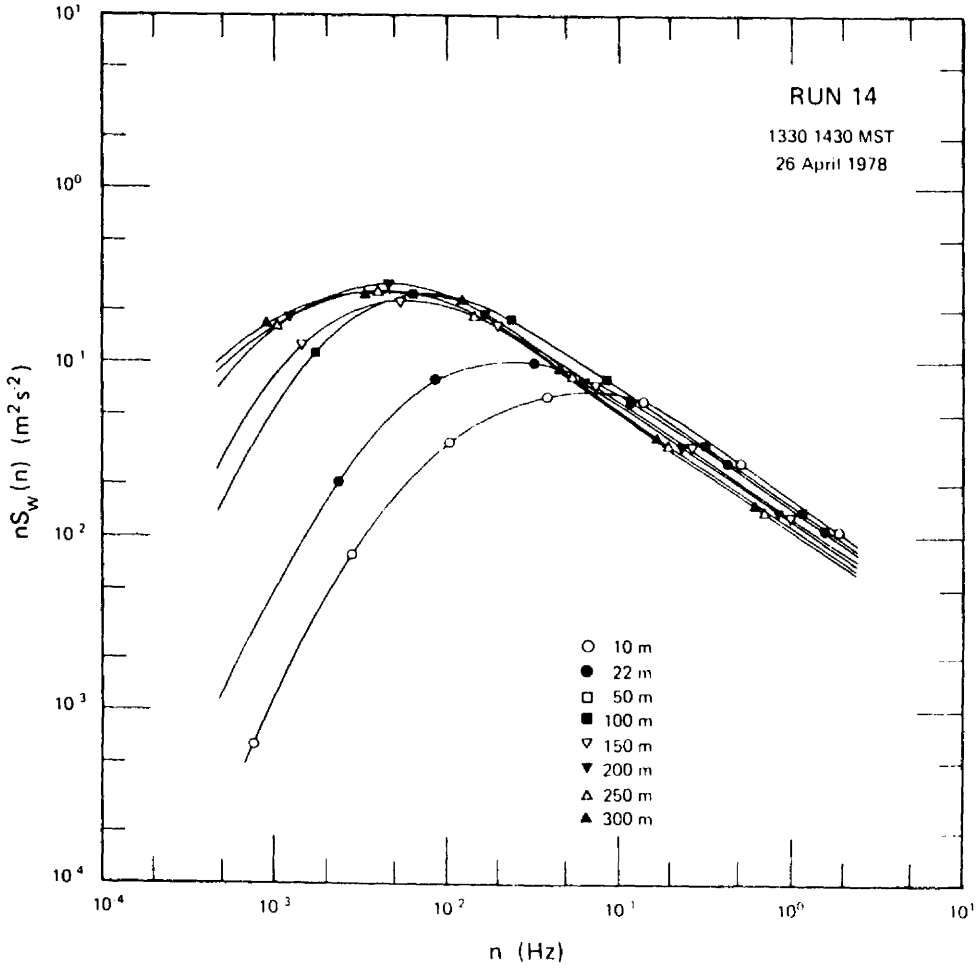

Figure 51. Vertical velocity spectra for Run 14.

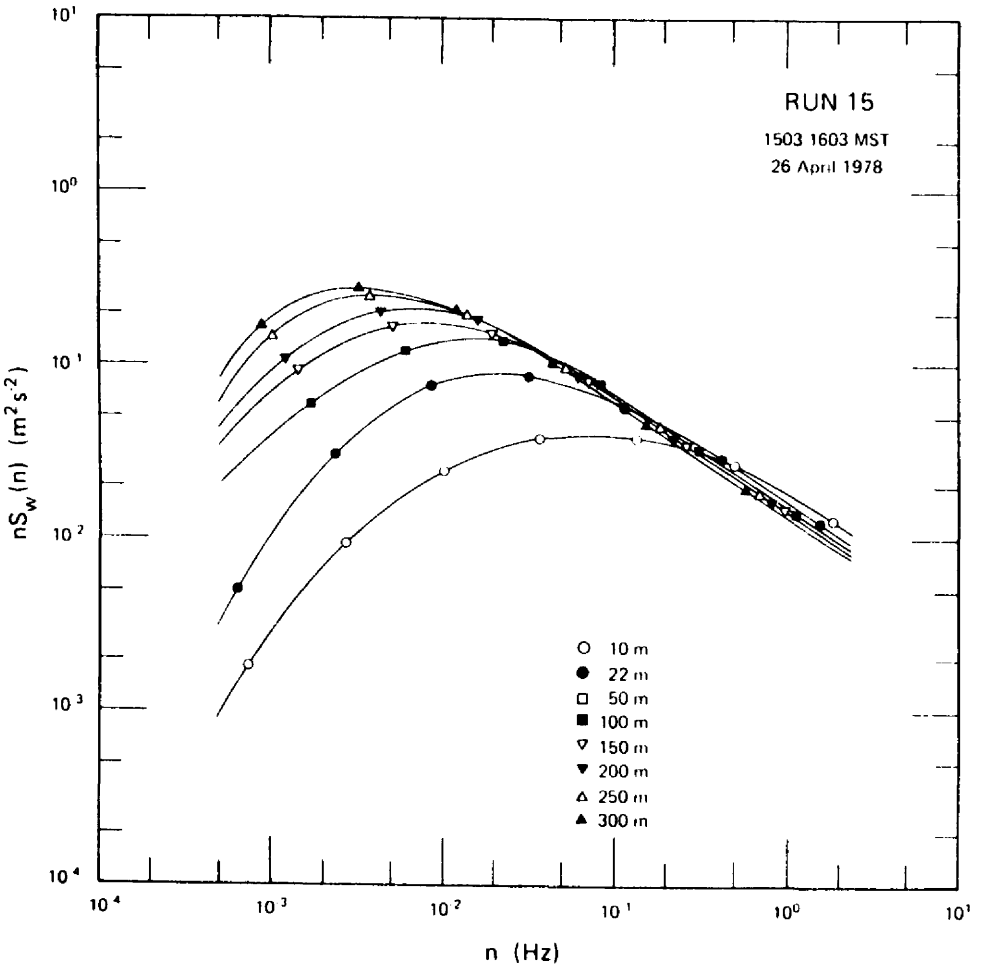

Figure 52. Vertical velocity spectra for Run 15.

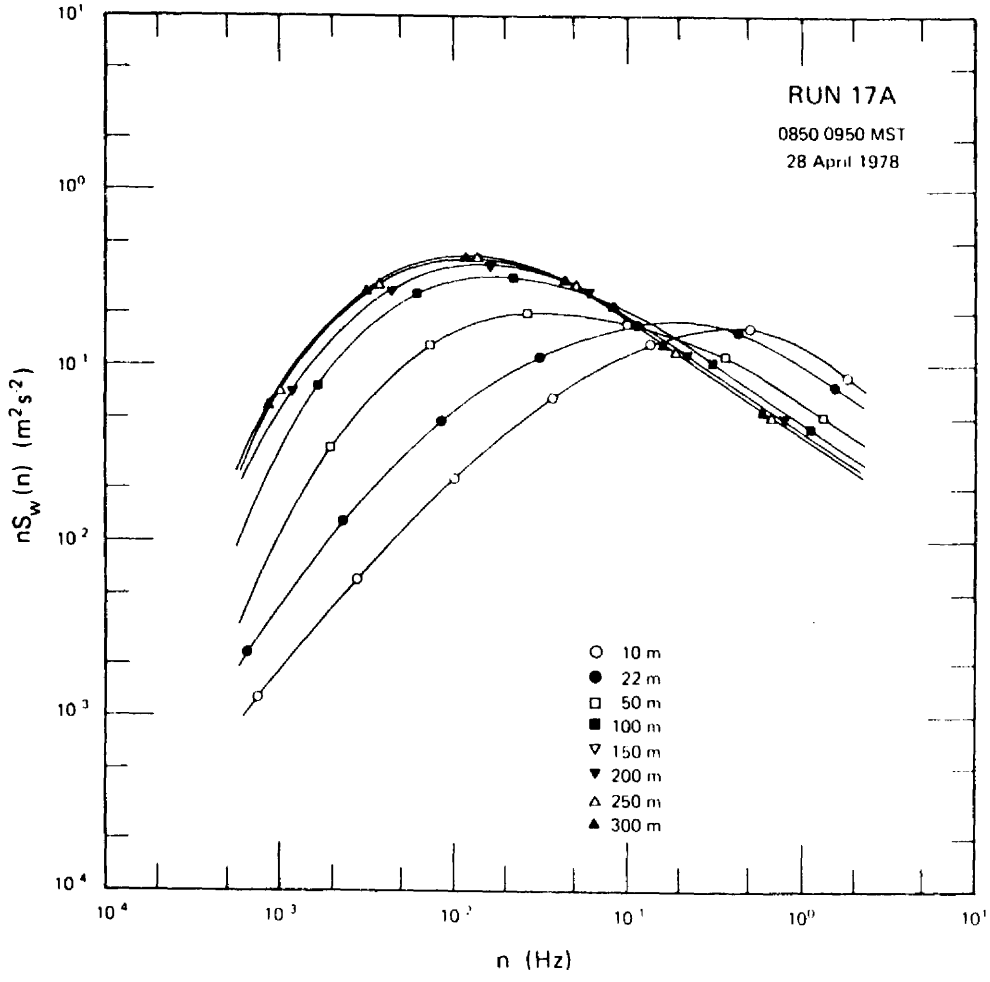

Figure 53. Vertical velocity spectra for Run 17A.

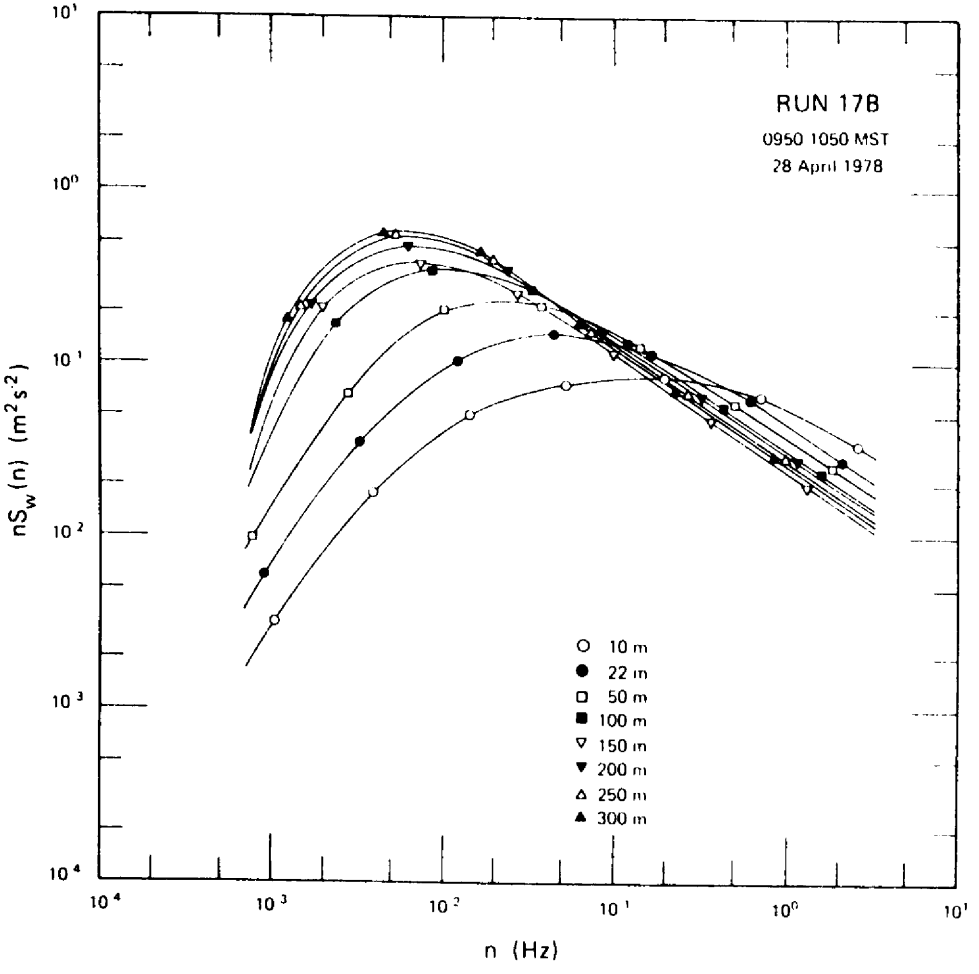

Figure 54. Vertical velocity spectra for Run 17B.

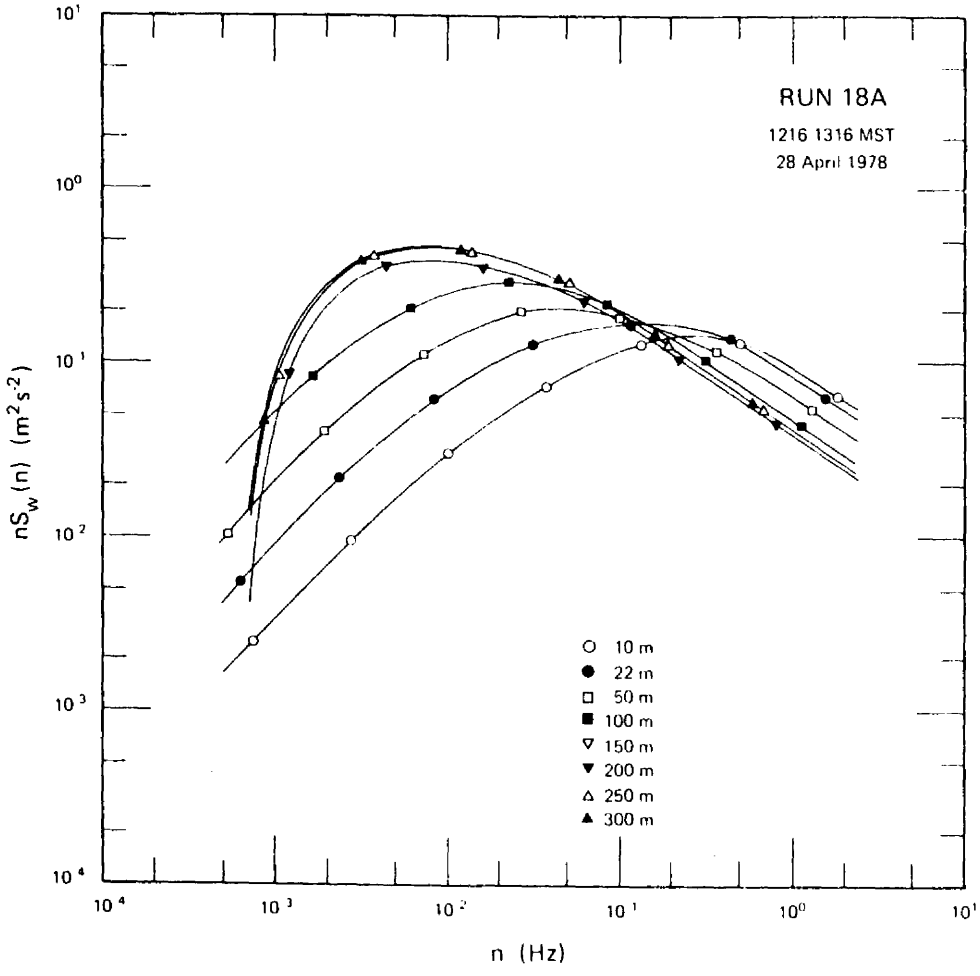

Figure 55. Vertical velocity spectra for Run 18A.

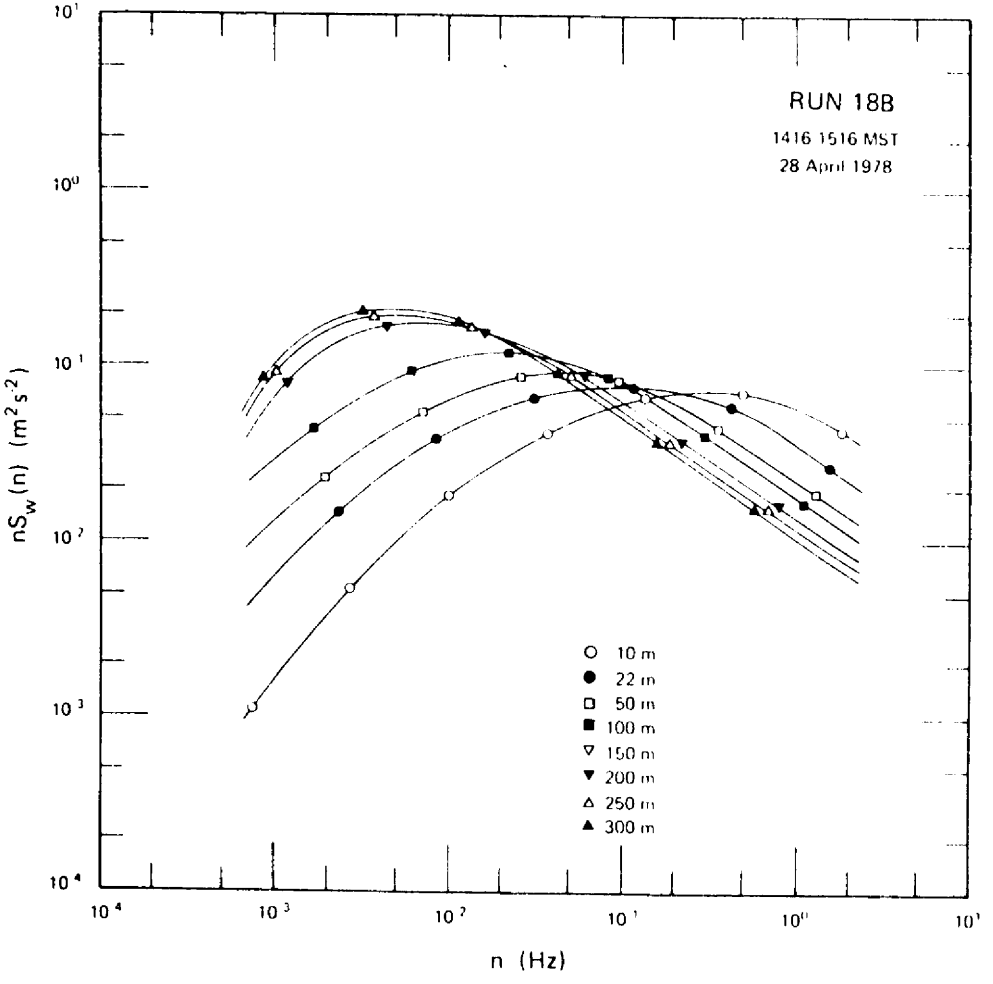

Figure 56. Vertical velocity spectra for Run 18B.

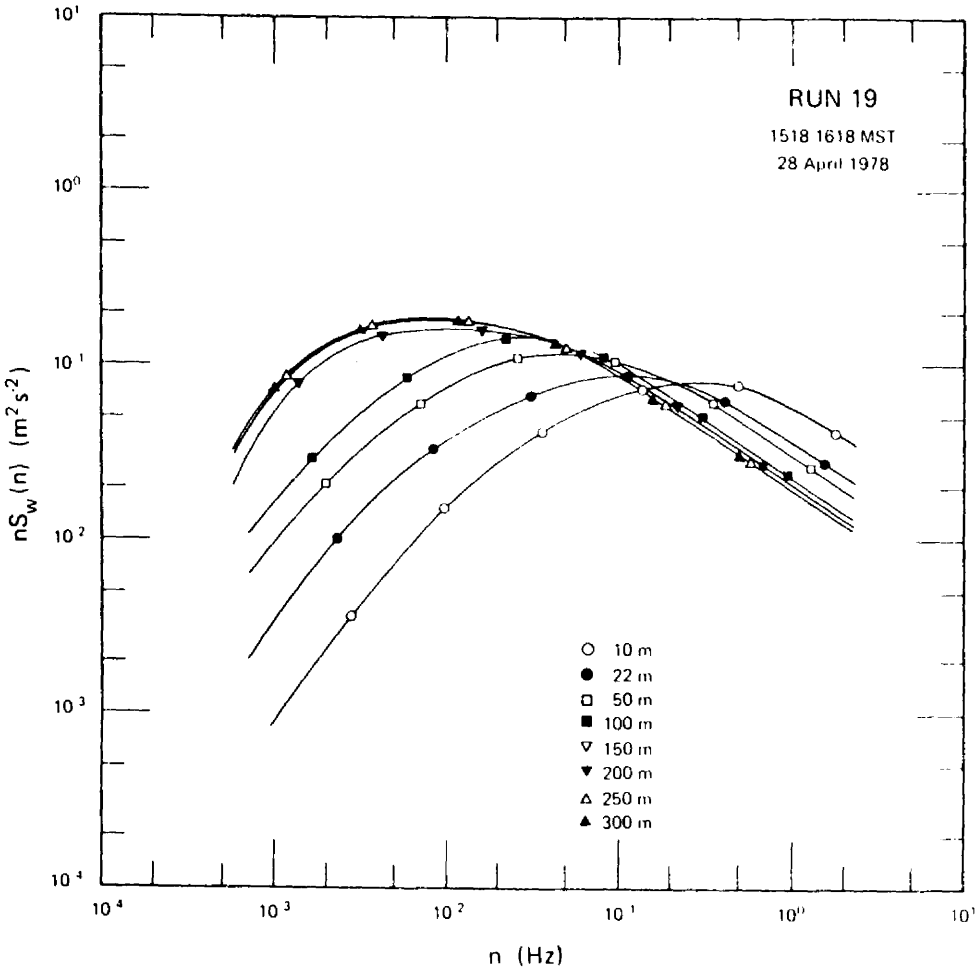

Figure 57. Vertical velocity spectra for Run 19.

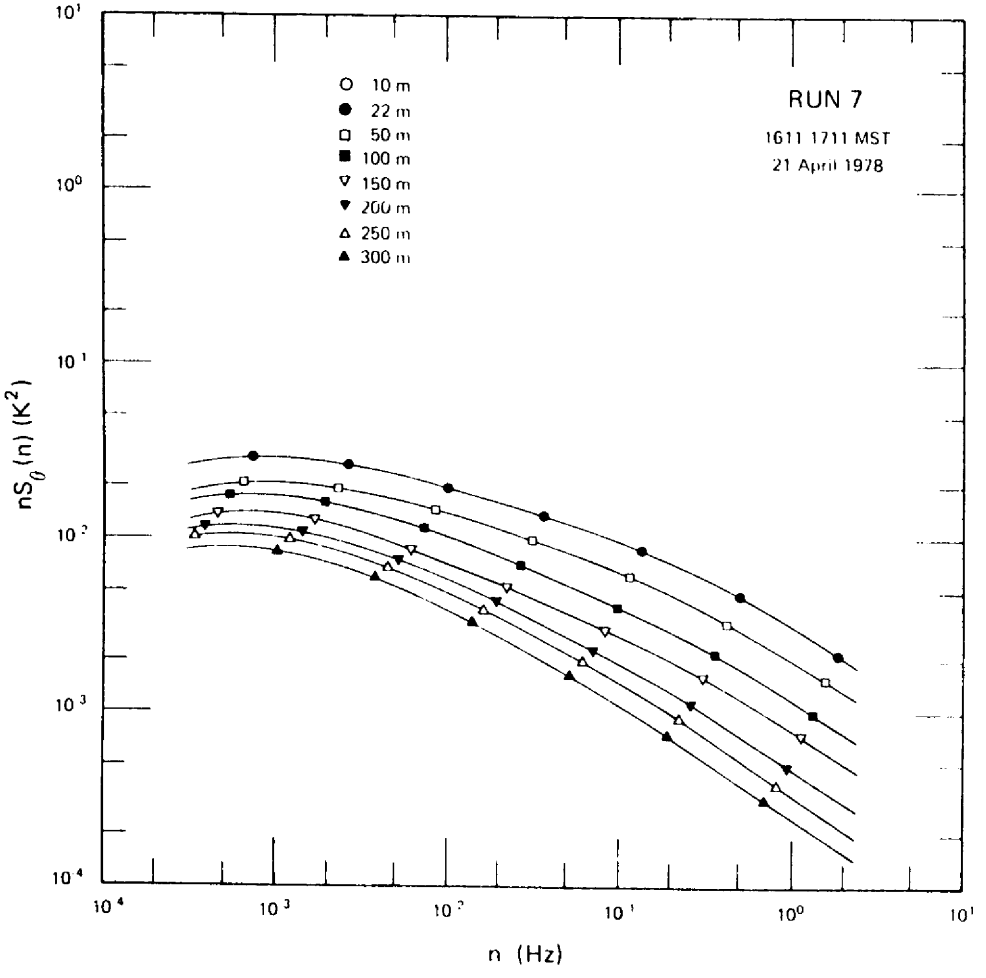

Figure 58. Temperature spectra for Run 7.

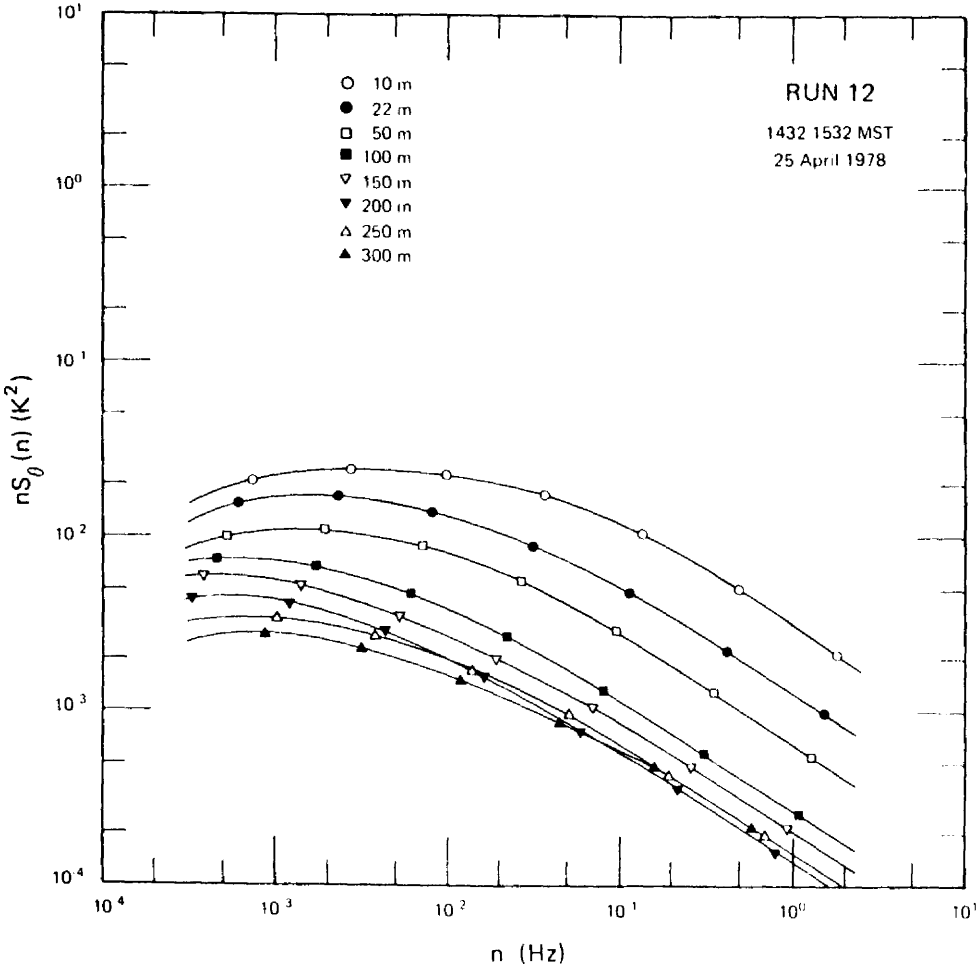

Figure 59. Temperature spectra for Run 12.

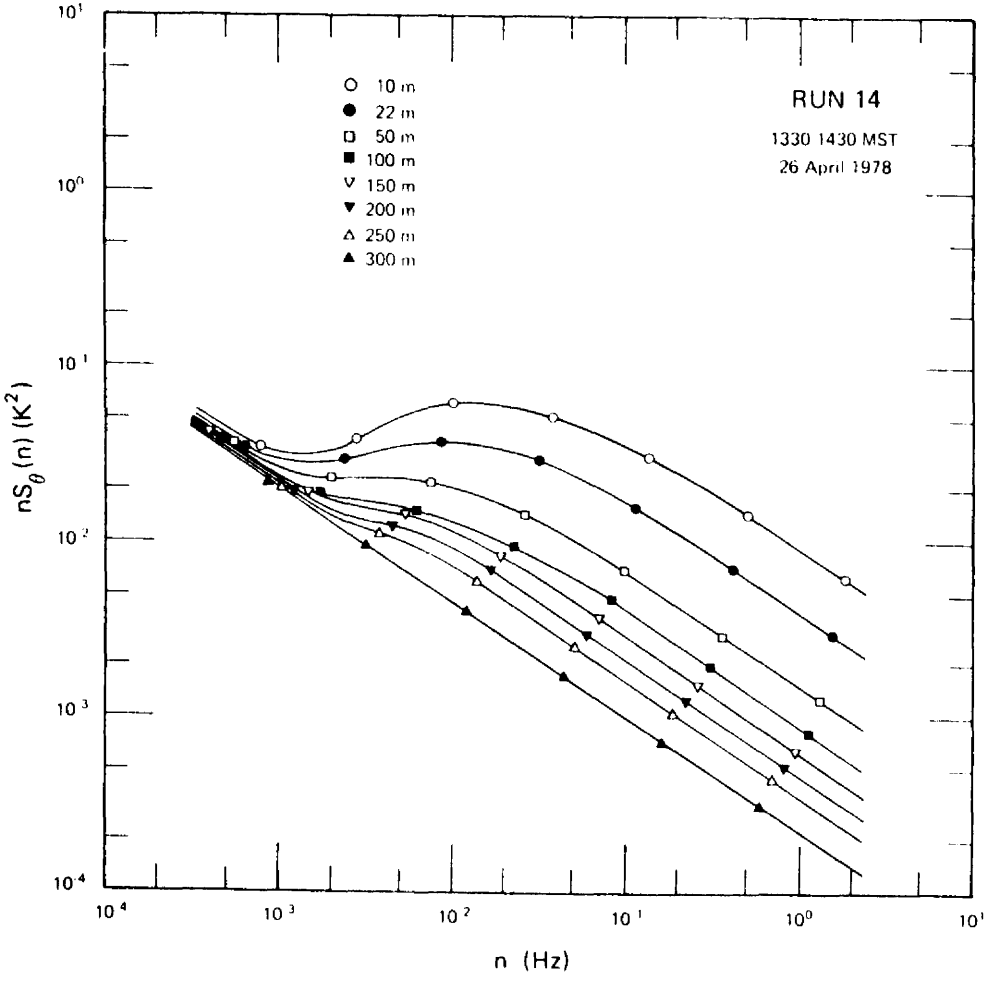

Figure 60. Temperature spectra for Run 14.

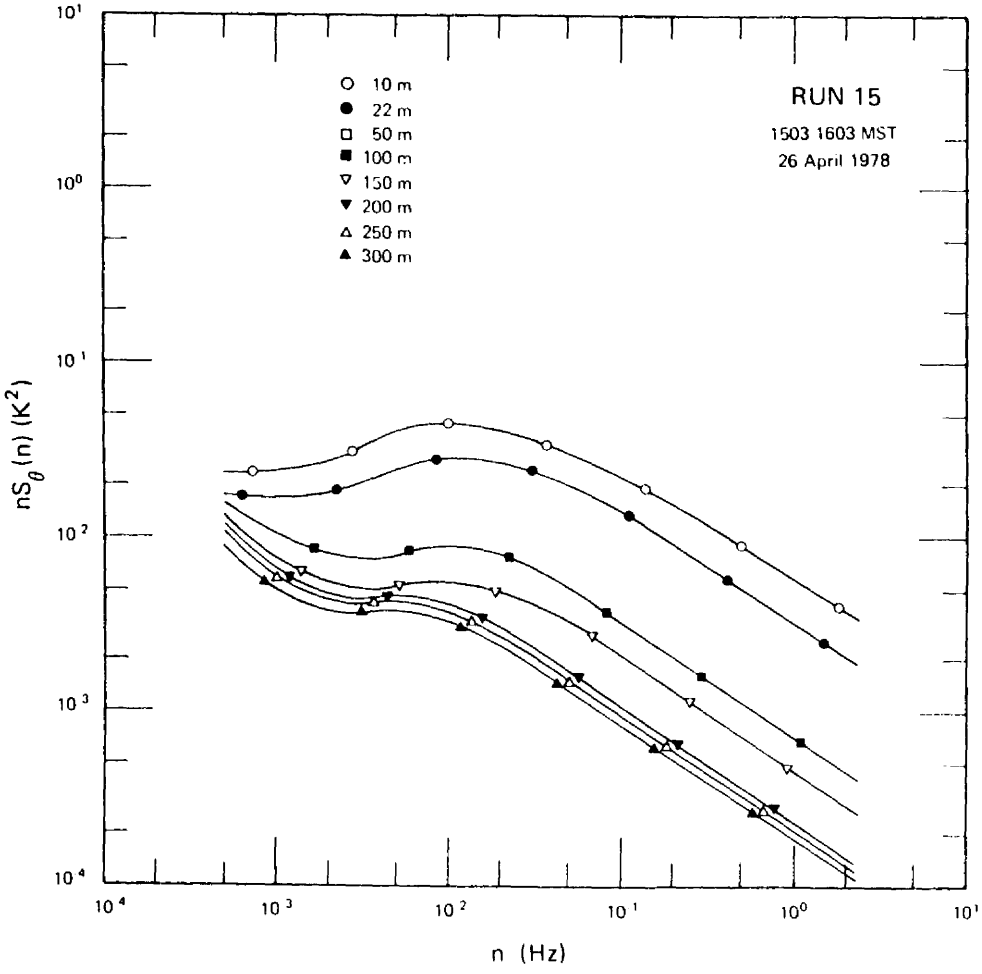

Figure 61. Temperature spectra for Run 15.

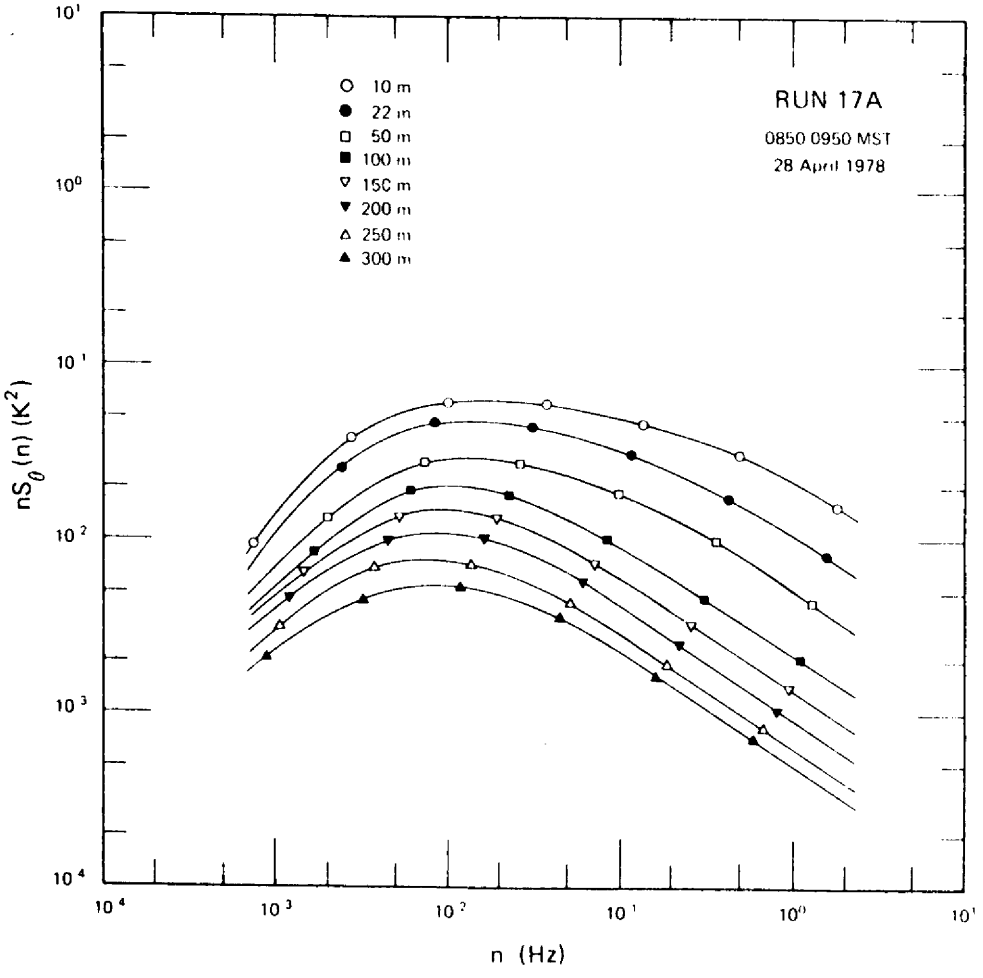

Figure 62. Temperature spectra for Run 17A.

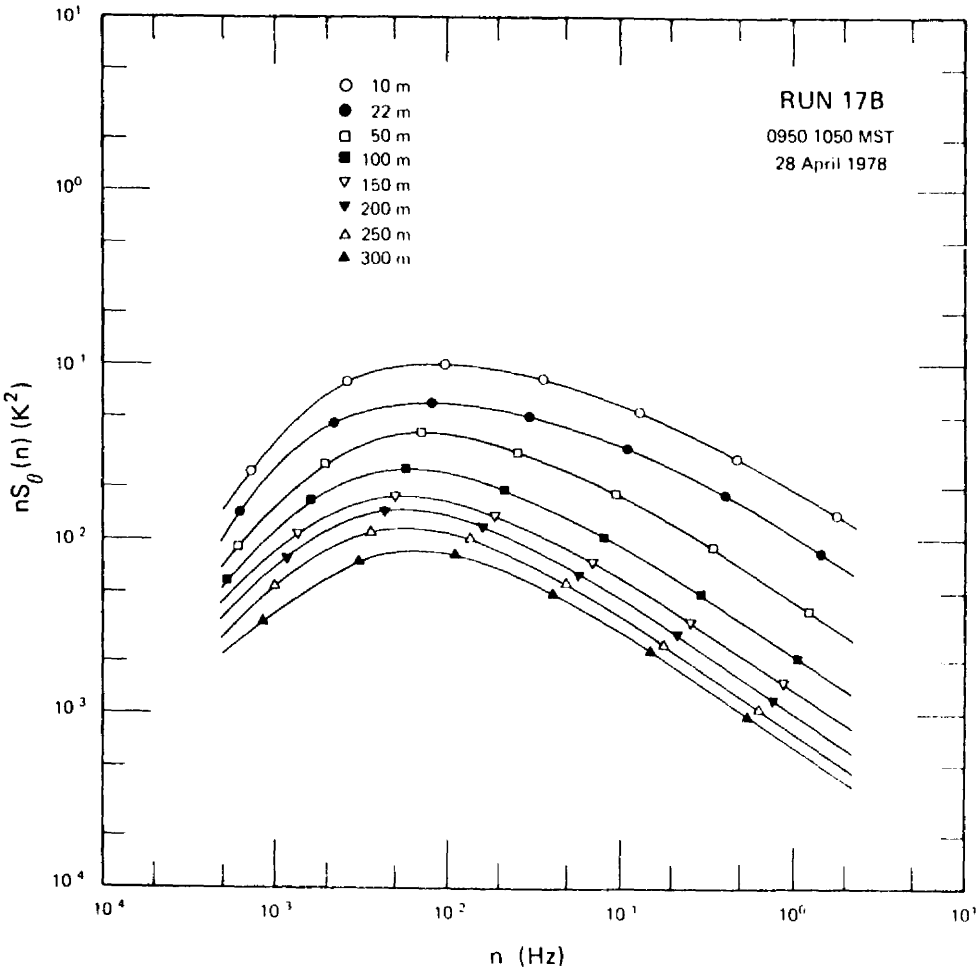

Figure 63. Temperature spectra for Run 17B.

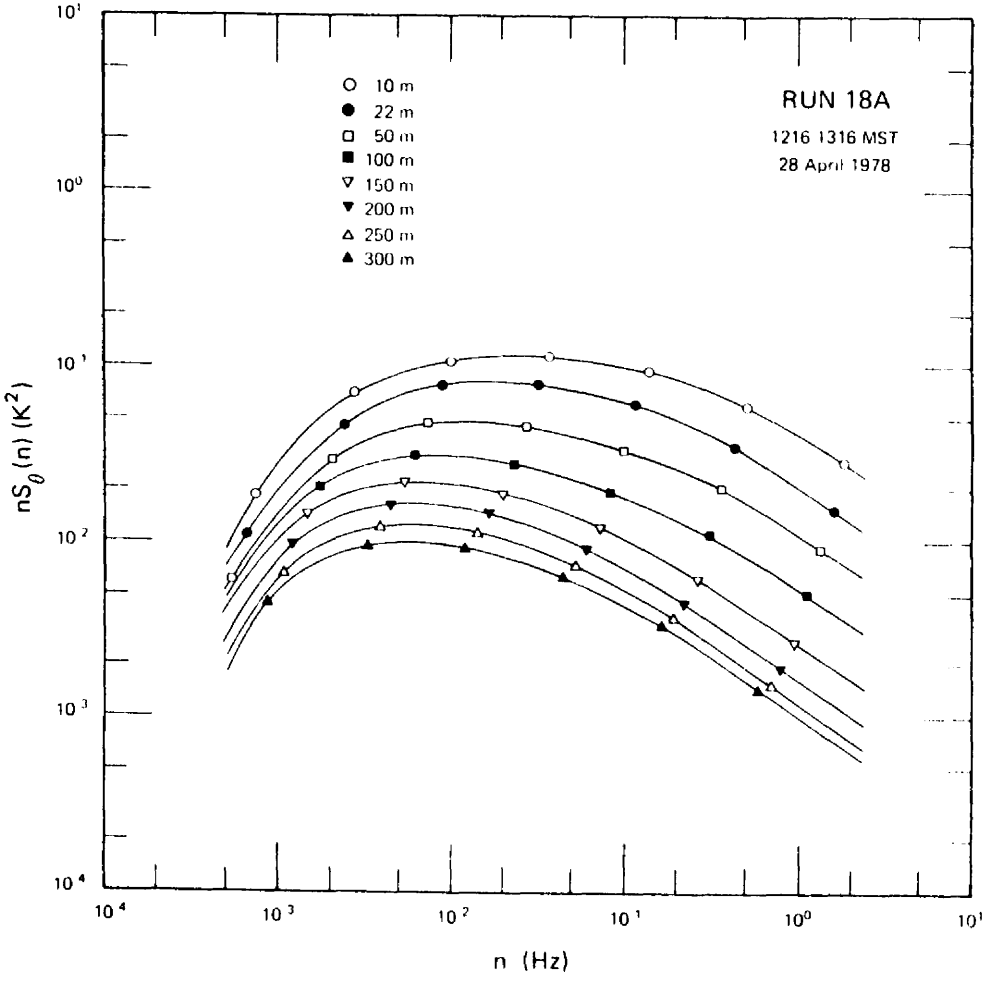

Figure 64. Temperature spectra for Run 18A.

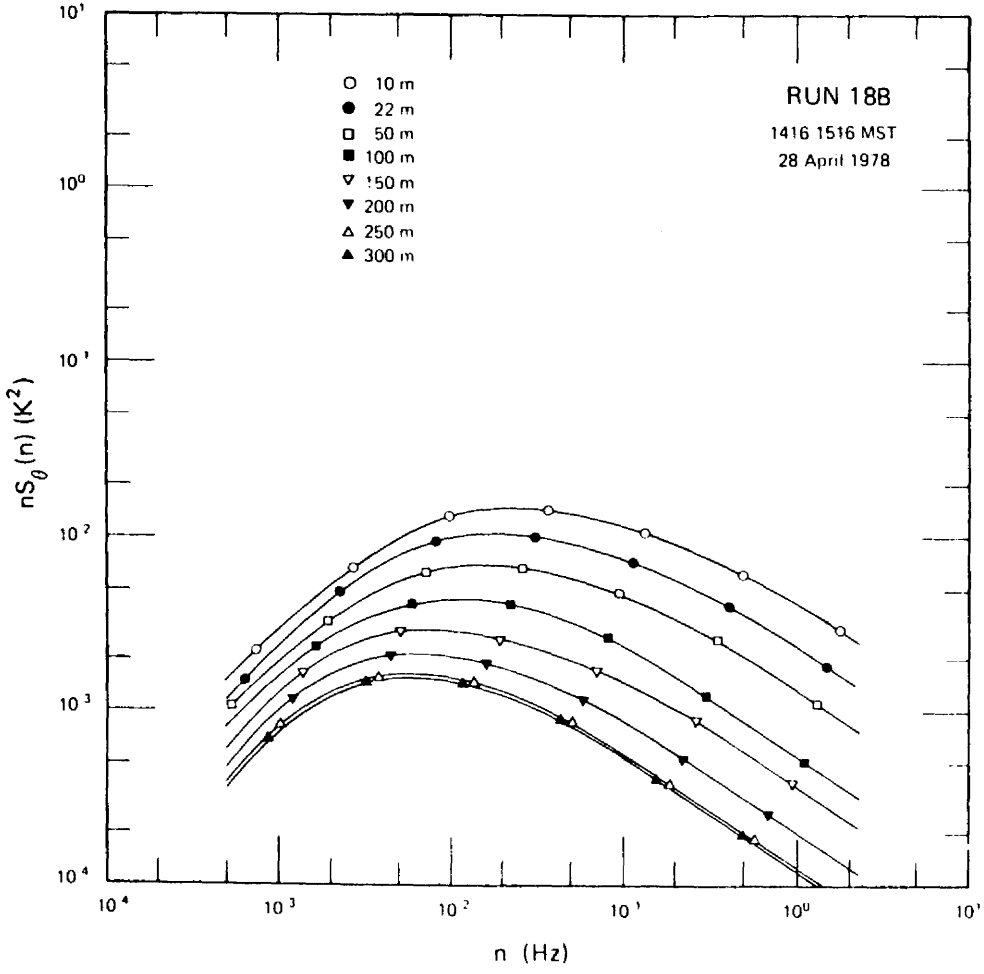

Figure 65. Temperature spectra for Run 18B.

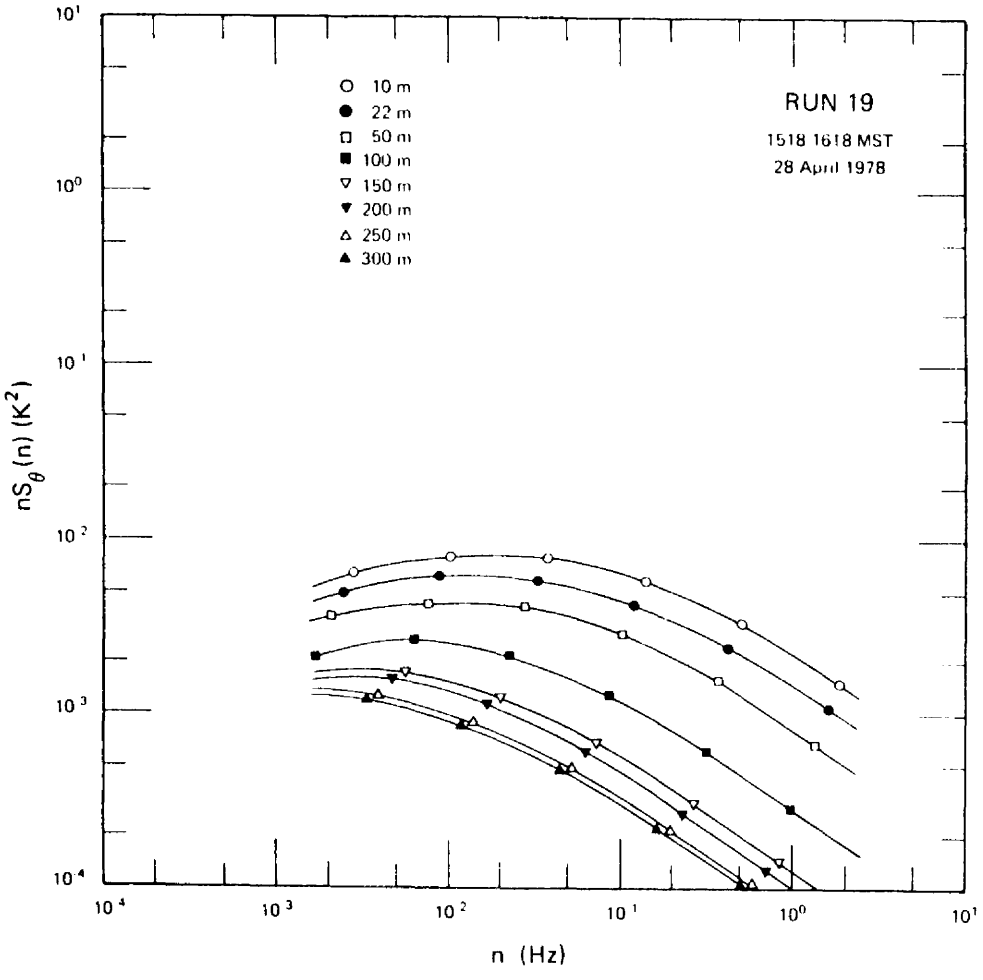

Figure 66. Temperature spectra for Run 19.

APPENDIX B

LIST OF SYMBOLS

$F_x(\kappa)$	one-dimensional wavenumber spectrum density	-	$m^3 s^{-2}$
f	dimensionless frequency in the surface layer	nz/U	-
f_i	dimensionless frequency in the mixed layer	nz_i/U	-
f_m	dimensionless frequency of the spectral peak in the surface layer	$n_m z_i/U$	-
g	acceleration due to gravity (g/T = buoyancy parameter)	-	$m\ s^{-2}$
k	von Kármán's constant	0.35	-
L	Obukhov length	$-u_*^3/[k(g/T)Q_o]$	m
N	dissipation rate for one-half of the temperature variance	-	$K^2 s^{-1}$
n	cyclic frequency	-	Hz
n_m	frequency of the logarithmic spectral peak	-	Hz
n_o	Nyquist frequency, one-half of the sampling rate	-	Hz
Q_o	surface kinematic heat flux	$(\overline{w\theta})_{surface}$	$K\ m\ s^{-1}$
$S_x(n)$	one-dimensional frequency spectral density	$X(n)X^*(n)$	$m^2 s^{-1}, K^2 s^{-1}$
T	mean temperature	-	°C
T_f	scaling temperature for the matching layer	Q_o/u_f	K
T_*	scaling temperature for the surface shear layer	$-Q_o/u_*$	K
t	time	-	s
U	mean wind speed	-	$m\ s^{-1}$
u	longtiudinal fluctuating wind component	-	$m\ s^{-1}$
u_f	scaling velocity for the matching layer	$[Q_o z(g/T]^{1/3}$	$m\ s^{-1}$

u_*	friction velocity, scaling velocity for the surface shear layer	$(\tau_o/\rho)^{1/2}$	$m\ s^{-1}$
$\overline{uw}$	kinematic momentum flux	-	$m^2 s^{-2}$
v	lateral fluctuating wind component	-	$m\ s^{-1}$
w	vertical fluctuating wind component	-	$m\ s^{-1}$
w_*	scaling velocity in the mixed layer	$[Q_o z_i (g/T)]^{1/3}$	$m\ s^{-1}$
$\overline{w\theta}$	kinematic heat flux	-	$K\ m\ s^{-1}$
$X(n)$	complex Fourier transform of the initial time series	-	$m\ s^{-1}$, K
$X^*(n)$	complex conjugate of the frequency domain series, $X(n)$	-	$m\ s^{-1}$, K
$x(t)$	initial time series	-	$m\ s^{-1}$, K
z	height above the ground (z/L = stability parameter)	-	m
z_i	height of the lowest inversion base	-	m
α_1	spectral constant for the one-dimensional u spectrum	0.5	-
β_1	spectral constant for the one-dimensional θ spectrum	0.8	-
ε	dissipation rate for turbulent kinetic energy	-	$m^2 s^{-3}$
θ	fluctuating temperature	-	K
θ_*	scaling temperature in the mixed layer	Q_o/w_*	K
κ	wavenumber	$2\pi n/U$	m^{-1}
λ	wavelength	U/n	m
λ_m	wavelength corresponding to the logarithmic spectral peak	U/n_m	m
ρ	density of air	-	$g\ m^{-3}$

σ_θ, σ_w	standard deviations of θ and w	-	-
τ_o	surface shear stress	$-\rho(\overline{uw})_{surface}$	$g\ m^{-1}s^{-1}$
ϕ_ε	dimensionless dissipation rate for turbulent energy in the surface layer	$kz\varepsilon/u_*^3$	-
ϕ_N	dimensionless dissipation rate for temperature variance in the surface layer	$kzN/u_*T_*^2$	-
ψ_ε	dimensionless dissipation rate for turbulent energy in the surface layer	$\varepsilon/[Q_o(g/T)]$	-
ψ	dimensionless dissipation rate for temperature variance in the mixed layer	$Nz_i/w_*\theta_*^2$	-

BIBLIOGRAPHIC DATA SHEET	CSU-ATSP-314	

4. Title and Subtitle

SPECTRAL CHARACTERISTICS OF BOUNDARY LAYER TURBULENCE OVER IRREGULAR TERRAIN

5. Report Date: June, 1979

6.

7. Author(s): Rae Ann Eversole

8. Performing Organization Rept. No. # 314

9. Performing Organization Name and Address

Department of Atmospheric Science
Colorado State University
Fort Collins, CO 80523

10. Project/Task/Work Unit No.

11. Contract/Grant No.

12. Sponsoring Organization Name and Address

National Oceanic and Atmospheric Administration--Wave Propagation Laboratory

13. Type of Report & Period Covered

14.

15. Supplementary Notes

16. Abstracts

The spectral behavior of turbulence in a convectively unstable boundary layer over undulating terrain is discussed. The wind and temperature fluctuations were measured with fast response sensors mounted on the 300 m tower at the Boulder Atmospheric Observatory (BAO). The boundary layer is divided into three layers (surface, matching, and mixed). The spectra of each layer are normalized using the appropriate scaling rules. The generalized spectra follow similarity theory. This paper compares the BAO results with the data obtained during AFCRL's field experiments in Kansas (1968) and Minnesota (1973) over flat, uniform terrain.

17. Key Words and Document Analysis. 17a. Descriptors

boundary layer
turbulence
Boulder Atmospheric Observatory
surface layer
mixed layer

17b. Identifiers/Open-Ended Terms

17c. COSATI Field/Group

18. Availability Statement	19. Security Class (This Report) UNCLASSIFIED	21. No. of Pages 115
	20. Security Class (This Page) UNCLASSIFIED	22. Price